SCIENTIFIC COMMITTEE
TWENTIETH REGULAR SESSION

Manila, Philippines

14–21 August 2024

Stock Assessment of Silky Shark in the Western and Central Pacific Ocean: 2024

WCPFC-SC20-2024/SA-WP-04-Rev2
14 August 2024

Philipp Neubauer[1], Kyuhan Kim[1], Kath Large[1] and Stephen Brouwer[2]

[1] **Dragonfly Data Science, Wellington, Aotearoa New Zealand**

[2] **Saggitus Environmental Science**

Revision 1:

Duplicated articles removed from References section.

Revision 2:

Fixed Figure 7 - inserted correct figure for year effects instead of flag effects for free-school purse-seine length compositions used with the corresponding CPUE index.

Stock Assessment of Silky Shark in the Western and Central Pacific Ocean 2024

Authors:
Philipp Neubauer
Kyuhan Kim
Kath Large
Stephen Brouwer

DRAGONFLY
Data Science

Cover Notes

To be cited as:

Neubauer, Philipp; Kim, Kyuhan; Large, Kath; Brouwer, Stephen (2024). Stock Assessment of Silky Shark in the Western and Central Pacific Ocean 2024, 121 pages. WCPFC-SC20-2024/SA-WP-04-Rev2. Report to the WCPFC Scientific Committee. Twentieth Regular Session, 14–21 August 2024.

CONTENTS

EXECUTIVE SUMMARY

This analysis assesses the southwest Pacific silky shark (*Carcharhinus falciformis*) stock in the Western and Central Pacific Ocean (WCPO). This is the third attempt at undertaking an assessment of Pacific silky sharks, with one previous attempt covering the entire Pacific (Clarke et al. 2018a), and the other for the WCPO area only (**Rice2013b**).

There are no target fisheries for silky sharks in the WCPO, and they are caught as bycatch in longline and purse seine fisheries. Since 2015 all silky sharks caught in fisheries managed by the Western and Central Pacific Fisheries Commission (WCPFC) are required to be released (WCPFC 2013). While silky sharks have been caught in Pacific fisheries since their inception in the 1950s, they have only been reported in catch records since the 1990s (Brouwer et al. 2023, Neubauer et al. 2023a). A catch history is required to be estimated prior to an assessment being undertaken because of the unreliability of both logsheet and observer data, due to: the use of generic reporting codes prior to 2015; the lack of logsheet reporting of bycatch data; and, poor and inconsistent (in time and space) observer coverage for most flags in the Pacific Ocean. However, general data improvements in recent years, along with the availability of biological data and the successful previous stock assessments led Brouwer and Hamer (2020) to conclude that a data rich assessment should be undertaken for this stock.

This assessment took a multi-model approach to assessing silky shark in the WCPO, resulting from large uncertainties in the underlying data and difficulties with fitting of integrated stock assessments for sharks generally. In an effort to understand overfishing risk to silky shark based on different lines of reasoning, a range of models were applied, with varying degrees of complexity and with different data requirements, including a fully integrated stock assessment in Stock Synthesis, and three alternative assessments: length and age structured assessment model (LAM), dynamic surplus production model (DSPM), and a length-based spatial risk assessment (SRA). These approaches were not strictly standardised, with no attempt to use consistent priors between them, and treating each approach as standalone to provide evidence from independent lines of reasoning. However, with a single set of data available, data inputs were standardised across all four assessment approaches.

Results across all assessment methods are largely in agreement that recent fishing mortality was low with respect to biological reference points for sharks. Therefore, while each modelling approach has limitations, we suggest that the weight of evidence is sufficient to conclude that fishing mortality has declined substantially for silky shark in the most recent decade, and that recent stock status is likely improving from previous low levels. We further suggest that the dynamic surplus production models provide the most parsimonious and robust available model for management advice. This suggestion derives from the consistency with other outcomes, but also because of stronger reservations about the robustness of other approaches. The stock synthesis assessment provided a number of challenges and some issues could not be resolved. We consider both the risk assessment and LAM models experimental at this stage, with further work required to use these model for management advice.

Main Assessment Conclusions

- The multi-model approach to assessing silky shark resulted in an uncertain stock status, but high confidence that recent fishing mortality is below levels that would preclude stock rebuilding.
- Based on considerations of model complexity, fit and estimation issues, we suggest that the dynamic surplus production model be used for providing management advice. We further suggest that the model ensemble across initial depletion priors may be over-representing uncertainty, and we suggest output from the intermediate assumption as a candidate model for management advice.
- The largest fishing mortality was estimated to have come from longline fisheries capturing nearly the full size-range of silky sharks, and reductions in interactions as a result of changes in fishing practices over the last decade may have substantially reduced this source of mortality, allowing the stock to rebuild.
- The stock status has been improving since 2010, and the recent fishing mortality rates are below biological reference points for the ensemble (Diagnostic F_{recent}/F_{crash}: 0.13 [0.01–0.25]; P(F_{recent}/F_{crash} >1)=0; P(F_{recent}/F_{lim} >1)=0).

With respect to other shark stocks with lower levels of information:

- Surplus production models should be used when composition data are problematic, and risk assessments should only be used in the context of prioritisation across species. However, alternative, data driven risk assessments could provide an avenue to use a risk assessment approach when time-series are not sufficiently long or reliable to estimate fishing mortality rates relative to biological reference points.
- With non-retention measures leading to sharks and other bycatch species being cut free from longlines, data colection may be problematic. In these cases, the only alternative to provide estimates of risk would be methods such as EASI-fish, which estimate risk from assumptions about fishery overlap with the species distributions and vulnerability to fishing effort.

Given some of the fundamental uncertainties highlighted above, we recommend:

- Additional tagging should be carried out using satellite tags in a range of locations as well as high seas areas to resolve fundamental questions about the species interactions with local oceanography and the dynamics of ENSO. Such tagging may help to resolve questions about the degree of natal homing and limited mixing of the stock, as suggested by genetics. This work is currently scheduled as part of the SRP as work theme 3 (a)vii and is due to begin in 2025 (Brouwer and Hamer 2024), and it is recommended that CCMs prioritise this work and ensure that satellite tagging options are included in the project specification.

- Additional growth studies and validation of aging methods from a range of locations could help build a better understanding of typical growth, as well as regional growth differences. Current growth data are conflicting, with insufficient data to understand the underlying process. This work is currently scheduled as part of the SRP as Project P19X11 and is due to begin in 2025 (Brouwer and Hamer 2024), and it is recommended that CCMs prioritise this work.
- Additional genetic/genomic studies across a broader set of locations could be undertaken to augment the tagging and existing genomics work to help resolve the stock/sub-stock structure patterns. To support this work, a strategic tissue sampling program for sharks is recommended with samples to be stored and curated in the Pacific Marine Specimen Bank. This work is currently scheduled as part of the SRP as work theme 3 (a)xii and is due to begin in 2026 (Brouwer and Hamer 2024), and it is recommended that CCMs maintain this project in the current work stream.

1. INTRODUCTION

Silky sharks (*Carcharhinus falciformis*) are wide ranging across the Pacific Ocean where they inhabit coastal and oceanic waters, but are most abundant in the tropical and subtropical waters (Bonfil 2008).

Globally, silky sharks are one of the most frequently caught sharks in tropical fisheries either as a target, or as bycatch (Bonfil 2008). In the Western and Central Pacific Ocean (WCPO) they are caught as bycatch in tropical and sub-tropical longline fisheries targeting tuna, billfish and blue sharks throughout the area and they are also caught in the purse seine fisheries of the WCPO (Brouwer et al. 2023). There are no target fisheries for silky sharks in the WCPO and since 2015 all silky sharks caught in fisheries managed by the Western and Central Pacific Fisheries Commission (WCPFC) are required to be released (WCPFC 2013).

Sharks, including silky sharks, have been caught in Pacific longline fisheries since their inception in the 1950s, but they have only been reported in catch records since the 1990s (Brouwer et al. 2023, Neubauer et al. 2023a). At that time, sharks were often lumped together and reported to a generic shark code (SHK). The generic shark code is seldom used after 2015 (Brouwer et al. 2023). These reporting issues have led to a paucity of data on silky shark catch which is exacerbated by a lack of logsheet reporting of bycatch in general, but particularly for sharks. Additionally, poor observer coverage for most flags in Pacific Ocean longline fisheries (Williams et al. 2020) means that catch records for this species are relatively sparse compared to the target tunas and blue sharks. The data that do exist are inconsistent in time and space and between fleets (Brouwer et al. 2023), suggesting the data which would usually be used in a stock assessment are sparse. This paucity of data requires that prior to an assessment being undertaken, catch histories need to be estimated as one cannot rely on reported or observed data alone. Catch histories have therefore been developed for some previous assessments (Rice 2012) and have again been attempted for this assessment (Neubauer et al. 2023a).

This paper reports on the 2024 stock assessment of silky sharks in the Western and Central Pacific Fisheries Commission Convention Area (WCPFC-CA). This is the third attempt at undertaking an assessment of Pacific silky sharks, with one previous attempt covering the entire Pacific (Clarke et al. 2018b), and the other for the WCPO area only (Rice and Harley 2013).

This report documents phase 2 of the 2024 silky shark assessment project, with phase 1 having been conducted in 2023. This is the first WCPFC shark assessment project to be conducted over a two year period, with the aim of allowing sufficient time to explore the issues associated with problematic data available to shark assessments, and have these considered by Scientific Committee prior to an assessment being conducted. This approach was recommended after both the recent blue shark and mako shark assessments (Neubauer et al. 2022, Large et al. 2022b), and was agreed at SC18.

Along with general data improvements in recent years (as well as the availability of biological data, and the successful previous stock assessments), the results of

investigative data work in phase 1 and the recommendations from SC19 led Brouwer and Hamer (2020) to conclude that a data rich assessment[1] should be undertaken for this stock.

A catch data series has been estimated and CPUE indices have been developed from multiple fleets (Neubauer et al. 2023a). These data along with estimates of growth, and observed length data from the population were available as inputs to this assessment (as part of the work in phase 1 reported to SC19). The assessment results are presented here, but as there are no agreed reference points for sharks managed by the WCPFC, where possible a range of metrics are provided as recommended by Brouwer and Hamer (2020) for SC20s consideration. This report should be considered along with the data inputs report (Neubauer et al. 2023a) and fisheries characterisation work (Brouwer et al. 2023) that were undertaken and reported to SC19 as part of this assessment.

2. ASSESSMENT INPUTS

2.1 CPUE indices

Observer-based CPUE indices were presented in Neubauer et al. (2023a). Long-line CPUE indices were used in Clarke et al. (2018a), as well as prior silky shark stock assessments (Rice & Harley 2013). However, the derived indices for the respective assessments were from different subsets of observer data (e.g., a regional CPUE was used in Clarke et al. (2018a), which differed markedly between assessments, and showed high inter-annual variability. Recent analyses suggest that this is likely due to high variability in longline CPUE between different regions and observer programmes (Neubauer et al. 2023a), all of which showed noisy CPUE with unclear over-all trends across the WCPFC convention area. Although silky shark are thought to show environmentally-mediated availability to fishing gear (Clarke et al. 2018a, Lennert-Cody et al. 2019), standardisation by environmental covariates (such as remote-sensed sea-surface temperature, chlorophyll-a or ENSO) did not standardise longline CPUE to produce interpretable indices.

Purse-seine indices, by contrast, showed a remarkable level of consistency, especially those derived from free-school sets (Figure 1). Despite effort being difficult to quantify for purse-seine indices, the non-target nature of silky shark in purse seine sets provides an argument that per-set indices may provide a reflection of silky shark abundance. While length compositions indicate that object associated sets mainly capture small silky shark, free-school sets catch all sizes, and with larger individuals than reported in longline data. Standardised free-school CPUE may therefore provide a suitable index of total biomass (Figure 2). As noted in Neubauer et al. (2023a), purse seine CPUE prior to 2000 is possibly biased as it largely comes from a single observer programme. In recent years, with poor coverage within the COVID-19 years (2021 and 2022), the index is poorly estimated and therefore these years are not included. The CPUE input for all

[1]Fully integrated stock assessment model using multiple sources of data including catch, effort and biological information in a model such as MULTIFAN-CL, Stock Synthesis or similar.

assessments therefore started in 2000, and ended in 2020. As a result, we defined recent status as stock status in 2019–2020, as status for more recent years is largely based on catch based projections (for the SS3 model).

The 2018 assessment for silky shark used a ENSO-related catchability in the model to account for environmentally driven availability of silky shark to the regional CPUE fleet (Clarke et al. 2018a). In comparison, we take the approach of standardising for environmental drivers outside of the stock-assessment model. We did so by adding environmental covariates to the CPUE standardisation (Figure 3 Neubauer et al. 2023a), which showed a strong ENSO signal present in purse-seine CPUE data. This signal may be due to a longitudinal shift in distribution of target species during ENSO years. To test that our indices were robust to spatio-temporal shifts in target species and fishing effort, we repeated our CPUE analysis with additional models using splines over longitude and latitude by year (with year treated as a random effect), and predicting CPUE in space and time (i.e., a spatio-temporal index; Figure 4). The latter was very similar to the initial purse-seine index (Figure 5). In addition, the strong coherence of the index between different observer programmes suggests that patterns of recent increase in CPUE are not due to the spatio-temporal extent of the fishery alone.

2.2 Length compositions and stock structure assumptions

Little is known about the stock structure of silky sharks in the Pacific Ocean. Initial studies based on mitochondrial DNA markers found differences between eastern and western Pacific stocks (Galván-Tirado et al. 2013), and there is some evidence to support multiple management units across the Pacific and the WCPFC, where nuclear markers yielded significant population structure between five regions and mitochondrial markers supported most of these differences. In addition, life history studies appear to corroborate this finding of stock structure, showing demographic differences between populations in Taiwan, Papua New Guinea, and the Central Pacific (Oshitani et al. 2003, Joung et al. 2008, Grant et al. 2018). However, sampling variability and study design may at least partly confound findings of demographic variability (Grant et al. 2018), and tagging studies have shown wide-ranging movement across national jurisdictions and international waters (Hutchinson et al. 2019, Francis et al. 2023).

Due to the standardisation effect on CPUE, especially with regards to ENSO variability, it was not reasonable to assume that the length-composition of the standardised index (i.e., index fleets in the model) ought to be the same as that of the catches. Maunder et al. (2020) suggested that composition data for index and capture fisheries should be separately specified, and selectivity estimated separately for each type of model fleet. This allows for temporal variability in catch to be resolved via time-varying selectivity, whereas a standardised index should correspond to a single selectivity.

We separated length compositions for purse seine fleets (object associated and free-school) into those of capture fleets and index fleets. The former used predicted compositions based on model-based scaling employed in Neubauer et al. (2023a). These

compositions estimate the effect of covariates on compositions on the basis of observed length frequencies, and then predict the capture length frequencies for unobserved effort to derive a length composition for total captures.

For index fisheries, we repeated this modeling approach, however, we included the same standardising variables as for the standardised CPUE index. Notably, we included effects for month, year, area (based on a 10-degree grid), observer programme-code, area and observer programme interactions with year, and an effect for ENSO variability (meiv2). The ENSO effect was formulated as two-dimensional spline over meiv2 and bins, using 5 knots across meiv2 and 10 knots across bins. The spline coefficients were estimated as random effects within brms (Bürkner 2018), and are therefore drawn towards a common mean of a linear effect unless data are sufficiently informative to suggest a more flexible form is required. Standardised length compositions corresponding to indices could then be derived by predicting the compositions of standardised catch and effort data used in CPUE models.

The LF scaling model used for catch was:

```
tot_by_bin ~ offset(log(n)) +
             (1 | bin) +
             (1 | bin:area) +
             (1 | bin:yy) +
             (1 | bin:mm) +
             (1 | bin:area:yy) +
             (1 | bin:flag_id) +
             (1 | bin:flag-id:yy),
```

where tot-by-bin is the total observations by length bin, modeled with a Poisson error distribution, n is the total observations across length bins in a stratum, and all factors are included as interactions with length bins. The corresponding model used for CPUE was:

```
tot_by_bin ~ offset(log(n)) +
             (1 | bin) +
             (1 | bin:area) +
             (1 | bin:yy) +
             (1 | bin:mm) +
             (1 | bin:area:yy) +
             (1 | bin:program_code) +
             (1 | bin:program_code:yy) +
             t2(meiv2, bin, k = c(5, 10)).
```

Input weights for compositions in the stock assessment were calculated as the trace

of covariance matrix across bins per year. This ensures that the relative uncertainty between compositions is correctly represented.

The latter model was used to standardise for ENSO by setting the meiv variable to zero (i.e., no ENSO influence) and predicting from the year effects only. Models were implemented using the ComPoM (Composition models using Poisson factorised Multinomial regression; Neubauer & Webber, in prep).

The model showed that length compositions were strongly influenced by the ENSO effect as measured by the meiv2 index (Figure 6). For free-school sets, positive ENSO conditions were associated with the presence of larger sharks in purse-seine sets, whereas during months of negative ENSO conditions, small individuals were present. A similar, albeit more uncertain pattern was observed for sharks caught in object associated sets.

The resulting effect was a strong standardisation on length compositions for index fisheries, especially for free-school sets (Figure 7). Due to the over-all restricted range of sizes seen in object associated sets, the standardisation effect for object-associated sets was smaller (Figure 8).

2.3 Catch assumptions

Fisheries interactions were reconstructed between 1995 and 2022 using an ensemble of spatial GLMM models (Neubauer et al. 2023a) that included effects for oceanographic predictors as well as targeting and total effort per stratum (5x5 degree grid, flag, year, month). Interaction estimates for longline and purse-seine were combined with a model for annual discard rates per flag (Figures 9, 10), which was used to produce scenarios of total fishing-induced mortality. Due to high discard uncertainties, especially before increased observer coverage in the 2010s, we considered the possibility of high and low discards alongside the base assumption of the median discard estimate from the discard model (Figures 11, 12, 13, 14). Post-release mortality was included at a rate of 15% in the calculations of total fishing-related mortality for long-line fisheries (Francis et al. 2023), and was applied at a rate of 85% for purse-seine fisheries (Hutchinson et al. 2015).

We only considered median estimates of interactions and discard fate. Uncertainty in modeled predictions of reconstructed catch, discards and post-release mortality was considered to be relatively small compared to over-all trends in catch and CPUE, and fundamental uncertainties about productivity-related parameters were thought to be more important for over-all model outcomes. We did, however, include a scenario of high and low initial equilibrium catch to reflect uncertainty of pre–1990s catch in estimates, as these remain highly uncertain. Our base assumption was that catches in years prior to the reconstructed catches were lower, and that catches increased with an expansion in longline fishing effort in the later 1990s and 2000s. Full exploration of fishing mortality, other catch and discard scenarios could be tested in the future.

3. REFERENCE POINTS

Clarke and Hoyle (2014) and Zhou et al. (2018) evaluated methods to derive reference points for elasmobranchs in the Western and Central Pacific Ocean (WCPO). However, to date, there are no formally agreed reference points for sharks in the WCPO. Recent assessments of oceanic whitetip shark, for example, compared fishing mortality to F_{lim} as a tentative limit reference point for sharks, and to F_{crash}, the fishing mortality that would lead to extinction in the long-term. If one assumes a simple Schaefer surplus production model, then $F_{crash} = R_{max}$, the maximum population growth rate (intuitively, a population cannot be sustained if fishing removes more individuals than the population can maximally produce), and $F_{lim} = 0.75R_{max}$. Because the versions of these reference points as used in the integrated assessment were approximated from integrated stock assessment runs, we use a subscript AS to show that these are not derived from R_{max}, but from the yield curve estimated in Stock Synthesis. Unlike for blue shark, which have higher productivity than many other shark species, we did not apply alternative reference points used for target fisheries.

4. STOCK SYNTHESIS ASSESSMENT METHODS

4.1 Model setup

The model used Stock Synthesis (Version V.30.22.1; Methot et al. 2021). We used Pacific specific parameters where possible (Clarke et al. 2015). CPUE data were included from 1995 (when suitable CPUE data became available) up to and including 2020. Models were run from 1995 to 2022, and outputs were analysed with respect to stock status in 2022.

4.1.1 Growth

Growth assumptions were based on Oshitani et al. (2003). We note that previous studies used growth estimates from Joung et al. (2008), but the latter study was based on a smaller sample in a small geographic area off the coast of Chinese Taipei, and found slower growth and larger asymptotic size. A size-at-birth was inferred to be near 50 cm for both males and females based on growth studies as well as measured lengths in tropical tuna fisheries. Growth variability was parametrised as a mixture of a CV for length-at-age (fixed at 0.085) with a constant standard deviation of 5 cm added to reflect variability observed at age zero (presumed age-0 silky shark have been observed as small as 30–35 cm). We assumed a maximum age of about 25 years, with females maturing at about 5-6 years old (Oshitani et al. 2003).

4.1.2 Natural mortality

Natural mortality was set to 0.18 in previous assessments (Rice and Harley 2013, Clarke et al. 2018b), citing work by Cortés (2002). However, while a range of 0.17-0.21 was cited, that same study also included a second sub-population with estimated M of 0.1-

0.15. Using a meta-analytic approach based on growth (assuming K of 0.148, and L_∞ of 216.4 cm fork length) and longevity (assuming longevity of 30 years) assumptions lead to an estimated median M of 0.21 with a lognormal SD of 0.08 under an input CV of 0.2 (Figure 15; based on https://connect.fisheries.noaa.gov/natural-mortality-tool/ Cope and Hamel 2022). We used this value to construct a prior, but given lower estimates found in Cortés (2002), we increased the SD of the lognormal prior from 0.08 to 0.3.

4.1.3 Reproductive output and recruitment

Stock recruitment assumptions for sharks have been problematic due to the low fecundity of many species. The low fecundity leads to a high vulnerability to fishing for many species, and it remains unclear how well stock-recruitment assumptions made in standard stock-recruitment relationships (SRR) for bony fishes, with often millions of eggs per female, translate to shark species. Taylor et al. (2013) suggested that standard stock-recruit relationships such as the Beverton-Holt model can make unreasonable assumptions about pre-recruit survival at low biomass (i.e., lead to survival greater than 1), especially if pre-recruit survival is high, a condition that is likely for many sharks. These authors proposed a survival-based stock recruit (SBSR) relationship as a three-parameter model with a shape parameter controlling the shape of the stock recruitment relationship. With a shape parameter $\beta < 1$, the model can emulate the shape of the Beverton-Holt (BH) SRR, whereas a shape of $\beta > 1$ leads to an over-compensatory SRR, with maximum recruitment at intermediate stock sizes.

Previous shark assessments in the WCPFC have employed the survival relationship for blue shark, for example (Neubauer et al. 2021, ISC 2018), deriving parameters for the function based on simulations run in the context of a Beverton-Holt (BH) model, and translating to corresponding parameters for the SBSR model. Other models have assumed BH SRRs, largely for convenience as it is somewhat easier to reflect on the associated steepness parameter than about the joint effects of the SBSR shape and the second parameter (the z_{frac}) which, loosely, determines the rate of density-dependent increase in survival as the stock is depleted (i.e., the strength of density dependence). In the context of the present model, however, we found that applying a BH SRR led to estimates of survival of >1 in some years, and led to highly unstable models with poor diagnostics. In addition, the BH model is essentially equivalent to a model with a low value for the shape parameter ($\beta < 1$; Taylor et al. (2013)), which assumes that density dependence is greatest near stock collapse, leading to an assumed high resilience at very low stock size, but limited density dependence at larger stock sizes. This is likely unrealistic for sharks if cannibalism and intra-specific competition are important. Lastly, models attempting to estimate the beta-parameter using priors with a prior median of 1 (i.e., giving equal prior weight to BH-like models with $\beta < 1$ and over-compensatory models with $\beta > 1$ consistently estimated $\beta > 1$, with preliminary Bayesian analyses (albeit with poor mixing performance for MCMC) pointing to $\beta \approx 1.5$ as a lower bound for β. We attempted both models with estimated β as well as using fixed values to ensure that uncertainty in the location of peak recruitment was considered.

4.1.4 Selectivity

We employed flexible selectivity assumptions for capture fisheries, reflecting the idea that they likely encounter different components of the stock from year to year, depending on oceanographic and fishing conditions. The flexibility in selectivity allows the model to remove the correct catch composition from the population. By contrast, the index fishery for the CPUE index was specified using a single selectivity that does not vary over time (Maunder et al. 2020).

For capture fisheries, we used a spline selectivity with 4 knots (longline and purse-seine), while assuming full selectivity for all sizes on average for the free-school purse-seine fleet. For all capture fisheries, we used a 2D auto-regressive prior (Xu et al. 2019) across length bins and years, with the first year for longline held fixed at the mean selectivity to allow for estimation of initial fishing mortality conditional on mean selectivity (otherwise random variation in year one is confounded with initial fishing mortality). We used the 2D-AR prior with a fixed auto-correlation of 0.3 and a standard-deviation of the log of deviations of 1, 1.5, and 2 for longline, associated purse-seine and free-school purse-seine, respectively. Although these standard deviations can (in theory) be tuned, we found that it was necessary to fix this deviation at a large number to mitigate issues with MCMCs (see below).

For the associated purse-seine index, the selectivity from the capture fishery was mirrored to the index fishery. However, this index was not used for fitting and served for visual inspection only. For the free-school index, we used a spline selectivity with 6 knots, but no time-variation. All selectivity parameters were given minimally informative normal or lognormal priors to improve MCMC performance, and ensure parameters cannot hit bounds during sampling as this can result in poor sampling.

4.1.5 Diagnostic model

As opposed to other recent shark stock assessments, which used model ensembles to integrate over key uncertainties in data and parameters (Neubauer et al. 2022, ISC 2024), we took an approach of attempting to integrate over key parameter uncertainties within the diagnostic model, and only addressing structural (in the sense of using different likelihoods) or data uncertainties for a range of uncertainties. Simulations developed for Neubauer et al. (2023b) suggested that this may be a preferable approach, rather than attempting an ensemble across fixed values of key parameters, as it maintains important correlations and avoids fixed parameter combinations that are unlikely *a posteriori* (*a priori* unlikely combinations can be accounted for by using multivariate priors with appropriate prior correlation). It is worth noting that this approach was feasible due to contrast in catch history (declining catch in recent years) and a corresponding increase in the CPUE index (Magnusson 2016).

For the diagnostic model, we fixed $beta$ at 2.69, the estimate from a MAP run aiming to estimate $beta$. The latter run presented a number of divergent iterations during MCMC, and was therefore not considered as a diagnostic model.

Priors Our diagnostic model used vaguely informative priors for all parameters to aid estimation and Markov Chain Monte Carlo. Specifically, we used an informed prior on natural mortality (median 0.2, CV 60%). A slightly domed beta-prior for z_{frac} was employed to reflect that this parameter is unlikely to be near the bounds of zero or 1 in reality. A relatively wide normal prior (mean 8, SD 4) was used for the log of unfished recruitment $ln(R_0)$.

Initial fishing mortality Equilibrium catch was set to 120 000 individuals, which corresponds to an assumption that catch was at the lower end of estimated catches in the mid 1990s prior to the expansion of the longline effort observed in the WCPFC during the late 1990s and early 2000s. We estimated initial F by assuming the population is at equilibrium with mortality from the longline fleet. In an attempt to provide minimal curvature (information) to the model to aid estimation of initial fishing mortality, we set a log-normal normal prior with mean 0.1 and CV of 65%.

MCMC While most initial models and some sensitivities were run using MAP estimates only, uncertainty for the diagnostic model and key sensitivities were estimated using full Bayesian inference, using the No-U-Turn sampler as implemented for ADMB (Monnahan & Kristensen 2018). We ran eight chains with different random seeds, and used 500 iterations for adaptation; these iterations were subsequently discarded as burn-in. Due to the complexity of the selectivity assumptions and parameter correlations, we had to use adaptation based on the dense covariance matrix in order to minimise divergent iterations, rather than the diagonal of the covariance matrix (the default). Divergent iterations arise when the sampler cannot adequately explore certain regions of parameter space due to the shape of the posterior surface, leading to potentially biased outcomes.

To diagnose the divergences, we ran a logistic regression against all parameters to understand the link between numerical values for each parameter and divergences. This diagnostic suggested that divergences were related to estimation of selectivity parameters, and specifically the 2D-AR structure, with random deviates from the mean selectivity consistently being the best predictors of divergent transitions. It is therefore likely that these failures to sample the parameter space largely influence the fit to length data.

While we were able to derive a diagnostic model without divergences, the same was not true for all sensitivities, and we therefore used sensitivities to understand the extent of structural uncertainty, without explicitly integrating this uncertainty into a model ensemble. This said, models with few divergent iterations appeared to give very similar outcomes to the diagnostic model without divergences. While it is clearly undesirable to maintain models with potential bias, it appears likely that this bias is minimal relative to uncertainties that persist with respect to data and life-history inputs for sharks.

All models were checked to ensure that $\hat{R}$ values were close to 1 and effective sample size for management quantities was >500.

4.1.6 Data weighting

Data weighting followed Francis (2011), first fitting a smoother through the CPUE index, and calculating the expected CV for CPUE from this fit on the basis of the SD of the residuals (Figure 16). The latter was found to be near 0.18, and the input SE for CPUE was therefore set to this level. Weights for length frequencies were adjusted iteratively, however, this adaptation was stopped after three iterations as the calculated weights did not stabilise. This behaviour may be due to the use of the 2D-AR selectivity influencing the calculation of weights.

4.1.7 Diagnostics

We used retrospective analysis, using 5 peels, to understand how recent data changes the estimated stock depletion and fishing mortality levels. In addition, we used profiles for M, $ln(R_0)$ and $beta$ to gain an understanding of the influence of data and model assumptions (such as initial catch) on natural mortality and stock recruitment.

4.1.8 Sensitivities

Data weighting Due to conflicts between CPUE and length data with regards to mortality and stock size, as well as the dubious performance of the Francis re-weighting method, we employed a sensitivity to halve the assumed standard error for the CPUE index, and set all length-composition weights to 1 (i.e., 5-80 times lower than after re-weighting), to understand the relative influence of these data.

Alternative values for beta The shape of the stock-recruit function is inherently uncertain. Estimates from a full MCMC estimation run for $beta$ suggested a range of 2-5 for this parameter under low catch assumptions, with a central estimate of 2.69. We therefore ran three alternative models with beta fixed at 1.5 and 4 in addition to model runs with $beta = 2.69$.

Initial catch We ran all options for $beta$ across low and high initial catch assumptions. For low catch, we set catch to the lowest figure estimated for the first 5 years of predicted catch (120 000 individuals), whereas for high catch, we doubled this figure.

Selectivity Alternative models were attempted with a fixed selectivity (i.e., not a 2D AR time-varying selectivity) for the longline fleet. An alternative run with no time-varying selectivity was run to confirm that the 2D-AR selectivity is indeed to blame for divergent iterations. While this run showed poor fits to length data and implausible outcomes (an initial biomass near B_0 with nearly no depletion), this run confirmed that without time-varying selectivity, no divergences occur.

5. ALTERNATIVE ASSESSMENTS METHODS

5.1 Length and age structured assessment model

5.1.1 Background

Conventional length-based age-structured models (Fournier et al. 1998, Methot Jr & Wetzel 2013) often overlook the cumulative impacts of length-dependent processes on a population. For instance, if large individuals are selectively removed by fishing, the surviving populations will become dominated by slower-growing individuals. In most age-structured models, as the population transitions from one age class to the next, it is typically assumed to be independent of the length distribution (i.e., the population is partitioned into age classes, and the length distribution within each age class is assumed to be constant). Although some age-structured models have considered partitioning fish of the same age into different growth groups (platoons) to account for fishing-induced selection (Taylor & Methot Jr 2013), this approach requires additional assumptions about partitioning to determine how each platoon distributes across length classes. Unlike such age-structured dynamics, length-structured dynamics can directly account for the cumulative impacts of length-dependent processes on population dynamics without additional assumptions about partitioning.

The cumulative impacts of length-dependent processes can be substantial, particularly for species with low fecundity and late maturation, such as sharks. The removal of large individuals can have more severe effects on population growth rates than in species with high fecundity and early maturation. Moreover, in shark assessments, information on age structure is typically unavailable, rendering age-structured dynamics no more beneficial than length-structured dynamics, aside from the ability to track the age structure of the population. Combining length-based dynamics with age structure can provide a more realistic representation of population dynamics by incorporating the cumulative impacts of length-dependent processes while tracking the age structure. This motivated us to develop a length- and age-structured model (LAM) that incorporates these cumulative impacts while maintaining the population's age structure.

The model was developed in Stan (Stan Development Team 2018) and based on previous research on length-based age-structured models (Quinn et al. 1998, Kim 2022), where the cohort-specific length distribution was used to calculate length-dependent mortality rates for each age class over time. Our LAM is similar to these previous models, but the major difference is that a vector of length bins for each age class and time step is explicitly used to describe the transition of the population between age, length, and time steps through a matrix equation.

5.1.2 Model structure

We largely retained the structure of submodels (e.g., growth, maturity, weight-at-length, and stock-recruitment relationship) from the Stock Synthesis models to maintain consistency with their biological assumptions. Only the model structure

unique to the LAM is described here. Prior distributions for all biological parameters are the same as those used in the diagnostic cases of the Stock Synthesis models, except for the CV of the growth variability parameter, which was fixed in the Stock Synthesis models but is estimated in the LAM. The technical details of these components are described in the appendix.

The length and age-structured dynamics are described by the following matrix equation:

$$\mathbf{N}_{t,a} = \begin{cases} \mathbf{R}_t & \text{for} \quad a = 0 \\ \mathbf{G}_{a-1}\mathbf{S}_{t-1}\mathbf{N}_{t-1,a-1} & \text{for} \quad 0 < a < A \\ \mathbf{G}_{a-1}\mathbf{S}_{t-1}\mathbf{N}_{t-1,a-1} + \mathbf{S}_{t-1}\mathbf{N}_{t-1,a} & \text{for} \quad a = A \end{cases}, \tag{1}$$

where $\mathbf{N}_{t,a}$ is the number of fish at age a in year t, represented as a vector of length classes. $\mathbf{R}_t$ is the recruitment vector, $\mathbf{G}_a$ is the growth transition matrix for age a, $\mathbf{S}_t$ is the survival matrix in year t, which is a function of length-dependent fishing mortality and length-independent natural mortality, and A is the plus group age.

The key component of the model is the age-specific growth transition matrix $\mathbf{G}_a$, which allows transitions between length and age classes. The growth transition matrix is calculated based on the von Bertalanffy growth function and growth variability for each age class, using the same parameters (and no additional parameters) as in the Stock Synthesis models. The details of the growth transition matrix are also described in the appendix.

5.1.3 Selectivity

Length-dependent selectivity was modelled using an exponential logistic function (see pattern 25 in the Stock Synthesis manual v3.30.17), except for the free-school purse-seine fleet:

$$\text{Sel}_i = \frac{\exp(p_3 \cdot p_1 \cdot (\text{peak} - L_i))}{1 - p_3 \cdot (1 - \exp(p_1 \cdot (\text{peak} - L_i)))} \tag{2}$$

where Sel_i is the selectivity for length bin i, L_i is the length of fish in length bin i (i.e., midpoint), p_1 is the ascending rate, p_2 is the parameter to adjust the peak of the selectivity curve, p_3 is the descending rate, and $\text{peak} = \min(L_i) + p_2 \cdot (\max(L_i) - \min(L_i))$.

For the free-school purse-seine fleet, the selectivity was modelled using a logistic function. The logistic selectivity function, where two parameters indicate the length at 5% and 95% selectivity rather than the conventional 50% and 95% selectivity, setting

reasonable bounds for the selectivity curve to aid in model convergence, is given by:

$$\text{Sel}_i = \frac{19}{19 + \exp\left(\log(361) \cdot \frac{L_i - L_{95}}{L_5 - L_{95}}\right)}, \tag{3}$$

where L_5 and L_{95} are the length at 5% and 95% selectivity, respectively.

All selectivity parameters were estimated in the model with bounded logit-normal priors, where the logit-transformed parameters follow a normal distribution with a mean of 0 and standard deviation of 1.6, to form weakly informative priors. Reasonably wide bounds were set for the selectivity parameters (see Table 3).

Similarly to our exploration with Stock Synthesis models, we also tested 2D-AR structures for time-varying selectivity with LAMs. As with the Stock Synthesis models, the 2D-AR structure rendered the LAM model unstable and it did not converge, with divergent transitions in the MCMC chains. Therefore, only time-invariant, fleet-specific selectivity was considered in the LAMs.

5.1.4 Initial fishing mortality

Our preliminary analyses indicated that the model was sensitive to the initial fishing mortality that determines the equilibrium population size in the first year. We attempted to estimate the initial fishing mortality in the model, but model convergence was not achieved. Therefore, we fixed the initial fishing mortality at different levels as a sensitivity analysis to determine the impact of the initial fishing mortality on the model results. The initial fishing mortality was fixed at 0.05, 0.1, and 0.15.

5.1.5 Catch-conditioned model

Catch data were assumed to be without error, requiring LAMs to internally estimate the instantaneous fishing mortality rate for each fleet. A Newton-Raphson method was implemented to internally search for the fishing mortality rate that matched the observed catch. We validated the Newton-Raphson algorithm by comparing the model-predicted catch for each fleet with the corresponding observed catch.

5.1.6 MCMC settings and diagnostics

We ran 10 chains with different random seeds, and used 400 iterations for adaptation; these iterations were subsequently discarded as burn-in, and the remaining 400 iterations were drawn as samples from each chain. We assessed convergence using the Gelman-Rubin statistic, trace plots, and effective sample size. We used the same convergence criteria as the Stock Synthesis models, where the Gelman-Rubin statistic $\hat{R}$ values were close to 1 and effective sample size for management quantities was >500. We also visually inspected the trace plots to ensure that the chains mixed well.

5.2 Dynamic surplus production model

As length frequency data are highly temporally variable, and spatio-temporal coverage is highly skewed over time, we sought to check trends found with the integrated assessment model against simpler models, namely dynamic surplus production models. The latter can be straightforwardly fitted to CPUE time series, and we applied the Schaefer surplus production model implemented in the *bdm* R package (Edwards 2017) to aggregated catch across fisheries and CPUE from the free-school purse-seine CPUE time series, used in the integrated assessment model.

Neubauer et al. (2019) provided context for the application of dynamic surplus production models (DSPM) to sharks in the WCPFC, and other recent assessments have applied these models when the available information lead to difficulties with integrated stock-assessment models (ISC 2024). DSPM are fitted based on state-space equations (McAllister & Edwards 2016, Froese et al. 2017) and do not require equilibrium assumptions that make traditional approaches to surplus production assessments difficult to justify (Bonfil 2005). Examples of packages that implement DSPMs are JABBA ("Just Another Bayesian Biomass Assessment"; Winker et al. 2018) and BDM ("Bayesian biomass dynamics model"; Edwards 2017). As such, the DSPM operates similarly to integrated assessments, where recruitment essentially functions as a process error term. The DSPMs tend to use an index of abundance (usually CPUE) to constrain the time series of abundance. Although productivity is usually estimated within DSPMs, it is useful to also constrain productivity via an informative prior (Edwards 2017).

We used a classic Schaefer production model implemented in the BDM package (although other hybrid production functions can be used with this R package). The population dynamics are parameterised in terms of the relative depletion ($x_t = N_t/K$), with relative harvest H_t also expressed in relative terms ($H_t = C_t/K$):

$$x_{t+1} = x_t + g(x_t) - H_t \tag{4}$$

$$g(x_t) = R_{max} x_t \left(1 - x_t\right). \tag{5}$$

5.2.1 Priors for dynamic surplus production models

Population growth R_{max} was calculated from methods in Pardo et al. (2018) based on the Euler-Lotka equation (see also Zhou et al. 2018), adjusted for survival to age at first maturity (Pardo et al. 2016). Estimating R_{max} serves a dual purpose here: it can act as a reference point for methods that cannot estimate stock productivity independently (e.g., risk assessments), but can also act as a prior for a DSPM for which R_{max} is the productivity parameter.

Life history input values for the Euler-Lotka equation were compiled from ranges and point estimates reported in Clarke et al. (2015) and recent stock assessment reports (Clarke et al. 2018b). Specifically, growth rate K was taken as 0.148 with sufficient

variability to encompass uncertainty and potential bias in estimates life-history values (Grant et al. 2018, Figure 17) for the simulated inputs, and for the resulting value of R_{max} (Figure 18). When only ranges were reported, the distributions were constructed to encompass those ranges as extreme quantiles (i.e., near the 5th and 95th percentile).

We also integrated over methods to derive natural mortality in the simulation procedure. Specifically, we used methods described in Jensen (1996) (age-at-maturity based), Hewitt and Hoenig (2005) (maximum age based), and Pardo et al. (2016) (expected life-span derived), by simulating R_{max} from the inputs under these mortality assumptions and combining the outputs. This led to a broader distribution for R_{max} than would be obtained if one considered a single method to estimate natural mortality.

Priors for the carrying capacity, K, and initial population depletion in 1995 were formulated as vague log-normal distributions, encompassing scenarios of high initial depletion as well as high initial biomass (i.e., $> B_0$). In order to ensure that these priors made sense in the context of observed catch, we simulated from the model using the prior for R_{max}, a wide prior for carrying capacity and and initial depletion ([0.01;0.6], and applied the catch to obtain a prior predictive/pushforward distribution for recent depletion. The obtained recent depletion values were then subset to values between 0.05% and 100% of carrying capacity, and only prior draws which led to these outcomes were retained (Figure 19). We note here that, due to the peaked and steeply declining catch history in recent years, the model invariably retained parameter combinations that led to high *a priori* current status and log over-fishing risk (Figure 19). We nevertheless used these values to estimate the parameters of a log-normal prior distributions for R_{max}, K and initial depletion. We subsequently manipulated the prior for initial depletion to investigate the sensitivity of the model to mis-specification of this prior. We fitted the model based on three sets of priors for the initial depletion level, with sensitivities assuming higher and lower levels of *a priori* initial depletion in 2000 (multiplying or dividing the prior mean of initial depletion by a factor of two). The process error standard deviation was fixed at 0.05.

Catch was summed across predicted purse-seine and long-line catches, as this appeared most appropriate for the assumption inherent in dynamic surplus production models that the population indexed by the CPUE index is fully vulnerable and affected by the specified catch.

5.2.2 Implementation

All estimation was done within the BDM package, with Markov Chain Monte Carlo (MCMC) in the underlying Bayesian estimation software Stan (Stan Development Team 2018) used to estimate parameters. We ran the MCMC for 110 000 iterations, discarding the first 10 000 iterations as burn-in, and keeping 1000 samples from each of 4 chains. All model were checked to ensure that $\hat{R}$ values were $<$1.01, and did not show any divergent iterations. Retrospectives were run with 5 peels, and Mohn's rho and predictive coverage were calculated as the proportion of the posterior for year y that is contained within the predictive distribution for that year from the retrospective

model ending in year $y - 1$.

5.3 Length-based spatial risk assessment

Spatial Risk Assessments (SRAs) incorporate spatially detailed relative abundance and effort information (vulnerability) and life-history (susceptibility). Neubauer et al. (2019) reviewed the utility of spatial risk assessments in the context of an application to oceanic whitetip shark. While we provide a brief description of this topic here, more detail and references can be found in Neubauer et al. (2019).

Briefly, spatial risk assessment approaches calculate fishing mortality and sustainability risk, often expressed as a risk-ratio comparing fishing mortality (F) to a life-history-derived sustainability threshold. These methods are typically employed when no reliable catch time-series can be derived. They therefore use recent catch data, avoiding the need for complete historical catch records or assumptions about catch completeness or CPUE data accuracy.

To compensate for the lack of temporal contrast, SRAs employ two main strategies. The first strategy involves pre-setting constraints on either current population size and relative abundance information. For some species, like seabirds and certain marine mammals, estimates may come from censuses or surveys. Genetic methods can also provide population size estimates, though these often involve significant assumptions or uncertainties. When dealing with regional stocks of wider-ranging populations, researchers may use spatial density data to estimate the relevant subpopulation or consider the impact of regional fishing on the entire population.

The second strategy assumes known gear efficiency. Methods such as SAFE and EASIfish can directly estimate fishing mortality conditional on assumptions of the spatial scale of gear impacts. This approach treats fishing effort as a survey, scaling estimated densities in fished areas to the overall habitat (i.e., akin to a swept-area approach for scaling trawl survey catch-per-unit-area (CPUA) to a total biomass).

By contrast to models that drive estimates of risk based on assumptions about gear efficiency, statistical risk assessment methods estimate population size or gear efficiency directly from spatial catch and effort data, conditional on gear-affected area assumptions. This method, exemplified by the e-SAFE approach, has advantages over CPUE trend-based estimates as it only requires assuming that current spatial CPUA reflects species distribution. A crucial parameter in this framework is the gear-affected area, which scales density estimates to total population size. While this area may be easier to determine for some gear types (e.g., trawls), these assumptions are far more challenging for other gear types like longlines and purse-seine, where effectiveness depends on gear characteristics (longline), search efficiency (purse-seine), environmental conditions, and species behavior.

In summary, while spatial quantitative risk assessments can estimate fishing mortality and risk using recent catch and effort data, in the absence of information on total population size and spatial abundance maps, they rely on strong assumptions about

gear efficiency and the area affected by each unit of fishing effort. Given this constraint, many authors have highlighted that spatial risk assessments are best suited to understand between-species differences in vulnerability and potential risk, as opposed to deriving risk for any single species (Neubauer et al. 2019, Griffiths et al. 2019b).

Here we propose an alternative hybrid method that is based on another class of data-poor assessments, namely those based on compositions (Ault et al. 2019, Chong et al. 2020). We combine a length-composition-based estimator of fishing mortality (Hordyk et al. 2015) with the e-SAFE spatial risk assessment method to jointly estimate relative abundance in space, relative gear efficiencies for longline and purse-seine set type, and fishing mortality. The latter is derived from recent length composition data, while other quantities are estimated from CPUA. This decomposition allows us to decompose the total fishing mortality into spatial impacts and impacts by gear of fleet, which is a useful feature of spatial risk assessments when aiming to prioritise conservation efforts. However, rather than being driven by assumptions, these impacts are estimated statistically within the model. While we demonstrate the feasibility of this approach, further work will be required to develop the approach into a more generally applicable tool.

5.3.1 Model description

We start with the description of an N-mixture model for decomposing spatial bycatch data into density (i.e., defining spatial overlap between fishing gear and abundance) and gear efficiency (describing the vulnerability of the species). This decomposition is common in spatial risk assessment methods (Griffiths et al. 2019b, Neubauer et al. 2019), and allows for attribution of fishing mortality and risk to individual components of effort such as gears, fleets or spatial units (noting that in SAFE or EASI-Fish the gear efficiencies are assumed rather than estimated as is done here). The model can be written as:

$$n_{i,k} \sim P(h_{i,k} a D_i, \phi), \tag{6}$$

$$C_{i,k} \sim B(n_{i,k}, Q_k), \tag{7}$$

where $n_{i,k}$ is the abundance of silky shark in the gear-affected area, $h_{i,k}$ is the number of observed effort units (i.e., hooks, sets) in area i for fleet k, and a, is the affected area per gear. The parameter $D_i = N_i/A_i$ is the density (numbers per grid area) of silky shark in grid i. The model can be considered a generative model: the number of sharks available per observed spatial unit of effort (i.e., the area affected by a unit of effort, e.g., a single hook or set) for each fleet in each grid cell i is random and follows a Poisson ($P()$) distribution with mean $D_i^a = aD_i = aN_i/A_i$, scaled by effort $h_{i,k}$. The catch for each fleet k in grid cell i is a binomial (B) draw given a specific fleet's gear efficiency Q_k.

For the purpose of this demonstration, fleets were defined as longline, object-associated

purse-seine and free-school purse-seine, though more detailed gear breakdowns may be desirable for longline gear. Although different set types may affect a, we subsumed this effect into the gear-efficiency parameter Q and modeled a single gear-affected area. We modelled Q as:

$$\log\left(\frac{Q}{1-Q}\right) = \beta_Q X + \omega_{\text{flag}} + \zeta_{\text{flag-gear}} \tag{8}$$

The parameter X is a design matrix with contrasts for set type, with coefficients β_Q estimated for both effects. Flag-gear ($\zeta_{\text{flag-gear}}$) measure differences between operational fishing gear deployments by different vessel-flags - this effect was treated as a random effect.

The spatial density of silky sharks was modelled as $\log D_i^a = \mu_D + f(\text{SST}_i) + f(\text{CHL}_i + f(d_i^{Coast})) + s(Lat_i, Lon_i, Month)$, where μ_D is the mean density per unit of effort and $f()$ is a smooth (spline) function of sea-surface temperature (SST), chlorophyll-a (CHL) and distance to coast (d^{Coast}) in grid i. $s()$ is a spatial residual spline over latitude, longitude and month, the latter treated as a random effect. The overall model differs from the catch-reconstruction model used in Neubauer et al. (2023a) in that the abundance and capture process are explicitly separated. This separation allowed extrapolation of shark density beyond fished grid cells. We used a 5-degree grid which allows for extrapolation of observed capture rates per cell to the full (unobserved) effort.

For the estimation, it is possible to explicitly integrate over the latent abundance process (the Poisson component of the model above), yielding a Poisson model $P(h_{i,k} D_i^a Q_k)$ (e.g., Raftery 1988). The expected number of individuals N_i in grid i is then $a^{-1} A_i D_i^a$. To account for the overdispersion of captures, we used a three-parameter version of the negative-binomial (NB) distribution (see Tremblay-Boyer & Neubauer 2019, for detail) instead of the Poisson distribution. The NB model is commonly interpreted in terms of overdispersion (e.g., aggregation of individuals) relative to a Poisson distribution (randomly-distributed individuals in space). The NB model used here has two additional parameters (compared to the Poisson): an overdispersion parameter (ϕ) and an exponent ν that describes how overdispersion varies with the mean of the distribution. We therefore get:

$$C_{i,k} \sim NB(h_{i,k} D_i^a Q_k, \phi, \nu) \tag{9}$$

and

$$\hat{CFULL}_{i,k} \sim NB(h_{i,k}^{FULL} D_i^a Q_k, \phi, \nu), \tag{10}$$

the latter describing the predicted catch across the full (unobserved) effort dataset.

The definition of current abundance $N_{curr} = \sum_i N_i = \sum_i a^{-1} A_i D_i^a$ implies that it is possible to estimate the current abundance N_{curr} in principle. However, this estimate

is reliant on an estimate of the gear-affected area. For this reason, the estimation of N_{curr} has the same limitations as the scaling of survey estimates of biomass to a total biomass estimate. Although the estimation of N_{curr} provides a method for not requiring knowledge of gear efficiency Q and the distribution of the focal species *a priori*, this method does not remove all unknowns from the estimation of N.

If estimation of N_{curr} is not the key focus, then it is possible to work backwards from an estimate of fishing mortality or harvest rate to estimate gear affected area and spatial and fleet specific impacts. Typically, a harvest rate is derived by summing estimated fatal interactions across space $\sum_{i,k} \hat{CFULL}_{i,k} \cdot S_k$ (where S_k is the survival rate for fleet k; the product of the discard rate and the post-release survival), and dividing by estimated abundance N_{curr} (Neubauer et al. 2019). Here we used the same post-release survival as for the stock assessment. The harvest rate can be easily decomposed into individual rates by doing the sum of estimated captures over discrete fleets or spatial areas.

As illustrated in Neubauer et al. (2019), the derived harvest rate is directly scaled by the assumption of gear affected area, which is difficult to derive for the main tuna gear types, such as longline and purse-seine. By introducing a more direct estimator of total fishing mortality from another commonly available data-source – namely length frequency data collected by observers, we can directly estimate a harvest rate, and use the spatial model described above to decompose the impact spatially, accounting for uncertainty in spatial distribution of the species (D_i) and relative gear efficiencies (Q_k), as well as spatial overlap. This method does not require a time-series, but uses recent data only. Due to the integrated nature of the model, data weighting becomes an issue, and we currently only explore somewhat ad-hoc weightings to give the length data comparable weight to the observed interactions (i.e., a weight of 1000).

We used the method described by Hordyk et al. 2015, which jointly estimates the length-based spawning potential ratio (LB-SPR) and the ratio F/M as well as selectivity (assumed logistic), using assumptions of von Bertalanffy growth parameters (k, L_∞ and growth CV) and natural mortality (typically input as M/k, derived from meta-analysis; Prince et al. 2015). Like most composition-based methods, the LB-SPR method assumes that the stock is at equilibrium with current fishing mortality, an assumption that may not be correct if fishing mortality is changing rapidly. Especially for long-lived species, this will lead to a lag between assessed status and fishing mortality. For a detailed mathematical description of the model, the reader is referred to Hordyk et al. 2015.

We used alternative values for M, and published values for k, as used in the integrated stock assessment. Selectivity is estimated using informed priors. The LB-SPR model was coded in Stan and integrated estimation was performed to directly estimate the gear-affected area from the LB-SPR estimate of fishing mortality. For this, fishing mortality was transformed to a harvest rate, and a vague gamma(1,1) prior was placed on fishing mortality. Other priors were vague (e.g., regression parameters for gear effects), or used brms default priors for standard deviations and splines, namely student-t priors (Table 1).

We tested the model against data from 2020 (base), 2019 and 2018, as well as sensitivities

Table 1: Priors employed in the hybrid length - based spatial risk assessment model.

Parameter	Notation	Prior
Fishing mortality	F	Gamma(1,1)
Regression coefficients	β_Q	Normal(0,100)
Density Intercept	μ_D	Normal(0,100)
Spline linear	β_{spline}	Normal(0,100)
Spline non-linear	sds_{spline}	Student-t(3,0,4.4)
Random effects	sd_{RE}	Student-t(3,0,4.4)
Selectivity	L50	Log-normal(log(50), 0.5)
Selectivity	L95	Log-normal(log(20), 0.5)

to growth (increasing growth CV, L_∞ by 20%) and natural mortality assumptions. Input data consisted of observed interactions (same as for catch reconstructions for sharks based on observer catch rates) as well as catch scaled length compositions (i.e., capture fishery compositions used in the Stock Synthesis assessment). Our base assumption for natural mortality was 0.16, based on an intermediate value cited in (Cortés 2002). As we assume a higher prior in the stock assessment, we ran a sensitivity with a prior of M=0.2.

The model was implemented in Stan, and run using MCMC for 500 iterations after discarding 500 iterations as burn-in for each of 8 chains. Due to long run-times and large size of outputs, we only kept a total of 500 samples from the posterior distribution. However, convergence and mixing were reasonable and we achieved effective sample sizes of close to 500 for most parameters. We used posterior predictive checks as well as residual analysis to confirm that the model provided a good fit to data.

6. ASSESSMENT RESULTS

6.1 Stock synthesis assessment (diagnostic model runs)

6.1.1 Model fits

The diagnostic model run showed reasonable fit to late CPUE, but predicted CPUE prior to the recent increase did not fit well, notably fitting a slightly increasing trend when CPUE was flat or slightly declining in early years (Figure 20). The residuals reflected the model's propensity to fit through the index rather than follow the concave shape of the CPUE index (Figure 21), with correspondingly high standard deviation of normalised residuals (SDNR), which should be around 1 after reweighting of length compositions.

The model produced a relatively good fit to over-all length composition data (Figures 22). In addition, trends in mean length were temporally aligned with CPUE trends (Figure 23) except in length compositions for longline data, which were down-weighted substantially relative to other compositions. It is evident from the mean length trends that the compositions are highly variable, especially the catch-scaled capture fishery

compositions; as a result, the model required time-varying selectivity with large fluctuations in selectivity for purse seine capture fisheries to produce acceptable fits, especially to free-school purse seine length frequencies (Figures 24–28, Figure 29). Another notable feature was that the standardised index fishery compositions for the free-school purse seine index showed markedly lower variation, with larger mean lengths and more consistent trend that aligned with CPUE, and was reasonably well fitted by the model (although model fits were somewhat more extreme than variation seen in the compositions).

6.1.2 Profiles

Negative log-Likelihood profiles of R_0 suggested that the lower bound of R_0 was largely driven by the compositions data, while the upper bound was given by the CPUE index (Figure 30). Log-Likelihood profiles for natural mortality showed a similar trade-off between composition and index likelihoods (Figure 31). The stock recruit parameter $beta$ was strongly constrained at the lower bound by the initial catch assumption (Figure 32; with low $beta$ values leading to higher catch). We repeated the profile with the high catch assumption, and at this point the lower bound becomes a lot less well defined - a slow gradient is given by the trade-off between index and length data.

6.1.3 Estimation uncertainty from MCMC

Most MCMCs for the Stock Synthesis models were deemed not usable due to a high number of divergent iterations. Our diagnostic model was the only model that ran with nearly no divergences (2 divergent iterations remained after burn-in). We assumed that the potential bias due to poorly explored regions of parameter-space was likely minor, as it appeared to occur with the 2D-AR selectivity deviations. The MCMC traces for key quantities appeared acceptable (Figure 33), and the resulting posteriors were consistent between 8 chains, with low $\hat{R}$ (Figure 34, Table 2). We therefore judged this model reasonable for exploration of trajectories of biomass and fishing mortality trends. However, due to our inability to obtain other reasonable models using full MCMC, we only used this model to explore uncertainty in the diagnostic case.

6.1.4 Estimated stock recruit relationship

The stock recruit relationship of the diagnostic base model can be compared to the alternative $beta$ assumptions using estimated values for pre-recruit survival and z_{frac} (Figure 35). At $beta$ = 2.69, the diagnostic model, pre-recruit survival remains high across a wide range of depletion levels from 0 to 0.5, before dropping steeply towards relatively low ($\sim$0.1) survival at high stock biomass. When $beta$ is increased to 4, this plateau of high survival is slightly lower, but extends to higher biomass levels. Conversely, at $beta$ = 1.5, the relationship between depletion and pre-recruit survival is near-linear. The corresponding stock-recruit functions mirror these differences with the function for $beta$ = 1.5 showing less doming in the stock-recruit function. We attempted

to fit models with $beta$ <1, but these were highly unstable and did not appear to converge to a global minimum for the negative log-likelihood.

Together with estimated recruitment deviations (Figure 35), the estimated pre-recruit survival showed a slowly increasing trend mirroring an increasing trend in recruitment deviations. After 2014, the trend in recruitment reverses, with a steady decline.

6.1.5 Model population trajectory - diagnostic case

The model suggested an over-all increase in fishing mortality up to the mid 2010's (Figures 37, 36), driven largely by an increase in longline and object-associated purse seine catches (Figure 38). Recent fishing mortality was estimated to have declined sharply since 2011, to levels well below F_{MSY}, from levels exceeding F_{crash} (the fishing mortality that would lead to population collapse in the long term). Despite increasing trends in F, the diagnostic model estimated a slow and steady increase in biomass over this period (Figure 39) — due to the steadily increasing trend in recruitment deviates (Figure 35) — from an initial biomass estimated to have been around 30% of unfished biomass (Figure 39). The population was estimated to have rebuilt rapidly from 2014, once fishing mortality rates declined below F_{MSY} levels (Figures 37). Good recruitment in 2012-2014, coupled with expected recruitment above unfished recruitment at intermediate depletion levels (Figure 35), led to an estimated stock rebuild to near unfished levels in recent years (Figure 39).

6.1.6 Retrospective patterns

Retrospective patterns were high for biomass related quantities, such as stock status (Figure 40), with initial relative biomass estimated to be high and near unfished levels when taking out 5 years from the estimation. Adding successive years then sees the biomass status drop to near current estimates for subsequent retrospective peels, albeit with very high uncertainty about stock status. With additional years of data, the stock depletion level increases slightly, though remains within confidence bounds of previous retrospective peels, suggesting that prior uncertainty correctly captures plausible future states over recent years. Although all patterns are within uncertainty intervals, these patterns suggest that biomass estimates are only just beginning to stabilise with the addition of recent data. The retrospective pattern and recent stabilisation of estimates is mirrored in fits to CPUE and the estimate of unfished average recruitment R_0 (Figure 40), with the peel that removes 5 years from estimation leading to poor CPUE fits. Fishing mortality related patterns were stable from peel 4 to recent estimates, as were fits to CPUE (Figure 40).

6.1.7 Sensitivities

Sensitivities over data weights showed very close outcomes for all three options, with higher CPUE weights leading to slightly lower stock status throughout the simulation, but similar current depletion near estimated unfished biomass levels (Figure 41). Lower

LF weights had a similar, if slightly more pronounced effect, with a slightly lower over-all stock status. Estimated fishing mortality levels were very close, as were CPUE fits, which differed only for most recent years, with higher CPUE weight models producing a slightly better fit (Figure 41).

Model runs over a grid of options for $beta$ and initial catch assumptions showed more variable outcomes than seen from data weighting (Figure 42). Models with low $beta$ (1.5) had lower over-all status, while models with high $beta$ (4) had the highest status and lowest over-all depletion levels. Higher catch levels and higher $beta$ led to higher estimated initial and current stock status. Estimated fishing mortality rates followed a similar pattern, with highest F estimated for lower assumed equilibrium catch levels. CPUE fits appear similar across models.

6.1.8 Ensemble over beta and initial catch

Give that uncertainties about $beta$ and initial catch appeared to capture the range of uncertainties associated with available model runs, we used draws from a multivariate log-normal distribution to construct an unweighted ensemble over this grid. The log-normal simulation approach was used here as alternative models in the grid had poor MCMC sampling with a relative large number of (>5%) of divergences indicating that the sampler could not adequately explore the posterior distribution.

The ensemble mirrored the range of model outcomes for the respective sensitivities (Figure 43), with recent (2019–2020) stock status showing a reasonable amount of uncertainty, whereas fishing mortality estimates were consistently below F_{MSY} and well below potential limit reference points (Figure 44).

6.2 Alternative assessments

6.2.1 Length and age structured assessment model

All LAM models converged well, with no persistent trends in the trace plots (Figures 45-50), no divergent transitions throughout the MCMC chains, and $\hat{R}$ values close to 1 (less than 1.02). The fits to the observed length compositions were generally satisfactory (Figures 51-55), except for the length frequencies collected from free-school sets, where the last two decades show bimodality with a high spike in larger groups (Figure 51). Although length frequency fits between sensitivity runs with different initial fishing mortality rates did not show significant differences, CPUE fits displayed small variations in the first and last five years (Figure 56). Specifically, lower values of F_{init} tended to be influenced more by the initial data points compared to higher values of F_{init}. The exact match between model-predicted catches and observed catches verified the internal calculation of fishing mortality rates through the Newton-Raphson algorithm that we implemented for the model (Figure 56).

Stock status trends over time from all three models showed increasing trends, similar to both the Stock Synthesis models and dynamic surplus production models (see panels

in the first row of Figure 60). As expected, the initial starting stock level changed with the initial fishing mortality rate. The model with the lowest initial fishing mortality rate ($F_{init} = 0.05$) showed the highest stock status, whereas the model with the highest initial fishing mortality rate ($F_{init} = 0.15$) showed the lowest stock status. Median fishing mortality rates for all three models were below F_{lim} across all years, but the model with the highest initial fishing mortality rate showed some years (between 1999 and 2012) with fishing mortality rates above F_{MSY} (see panels in the second row of Figure 60). For all three models, the longline fleet showed the highest fishing mortality rates, followed by purse-seine object-associated sets and purse-seine free-school sets (see panels in the third row of Figure 60). The model with the highest initial fishing mortality rate showed the highest fishing mortality rates for all three fleets.

Estimated selectivity for all three models was almost identical, except for the longline fleet, where the model with the lowest initial fishing mortality rate showed a slightly lower selectivity for larger fish than the highest initial fishing mortality rate model (Figure 57). The estimated length-at-age distributions for all three models were also similar, resulting in similar patterns of age compositions over time across all three models (Figure 59). Although the overall trends in the three models were similar, marginal posterior distributions for the key parameters differed significantly. Higher initial fishing mortality rates resulted in lower estimates of unfished recruitment R_0 and natural mortality M, and higher estimates of z_{frac}, whereas the opposite was true for the model with the lowest initial fishing mortality rate (Figure 58). The model with the lowest initial fishing mortality rate showed the largest uncertainty in the estimates of z_{frac}, but other parameters showed similar uncertainty across all three models. The parameter for growth variability CV_2 showed almost identical estimates across all three models.

Based on the Majuro plots, the stock status in the recent two years (2019–2020) underwent lower fishing mortality rates than the corresponding F_{MSY} across all three models (Figure 61), but stock levels varied across models. The highest initial fishing mortality rate model showed the lowest stock status, around 25% of its unfished status, whereas the lowest initial fishing mortality rate model showed the highest stock status, around 90% of its unfished status.

6.2.2 Dynamic surplus production model

Dynamic surplus production models converged rapidly, and showed good MCMC mixing for all key parameters (Figure 62), and good convergence diagnostics and effective sample size (Table 5, Figure 63).

Dynamic surplus production models were largely in agreement with the integrated assessment in terms of recent stock trajectories as well as fishing mortality rates relative to proposed reference points(Figure 64). The model fitted the CPUE series well, but as for the integrated assessment, the modeled population trajectory did not quite capture the slight decline observed in the early part of the time-series, but managed to capture trends in recent CPUE more accurately (Figure 65). The estimated process error by year

showed a similar pattern to the estimated recruitment deviations from the integrated stock assessment.

Retrospective patterns were observed for biomass (Mohn's $\rho = 0.30$) and harvest rate ($\rho = -0.43$). However, these were largely due to the model gaining new information from the recent increase in CPUE (Figure 66): Initial estimates of biomass were higher and highly uncertain; with recent reductions in fishing mortality and corresponding increase in CPUE, the model updates its estimate of depletion, fishing mortality and productivity. Nevertheless, the uncertainty in early years includes updated trajectories, with high predictive coverage of around 95% confirming that the posterior distribution of each new year in the retrospectives is 95% contained within the predictive distribution from the previous fit (Table 4).

The model estimated the stock to be slightly more productive than the integrated assessment did, with harvest rates only approaching, but not surpassing $F[crash]$. Conversely, recent depletion levels were estimated to be lower than those estimated from the integrated stock assessment across all three scenarios of initial depletion: the base assumption led to an estimated status in 2020 of 48% (95% CI: 26%–77%) of unfished abundance, with alternative depletion priors leading to estimates of 20% (95% CI: 10%–35%) for a prior suggesting a lower initial abundance, and 67% (95% CI: 39%–100%) for a model with *a priori* high initial stock status in 1995 (Table 5, Figure 67).

6.2.3 Length-based spatial risk assessment

The hybrid spatial risk assessment converged well and produced satisfactory MCMC diagnostics, despite the low number of retained MCMC draws (Table 6, Figure 68). Fits to observed interactions were good (Figure 69), with no clear trend in residuals both globally, by gear, and spatially (Figures 69, 70). Fits to length compositions across years were deemed satisfactory (Figure 71), but uncertainty did not capture the variability in the input LFs. The latter were highly variable, and 2018 showed the best fit to length compositions.

Although composition fits did not vary much between sensitivities (Figure 71), estimates for key quantities differed between years and sensitivities (Figure 72). The statistics of the sampling distribution (negative binomial parameters nu and phi) changed between years, whereas the estimated harvest rate was slightly higher in 2018 and 2019 than in 2020. Models with higher weight showed lower variance in the estimated harvest rate, but showed the same mean harvest rate. Assuming a higher M led to an estimate of lower harvest rates, whereas assuming a larger L_∞ led to an estimate of higher harvest rates; the growth CV did little to influence the results.

Predictions in space-based total effort (Figure 73) showed marked inter-annual spatial changes in harvest rates (Figure 74), reflecting variable effort, but also variable estimated distributions (Figure 75). In 2018 and 2019, the distribution was estimated to be strongly skewed towards Papua New-Guinea and the Solomon Islands, whereas in 2020, abundance hotspots were estimated to be further eastward and towards higher latitudes.

Decomposing the harvest rates into gear types showed that the highest harvest rates are due to object-associated purse-seine sets (Figures 76, 77), which often fish in areas of high density in western equatorial waters. Consequently, the total harvest rate from this gear-type was estimated to be nearly twice that of longline and free-school sets. The estimated F/F_{crash} was just over 0.5, with a probability of near 15% that F exceeds F_{crash} (Table 7), with a risk just over 25% for 2018 and 2019. Only with an assumption of larger L_∞ does the risk increase to >50% (Figure 77).

6.3 Model comparison

Stock status (SSB_{recent}/SSB_0), measured as recent (2019–2020) relative depletion, was highly variable across models, with mean estimates ranging from 0.44 (95% CI: 0.10–0.96) for an ensemble across dynamic surplus production model assumptions of initial depletion, to 0.76 (0.45–0.98) for the diagnostic stock synthesis model (Tables 8,9; Figure 78). Uncertainty about recent relative depletion across the range of models was high, especially across ensembles of models where initial fishing mortality could not be reliably estimated from data and had to be formulated as a prior (dynamic surplus production) or set explicitly (length and age based model). For the diagnostic case of the dynamic surplus production model, for example, uncertainty was still relatively high (0.22–0.82), but excluded extreme outcomes seen in the ensemble over initial conditions.

Fishing mortality was consistently estimated to be below possible limit reference points with high probability. Only the length-based risk assessment suggested a probability of fishing mortality exceeding F_{crash} of >5%. The length and age based models had the lowest estimated recent fishing mortalities (Diagnostic F_{recent}/F_{crash}: 0.04 [0.01–0.10]; P(F_{recent}/F_{crash} >1)=0), with dynamic surplus production (Diagnostic F_{recent}/F_{crash}: 0.13 [0.02–0.24]; P(F_{recent}/F_{crash} >1)=0) and Stock Synthesis models (Diagnostic F_{recent}/F_{crash}: 0.38 [0.26–0.54]; P(F_{recent}/F_{crash} >1)=0) providing intermediate estimates. Ensemble models had, as expected, higher uncertainty than single diagnostic models. However, this increase in uncertainty was not as marked for fishing-mortality related quantities as for stock status estimates.

7. DISCUSSION

Our assessment took a multi-model approach to assessing silky shark in the Western and Central Pacific Ocean. The approach resulted from large uncertainties in the underlying data and difficulties with fitting of integrated stock assessments for sharks generally. We therefore attempted a range of models with varying degrees of complexity and with different data requirements in an effort to understand overfishing risk to silky shark based on different lines of reasoning. We consciously did not standardise approaches strictly across models — meaning we did not attempt to use consistent priors between assessments — treating each approach as standalone and providing evidence from independent lines of reasoning. However, data inputs were standardised across assessments as we had a single set of data available from our prior analyses of available data for silky shark (Neubauer et al. 2023a).

Our results across all assessment methods were largely in agreement that recent fishing mortality was low with respect to possible limit reference points for sharks. Therefore, while each modelling approach has limitations, we suggest that the weight of evidence is sufficient to conclude that fishing mortality has declined substantially for silky shark in the most recent decade, and that recent stock status is likely improving from previous low levels. We further suggest that the dynamic surplus production models provide the most parsimonious and robust available model for management advice. This suggestion derives from the consistency with other outcomes, but also because of stronger reservations about the robustness of other approaches. Most importantly, the stock synthesis assessment provided a number of challenges that could not be resolved sufficiently to consider these models robust. We consider both the length-based risk assessment and LAM models experimental at this stage, with further work required to use these model for management advice.

Usually, an integrated assessment is preferred when sufficient data are available (Neubauer et al. 2019). However, we were concerned by the difficulties with fitting highly variable length compositions and the associated deficiencies with MCMC. The divergences we observed for integrated models were due to the flexible selectivity employed to fit length compositions. Without this flexibility, the model could not fit composition data, and led to estimates of little depletion across the full time-series, which did not appear believable. While the model appeared to converge well under MAP, the No-U-Turn (NUTS) sampler provides a useful tool in the form of divergences for diagnosing difficult posterior shapes that limit or bias accurate estimates of uncertainty. As such, the divergences may be seen as a sign of potential model mis-specification (Gelman et al. 2020), but it may also be a sign of a complex model that is difficult to sample from. In either case, however, these sampling difficulties suggest that the model requires further work to resolve these issues.

The slight increase in spawning biomass seen in the integrated model over the first 20 years of the time-series are not reflected in CPUE, and we could not derive a model where the stable or declining trend in early CPUE could be better fitted. Even models with higher weight on CPUE failed to lead to better fits of early CPUE. This may be due to deficiencies in the CPUE itself, or due to model mis-specification. For example, it is possible that life-history estimates used in the assessment are not representative due to sampling variability or bias (Grant et al. 2019). Growth specifically has been reported to be slower at higher latitudes (Joung et al. 2008), and may vary spatially and over time. Spatio temporal variation is obvious in catch-rates and lengths of silky shark caught across all fleets, and the influence of ENSO conditions is consistent across models for CPUE and compositions. Whether these relationships are the reflection of growth differences according to oceanographic conditions, or if it relates to migrations of different age classes, is poorly understood.

Mis-specification of variability in growth could be a partial cause of the poor fit of the integrated model in some years of the time series, as it largely determines the length distribution of the population. This argument was a key reason for our development of a length-and-age structured model in this assessment. Although the complexity of the LAMs was not well supported by the current information on LFs and CPUE data,

we believe that the model provides a useful avenue of research towards incorporating cumulative impacts of fishing pressure. The LAM we developed for this assessment uses the same number of parameters as the Stock Synthesis models, but provides a better representation of population dynamics, naturally incorporating the cumulative impact of fishing pressures on the length distribution of the population. This impact could be particularly important for long-lived and late-maturing species like sharks. Another advantage of the LAM is its ability to be easily extended to include both age- and length-dependent processes, where changes in each component depend on each other in a more natural way. For example, if both length- and age-dependent natural mortality need to be included (e.g., higher predation pressure on smaller individuals and higher senescence on older individuals), an age-specific survivorship matrix can be used in the LAM. Here, the diagonal elements represent the length-dependent natural mortality for each age class, while the overall scaling of the matrix represents the age-dependent natural mortality. Such extensions would make the LAM a more flexible and powerful tool, as it can also be used for performing simulation testing or developing priors for simpler models.

In a fully length-structured model—where fishing-induced changes in length distribution are naturally reflected in the model—productivity is even more dependent on such variability. We initially attempted to estimate the two parameters (CV_1 and CV_2) governing growth variations when fitting the LAMs, but fixing one of the parameters to a constant value—particularly CV_1, which determines the variability in length of the recruitment age class—was necessary to achieve convergence. When the selectivities were all assumed to be dome-shaped, using more flexible selectivity forms, the model struggled to estimate CV_2, even though CV_1 was fixed. This is likely due to the fact that fitting the LFs was largely explained by the flexible selectivity form, and the growth parameters were not well identified. More information on variability in growth would be needed to determine which selectivity form is most appropriate, and to estimate the growth parameters more accurately.

More generally, the strong standardisation of indices and lengths by the ENSO index suggests that there is an important process that is not currently well represented in our models. The importance of this process was previously highlighted by Lennert-Cody et al. (2019), but little is known about the reason or significance of this process, and we attempted to standardise all index fishery data to account for impacts of ENSO. However, this may not be sufficient to eliminate process error arising from ENSO-driven migrations and/or unresolved stock structure. Genomic data suggested strong population structure (Derek W. Kraft and Bowen 2018), and oceanographic conditions could be related to ontogenetic movements of separate stocks. Tagging data gave conflicting results between regions (Francis et al. 2023), with some long range movements in equatorial individuals and local within region movements at higher latitude. A key problem is that tagging studies are not replicated in time and space, and therefore provide little information to resolve spatio-temporal processes.

The surplus production model integrates over processes that impact composition data by assuming that the population reflected by the index is fully selected across time, and therefore do not need to resolve availability of lengths classes. This is supported

by the standardised length compositions showing much slower variation with slight early declines, and recent increases in mean lengths suggest that the standardised compositions reflect a consistently selected population. In addition, silky shark appear vulnerable from age 0, suggesting that full selection of size classes is a reasonable assumption. However, by not needing to resolve the catch composition, the model circumvents the need for a large number of parameters and complexity, and is able to fit CPUE better than the integrated model.

The recent increases in CPUE provide information to models about stock productivity and correspondingly adjust exploitation and depletion levels prior to the increase. It is well understood that stock assessment models generally require information from contrast in fishing mortality and biomass indices in order to estimate stock productivity (Magnusson 2016). As more of this information becomes available, the model will update estimates of productivity, which naturally leads to retrospective patterns in assessments. We argue that these patterns are to be understood as a learning process in the case of the present model, rather than a sign of model mis-specification, and that retrospective patterns need to be evaluated in the context of individual data and models in order to interpret them. Conversely, the information provided by the CPUE index to the model places an onus on CPUE being an informative measure of relative biomass. The high degree of consistency across all observer programs of the free-school purse-seine index, in conjunction with the non-target nature of the fishery, provides strong evidence that the index is measuring a large-scale and coherent pattern, and that the information is the best source of abundance and productivity information available. Together with declining estimated catch, the index therefore appears an appropriate choice to drive model estimates and learning.

While the dynamic surplus production model considers only the catch and index as data, the risk-assessment approach developed here used composition information alongside spatial catch rates (CPUA) and ignores CPUE. Given the complexity of composition information for silky shark this might appear a difficult proposition, and future iterations of this work could test if it is more appropriate to use standardised length compositions for this task. If compositions are highly variable, then pooling across years may be desired, to ensure that an average composition is reflected in the estimates of fishing mortality. Given the variability in available compositions it was difficult to judge if fits to length data in the spatial model were adequate. In addition, given the spatial variation in captures between years, estimates of underlying compositions varied between years, but it was difficult to gauge whether such estimates are reasonable given inter-annual variation in oceanography-driven distribution of silky sharks, or if this variability simply reflects sampling error. Nevertheless, the relative consistency of estimates of risk for recent years (higher F for 2018 and 2019, declining risk from 2019–2020) reflect inferences made from CPUE, and suggest the method has some merit when length-compositions reflect broad-scale fishing mortality. The link to spatial and fleet-specific impacts provides a useful avenue to test management options.

While the risk assessment provided a way to apply a method that does not require a long time series of inputs, future applications should explore integrating the model

across years of available data to ensure that between year variation in density and length are handled appropriately (e.g., catchability could be considered constant between years, while density varies). This would provide a more robust way to include inter-annual variability, while minimising the potential for between-year sampling variation to swamp signals of impact. In addition, the models could be applied in a more explicit grid across uncertainty in demographic parameters; like stock assessments, the methods are sensitive to natural mortality assumptions and growth inputs. Nevertheless, we suggest that the length-based method provides a method to apply a hybrid spatial risk assessment that does not require time-series data, yet is still applied in a statistical context that captures uncertainty and estimates key underlying parameters such as population density and catchability in a model-base framework. While the present application should be seen as a proof of concept, it could be extended and improved for a broader application to species for which length composition data is recently being collected, and which cannot be assessed. It also allows the application of a risk assessment framework to single-species applications, a task that is generally discouraged for most risk assessment frameworks (e.g., Hordyk and Carruthers 2018, Griffiths et al. 2019a) as estimates for individual species are often driven by assumptions rather than data.

Overall, our findings from applying a range of model types to silky shark data suggest that methods with lower data requirements hold promise for species where composition data are problematic. This is the case for many bycatch species, and sharks such as shortfin mako where large individuals do not appear in catches, likely due to dome-shaped selectivity (Large et al. 2022a, ISC 2024). Notably, ISC 2024 also proposed a dynamic surplus production model for north Pacific shortfin mako. Overall, our exploration across models support recommendations made at SC15 regarding the use of alternative assessment methods for sharks (Neubauer et al. 2019). Notably, Neubauer et al. (2019) suggested that surplus production models should be used when composition data are problematic, and risk assessments should only be used in the context of prioritisation across species, but were problematic for any single species. However, in the present study we suggested that alternative, data driven risk assessments could provide an avenue to use a risk assessment approach when time-series are not sufficiently long, or reliable, to estimate fishing mortality rates relative to biological reference points. However, the method relies on composition data and, with non-retention measures leading to sharks and other bycatch species being cut free from longlines, it may prove difficult to get useful amounts of data across a number of species. In that case, methods such as EASI-fish (Griffiths et al. 2019b), which estimate risk from assumptions about fishery overlap with bycatch species distributions and vulnerability to fishing effort, may be the only alternative to provide estimates of risk.

In summary, across methods, we found consistent evidence that recent fishing mortality is low relative to conservation reference points, driven by recent declines in fishing mortality from longline fisheries. Although the exact stock status in terms of relative depletion remains unclear and strongly dependent on assumptions about initial status, catch or fishing mortality, recent fishing mortality estimates are remarkably consistent across methods and sensitivities, suggesting that fishing mortality has

declined sufficiently to allow for a substantial increase in the population. The estimated decrease in fishing mortality and increase in populations coincides with non-retention measures coming into effect across all fisheries. Although post-release mortality is estimated to be high from purse seine fisheries (Hutchinson et al. 2015), the largest fishing mortality was estimated to have come from longline fisheries capturing nearly the full size-range of silky sharks, and reductions in interactions as a result of changes in fishing practices over the last decade may have substantially reduced this source of mortality, allowing the stock to rebuild.

In conclusion, we suggest the dynamic surplus production model as a reasonable model to base management advice on. We further suggest that although the uncertainty about absolute stock status is high across assumptions for initial depletion priors (Stock status SSB_{recent}/SSB_0: 0.10 – 0.96), the estimates of recent fishing mortality relative to biological reference points are consistent across models (the ensemble shows minimally higher uncertainty than the diagnostic case) and provide a sufficient basis for management advice. On this basis, we conclude that stock status has been improving since 2010, and that recent fishing mortality rates are below biological reference points for the ensemble (Diagnostic F_{recent}/F_{crash}: 0.13 [0.01–0.25]; P(F_{recent}/F_{crash} >1)=0; P(F_{recent}/F_{lim} >1)=0).

7.1 Main Assessment Conclusions

- The multi-model approach to assessing silky shark resulted in an uncertain stock status, but high confidence that recent fishing mortality is below levels that would preclude stock rebuilding.
- Based on considerations of model complexity, fit and estimation issues, we suggest that the dynamic surplus production model be used for providing management advice. We further suggest that the model ensemble across initial depletion priors may be over-representing uncertainty, and we suggest output from the intermediate assumption as a candidate model for management advice.
- The largest fishing mortality was estimated to have come from longline fisheries capturing nearly the full size-range of silky sharks, and reductions in interactions as a result of changes in fishing practices over the last decade may have substantially reduced this source of mortality, allowing the stock to rebuild.
- The stock status has been improving since 2010, and the recent fishing mortality rates are below biological reference points for the ensemble (Diagnostic F_{recent}/F_{crash}: 0.13 [0.01–0.25]; P(F_{recent}/F_{crash} >1)=0; P(F_{recent}/F_{lim} >1)=0).

With respect to other shark stocks with lower levels of information:

- Surplus production models should be used when composition data are problematic, and risk assessments should only be used in the context of prioritisation across species. However, alternative, data driven risk assessments could provide

an avenue to use a risk assessment approach when time-series are not sufficiently long or reliable to estimate fishing mortality rates relative to biological reference points.

- With non-retention measures leading to sharks and other bycatch species being cut free from longlines, data colection may be problematic. In these cases, the only alternative to provide estimates of risk would be methods such as EASI-fish, which estimate risk from assumptions about fishery overlap with the species distributions and vulnerability to fishing effort.

Given some of the fundamental uncertainties highlighted above, we recommend:

- Additional tagging should be carried out using satellite tags in a range of locations as well as high seas areas to resolve fundamental questions about the species interactions with local oceanography and the dynamics of ENSO. Such tagging may help to resolve questions about the degree of natal homing and limited mixing of the stock, as suggested by genetics. This work is currently scheduled as part of the SRP as work theme 3 (a)vii and is due to begin in 2025 (Brouwer and Hamer 2024), and it is recommended that CCMs prioritise this work and ensure that satellite tagging options are included in the project specification.
- Additional growth studies and validation of aging methods from a range of locations could help build a better understanding of typical growth, as well as regional growth differences. Current growth data are conflicting, with insufficient data to understand the underlying process. This work is currently scheduled as part of the SRP as Project P19X11 and is due to begin in 2025 (Brouwer and Hamer 2024), and it is recommended that CCMs prioritise this work.
- Additional genetic/genomic studies across a broader set of locations could be undertaken to augment the tagging and existing genomics work to help resolve the stock/sub-stock structure patterns. To support this work, a strategic tissue sampling program for sharks is recommended with samples to be stored and curated in the Pacific Marine Specimen Bank. This work is currently scheduled as part of the SRP as work theme 3 (a)xii and is due to begin in 2026 (Brouwer and Hamer 2024), and it is recommended that CCMs maintain this project in the current work stream.

8. ACKNOWLEDGEMENTS

The authors would like to thank SPC, particularly Peter Williams and Emmanuel Schneiter for providing the WCPFC Members data for these analyses. We would also like to thank Paul Hamer and the stock assessment team at SPC for constructive discussions throughout this work and for comments on earlier drafts of this report, and the SPC Pre-Assessment Workshop Members for their helpful feedback on the catch

reconstruction and CPUE proposals. Finally, we acknowledge the funding of this work from the WCPFC Scientific Committee Project 108.

9. REFERENCES

Ault, J. S.; Smith, S. G.; Bohnsack, J. A.; Luo, J.; Stevens, M. H.; DiNardo, G. T.; Johnson, M. W., & Bryan, D. R. (2019). Length-based risk analysis for assessing sustainability of data-limited tropical reef fisheries. *ICES Journal of Marine Science*, *76*(1), 165–180.

Bonfil, R. (2008). Sharks of the Open Ocean: Biology, Fisheries and Conservation. In M. D. Camhi; E. K. Pikich, & E. A. Babcock (Eds.), (Chap. The Biology and Ecology of the SilkyShark, *Carcharhinus falciformis*, pp. 114–127). Blackwell Publishing Ltd.

Bonfil, R. (2005). Fishery stock assessment models and their application to sharks. In R. Bonfil & J. A. Musick (Eds.), (p. 154). Rome: FAO.

Brouwer, S. & Hamer, P. (2020). *2021-2025 Shark Research Plan*. WCPFC-SC16-2020/EB-IP-01 (Rev 1). Report to the Western and Central Pacific Fisheries Commission Scientific Committee. Sixteenth Regular Session, 12–19 August 2020, Pohnpei, Federated States of Micronesia.

Brouwer, S. & Hamer, P. (2024). *Progress against the 2021-2030 Shark Research Plan - 2024*. WCPFC-SC20-2024/EB-IP-10. Report to the Western and Central Pacific Fisheries Commission Scientific Committee. Twentieth Regular Session, 14–21 August 2024, Manila, Philippines.

Brouwer, S.; Large, K., & Neubauer, P. (2023). *Characterisation of the fisheries catching Silky sharks (Carcharhinus falciformis) in the Western and Central Pacific Ocean*. WCPFC-SC19-2023/SA-IP-09. Report to the Western and Central Pacific Fisheries Commission Scientific Committee. Nineteenth Regular Session, 16–24 August 2023, Koror, Palau.

Bürkner, P.-C. (2018). Advanced Bayesian multilevel modeling with the r package brms. *The R Journal*, *10*(1), 395–411. doi:10.32614/RJ-2018-017

Chong, L.; Mildenberger, T. K.; Rudd, M. B.; Taylor, M. H.; Cope, J. M.; Branch, T. A.; Wolff, M., & Stäbler, M. (2020). Performance evaluation of data-limited, length-based stock assessment methods. *ICES Journal of Marine Science*, *77*(1), 97–108.

Clarke, S.; Coelho, R.; Francis, M.; Kai, M.; Kohin, S.; Liu, K. M.; Simpfendorfer, C.; Tovar-Avila, J.; Rigby, C., & Smart, J. (2015). *Report of the Pacific shark life history expert panel workshop, 28-30 April 2015* (tech. rep. No. SC11-EB-IP-13). WCPFC.

Clarke, S. & Hoyle, S. (2014). *Development of limit reference points for elasmobranchs*. WCPFC-SC10-2014/MI-WP-07. Report to the Western and Central Pacific Fisheries Commission Scientific Committee. Tenth Regular Session, 12–19 August 2014, Majuro, Republic of the Marshall Islands.

Clarke, S.; Langley, A.; Lennert-Cody, C.; Aures-de-Silva, A., & Maunder, M. (2018a). *Addendum to Pacific-wide silky shark (Carcharhinus falciformis) stock status assessment*. WCPFC-SC14-2018/SA-WP-08a. Report to the Western and Central Pacific Fisheries Commission Scientific Committee. Fourteenth Regular Session, 8–16 August 2018, Busan, Repbulic of Korea.

Clarke, S.; Langley, A.; Lennert-Cody, C.; Aures-de-Silva, A., & Maunder, M. (2018b). *Pacific-wide silky shark (Carcharhinus falciformis) stock status assessment*. WCPFC-SC14-2018/SA-WP-08. Report to the Western and Central Pacific Fisheries Commission Scientific Committee. Fourteenth Regular Session, 8–16 August 2018, Busan, Repbulic of Korea.

Cope, J. M. & Hamel, O. S. (2022). Upgrading from m version 0.2: An application-based method for practical estimation, evaluation and uncertainty characterization of natural mortality. *Fisheries Research*, *256*, 106493.

Cortés, E. (2002, August). Incorporating uncertainty into demographic modeling: Application to shark populations and their conservation. *Conservation Biology*, *16*(4), 1048–1062.

Derek W. Kraft, M. H. & Bowen, B. W. (2018). *Pacific stock structure of the Silky shark (Carcharhinus falciformis) resolved with next generation sequencing* (tech. rep. No. SC14-EB-IP-04). WCPFC.

Edwards, C. T. T. (2017). *Bdm: Bayesian biomass dynamics model*. R package version 0.0.0.9022.

Fournier, D. A.; Hampton, J., & Sibert, J. R. (1998). Multifan-cl: A length-based, age-structured model for fisheries stock assessment, with application to south pacific albacore, thunnus alalunga. *Canadian Journal of Fisheries and Aquatic Sciences*, *55*(9), 2105–2116. doi:10.1139/f98-100

Francis, M. P.; Lyon, W. S.; Clarke, S. C.; Finucci, B.; Hutchinson, M. R.; Campana, S. E.; Musyl, M. K.; Schaefer, K. M.; Hoyle, S. D.; Peatman, T., et al. (2023). Post-release survival of shortfin mako (isurus oxyrinchus) and silky (carcharhinus falciformis) sharks released from pelagic tuna longlines in the pacific ocean. *Aquatic Conservation: Marine and Freshwater Ecosystems*, *33*(4), 366–378.

Francis, R. I. C. (2011). Data weighting in statistical fisheries stock assessment models. *Canadian Journal of Fisheries and Aquatic Sciences*, *68*(6), 1124–1138.

Froese, R.; Demirel, N.; Coro, G.; Kleisner, K. M., & Winker, H. (2017). Estimating fisheries reference points from catch and resilience. *Fish and Fisheries*, *18*(3), 506–526.

Galván-Tirado, C.; Díaz-Jaimes, P.; García-de León, F. J.; Galván-Magaña, F., & Uribe-Alcocer, M. (2013). Historical demography and genetic differentiation inferred from the mitochondrial dna of the silky shark (carcharhinus falciformis) in the pacific ocean. *Fisheries Research*, *147*, 36–46.

Gelman, A.; Vehtari, A.; Simpson, D.; Margossian, C. C.; Carpenter, B.; Yao, Y.; Kennedy, L.; Gabry, J.; Bürkner, P.-C., & Modrák, M. (2020). Bayesian workflow. *arXiv preprint arXiv:2011.01808*.

Grant, M. I.; Smart, J. J.; Rigby, C. L.; White, W.; Chin, A.; Baje, L., & Simpfendorfer, C. A. (2019). Intraspecific demography of the silky shark (*Carcharhinus falciformis*): implications for fisheries management. *ICES Journal of Marine Science*, *77*(1), 241–255. doi:10.1093/icesjms/fsz196

Grant, M. I.; Smart, J. J.; White, W. T.; Chin, A.; Baje, L., & Simpfendorfer, C. A. (2018). Life history characteristics of the silky shark (*Carcharhinus falciformis*) from the central west Pacific. *Marine and Freshwater Research*, *69*(4). doi:10.1071/MF17163

Griffiths, S. P.; eyes, K. K.-R.; Garilao, C.; Duffy, L. M., & Román, M. H. (2019a). Ecological Assessment of the Sustainable Impacts of Fisheries (EASI-Fish): a

flexible vulnerability assessment approach to quantify the cumulative impacts of fishing in data-limited settings. *Marine Ecology Progress Series*, *625*, 89–113.
Griffiths, S. P.; Kesner-Reyes, K.; Garilao, C.; Duffy, L. M., & Román, M. H. (2019b). Ecological assessment of the sustainable impacts of fisheries (easi-fish): A flexible vulnerability assessment approach to quantify the cumulative impacts of fishing in data-limited settings. *Marine Ecology Progress Series*, *625*, 89–113.
Hewitt, D. A. & Hoenig, J. M. (2005). Comparison of two approaches for estimating natural mortality based on longevity. *Fishery Bulletin*, *103*(2), 433.
Hordyk, A. R. & Carruthers, T. R. (2018). A quantitative evaluation of a qualitative risk assessment framework: Examining the assumptions and predictions of the productivity susceptibility analysis (psa). *PloS one*, *13*(6), e0198298.
Hordyk, A.; Ono, K.; Valencia, S.; Loneragan, N., & Prince, J. (2015). A novel length-based empirical estimation method of spawning potential ratio (spr), and tests of its performance, for small-scale, data-poor fisheries. *ICES Journal of Marine Science*, *72*(1), 217–231.
Hutchinson, M.; Itano, D.; Muir, J., & Holland, K. (2015). Post-release survival of juvenile silky sharks captured in a tropical tuna purse seine fishery. *Marine Ecology Progress Series*, *521*, 143–154. doi:10.3354/meps11073
Hutchinson, M.; Coffey, D. M.; Holland, K.; Itano, D.; Leroy, B.; Kohin, S.; Vetter, R.; Williams, A. J., & Wren, J. (2019). Movements and habitat use of juvenile silky sharks in the pacific ocean inform conservation strategies. *Fisheries Research*, *210*, 131–142.
ISC (2018). *Stock assessment and future projections of blue shark in the North Pacific Ocean through 2015*. WCPFC-SC14-2018/SA-IP-13. Report to the Western and Central Pacific Fisheries Commission Scientific Committee. Fourteenth Regular Session, 8–16 August 2018, Busan, Republic of Korea.
ISC (2024). *Stock Assessment of Shortfin Mako Shark in the North Pacific Ocean through 2022*. WCPFC-SC20-2024/SA-WP-14. Report to the Western and Central Pacific Fisheries Commission Scientific Committee. Twentieth Regular Session, 14–21 August 2024, Manila, Philippines.
Jensen, A. (1996). Beverton and holt life history invariants result from optimal trade-off of reproduction and survival. *Canadian Journal of Fisheries and Aquatic Sciences*, *53*(4), 820–822.
Joung, S. J.; Chen, C. T.; Lee, H. H., & Liu, K. M. (2008). Age, growth, and reproduction of silky sharks, *Carcharhinus falciformis*, in northeastern Taiwan waters. *Fisheries Research*, *90*, 78–85. doi:10.1016/j.fishres.2007.09.025
Kim, K. (2022). *State-space stock assessment models for data-moderate fisheries* (Doctoral dissertation, Victoria University of Wellington, New Zealand).
Large, K.; Neubauer, P., & Brouwer, S. (2022a). *Stock assessment of the South Pacific shortfin mako shark*. WCPFC-SC18-2022/SA-WP-02. Report to the Western and Central Pacific Fisheries Commission Scientific Committee. Eighteenth Regular Session, 10–18 August 2020, Pohnpei, Federated States of Micronesia.
Large, K.; Neubauer, P.; Brouwer, S., & Kai, M. (2022b). *Input data for the 2022 South Pacific Shortfin Mako Shark stock assessment*. WCPFC-SC18-2022/SA-IP-13. Report to the Western and Central Pacific Fisheries Commission Scientific Committee.

Eighteenth Regular Session, 10–18 August 2020, Pohnpei, Federated States of Micronesia.

Lennert-Cody, C. E.; Clarke, S. C.; Aires-da-Silva, A.; Maunder, M. N.; Franks, P. J. S.; Román, M.; Miller, A. J., & Minami, M. (2019, January). The importance of environment and life stage on interpretation of silky shark relative abundance indices for the equatorial pacific ocean. *Fisheries Oceanography*, *28*(1), 43–53.

Magnusson, A. (2016). *Informative data and uncertainty in fisheries stock assessment* (Doctoral dissertation, University of Washington, United States).

Maunder, M. N.; Thorson, J. T.; Xu, H.; Oliveros-Ramos, R.; Hoyle, S. D.; Tremblay-Boyer, L.; Lee, H. H.; Kai, M.; Chang, S.-K.; Kitakado, T., et al. (2020). The need for spatio-temporal modeling to determine catch-per-unit effort based indices of abundance and associated composition data for inclusion in stock assessment models. *Fisheries Research*, *229*, 105594.

McAllister, M. & Edwards, C. (2016). Applications of a bayesian surplus production model to new zealand fish stocks. *New Zealand Fisheries Assessment Report*, *52*, 79.

Methot Jr, R. D. & Wetzel, C. R. (2013). Stock synthesis: A biological and statistical framework for fish stock assessment and fishery management. *Fisheries Research*, *142*, 86–99.

Methot, R. D.; Wetzel, C. R.; Taylor, I. G.; Doering, K. L., & Johnston, K. F. (2021). *Stock Synthesis User Manual Version 3.30.17*. NOAA Fisheries, Seattle, WA.

Monnahan, C. C. & Kristensen, K. (2018). No-u-turn sampling for fast bayesian inference in admb and tmb: Introducing the adnuts and tmbstan r packages. *PloS one*, *13*(5), e0197954.

Neubauer, P.; Large, K.; Kim, K., & Brouwer, S. (2023a). *Analysing potential inputs to the 2024 Stock assessment of Western and Central Pacfic silky shark)* (tech. rep. No. WCPFC-SC19-2023/SC19-SA-WP-10). WCPFC.

Neubauer, P.; Carvalho, F.; Ducharme-Bath, N.; Large, K.; Brouwer, S.; Day, J., & Hamer, P. (2022). *Improved stock assessment and structural uncertainty grid for Southwest Pacific blue shark*. WCPFC-SC18-2022/SA-WP-03. Report to the Western and Central Pacific Fisheries Commission Scientific Committee. Eighteenth Regular Session, 10–18 August 2022, Pohnpei, Federated States of Micronesia.

Neubauer, P.; Kim, K.; A'mar, T., & Large, K. (2023b). *Addressing uncertainty in WCPFC stock assessments*. WCPFC-SC19-2023/SA-WP-12. Report to the Western and Central Pacific Fisheries Commission Scientific Committee. Nineteenth Regular Session, 16–24 August 2023, Koror, Palau.

Neubauer, P.; Large, K., & Brouwer, S. (2021). *Stock assessment for South Pacific blue shark in the Western and Central Pacific Ocean*. WCPFC-SC17-2021/SA-WP-03. Report to the Western and Central Pacific Fisheries Commission Scientific Committee. Seventeenth Regular Session, 11–19 August 2021, Pohnpei, Federated States of Micronesia.

Neubauer, P.; Richard, Y., & Tremblay-Boyer, L. (2019). *Alternative assessment methods for oceanic white-tip shark*. WCPFC-SC15-2019/SA-IP-13. Report to the Western and Central Pacific Fisheries Commission Scientific Committee. Nineteenth Regular Session, 12–20 August 2019, Pohnpei, Federated States of Micronesia.

Oshitani, S.; Nakano, H., & Tanaka, S. (2003). Age and growth of the silky shark Carcharhinus falciformis from the Pacific Ocean. *Fisheries Science*, *69*, 456–464.

Pardo, S. A.; Kindsvater, H. K.; Reynolds, J. D., & Dulvy, N. K. (2016, August). Maximum intrinsic rate of population increase in sharks, rays, and chimaeras: The importance of survival to maturity. *Canadian Journal of Fisheries and Aquatic Sciences*, *73*(8), 1159–1163. doi:10.1139/cjfas-2016-0069

Pardo, S. A.; Cooper, A. B.; Reynolds, J. D., & Dulvy, N. K. (2018, January 5). Quantifying the known unknowns: Estimating maximum intrinsic rate of population increase in the face of uncertainty. *ICES Journal of Marine Science*. doi:10.1093/icesjms/fsx220

Prince, J.; Hordyk, A.; Valencia, S. R.; Loneragan, N., & Sainsbury, K. (2015). Revisiting the concept of beverton–holt life-history invariants with the aim of informing data-poor fisheries assessment. *ICES Journal of Marine Science*, *72*(1), 194–203.

Quinn, T. J.; Turnbull, C. T., & Fu, C. (1998). A length-based population model for hard-to-age invertebrate populations. *Fishery Stock Assessment Models*, 531–556.

Raftery, A. E. (1988). Inference for the binomial n parameter: A hierarchical bayes approach. *Biometrika*, *75*(2), 223–228.

Rice, J. (2012). *Alternate catch estimates for silky and oceanic whitetip sharks in Western and Central Pacific Ocean*. WCPFC-SC8-2012/SA-IP-12. Report to the Western and Central Pacific Fisheries Commission Scientific Committee. Eighth Regular Session, 7–15 August 2012, Busan, Korea.

Rice, J. & Harley, S. (2013). *Updated stock assessment of silky sharks in the Western and Central Pacific Ocean*. WCPFC-SC9-2013/SA-WP-03. Report to the Western and Central Pacific Fisheries Commission Scientific Committee. Ninth Regular Session, 6–14 August 2013, Pohnpei, Federated States of Micronesia.

Stan Development Team (2018). RStan: the R interface to Stan. R package version 2.17.3. Retrieved from http://mc-stan.org/.

Taylor, I. G.; Gertseva, V.; Methot Jr, R. D., & Maunder, M. N. (2013). A stock–recruitment relationship based on pre-recruit survival, illustrated with application to spiny dogfish shark. *Fisheries Research*, *142*, 15–21.

Taylor, I. G. & Methot Jr, R. D. (2013). Hiding or dead? a computationally efficient model of selective fisheries mortality. *Fisheries Research*, *142*, 75–85.

Tremblay-Boyer, L. & Neubauer, P. (2019). *Historical catch reconstruction and CPUE standardization for the stock assessment of oceanic whitetip shark in the Western and Central Pacic Ocean*. WCPFC-SC15-2019/SA-IP-17. Report to the Western and Central Pacific Fisheries Commission Scientific Committee. Fifteenth Regular Session, 12–20 August 2019, Pohnpei, Federated States of Micronesia.

WCPFC (2013). *Conservation and Management Measure for Silky Sharks*. WCPFC10/CMM2013-08. Western and Central Pacific Fisheries Commission. Tenth Regular Session, 2–6 December 2013, Cairns, Australia.

Williams, P.; Panizza, A.; Falasi, C.; Loganimoce, E., & Schneiter, E. (2020). *Status of Observer Data Management* (tech. rep. No. SC16-2020/ST-IP-02). WCPFC.

Winker, H.; Carvalho, F., & Kapur, M. (2018). JABBA: Just another bayesian biomass assessment. *Fisheries Research*, *204*, 275–288.

Xu, H.; Thorson, J. T.; Methot, R. D., & Taylor, I. G. (2019, February). A new semi-parametric method for autocorrelated age- and time-varying selectivity in age-structured assessment models. *Canadian Journal of Fisheries and Aquatic Sciences*, *76*(2), 268–285.

Zhou, S.; Deng, R.; Hoyle, S., & Dunn, M. (2018). *Identifying appropriate reference points for elasmobranchs within the WCPFC*. WCPFC-SC14-2018/MI-WP-07. Report to the Western and Central Pacific Fisheries Commission Scientific Committee. Fourteenth Regular Session, 8–16 August 2018, Busan, Korea.

10. TABLES

10.1 Stock synthesis assessment

Table 2: Estimates and associated uncertainty estimated using MCMC for model parameters and derived quantities for the 2024 diagnostic model for silky shark. SD: Standard deviation, MAD: median absolute deviation, credible intervals (5% and 95%), the $\hat{R}$ convergence diagnostic (should be as close as possible to 1.00) and the Effective Sample Size (ESS).

Variable	Mean	Median	SD	MAD	5%	95%	$\hat{R}$	ESS
Objective function	1799.90	1799.65	25.75	26.16	1758.32	1842.15	1.00	1600.30
SSB_{recent}/SSB_0	0.97	0.97	0.06	0.06	0.86	1.06	1.00	1268.64
F_{Init}	0.12	0.12	0.01	0.01	0.11	0.14	1.00	887.93
$\ln(R_0)$	6.46	6.46	0.17	0.17	6.20	6.75	1.00	1313.56
M	0.16	0.16	0.01	0.01	0.14	0.18	1.00	1052.85
z_{frac}	0.66	0.66	0.03	0.03	0.61	0.71	1.00	412.19

10.2 Alternative assessments

10.2.1 Length and age-structured model

Table 3: Lower and upper bounds for the parameters of the exponential logistic and logistic selectivity functions. The three parameters for exponential logistic selectivity (i.e., p_1, p_2, and p_3) are defined in Equation (2), and the two other parameters for logistic selectivity (i.e., L_5 and L_{95}) are defined in Equation (3).

	Exponential logistic	Logistic
p_1 (or L_5)	$(0.02, 1)$	$(30, 90)$
p_2 (or L_{95})	$(0.1, 0.8)$	$(90, 150)$
p_3	$(0.001, 0.5)$	

10.2.2 Dynamic surplus production model

Table 4: Predictive coverage: proportion of the posterior distribution for year y.

Year	Coverage	
	Harvest rate	Depletion
2016	0.96	0.96
2017	0.95	0.98
2018	0.95	0.93
2019	0.93	0.98
2020	0.94	0.96

Table 5: Parameter estimates and derived quantities for different model runs with alternative prior assumptions about initial depletion (start_N). SD: Standard deviation, MAD: median absolute deviation, credible intervals (5% and 95%), the $\hat{R}$ convergence diagnostic (should be as close as possible to 1.00) and the Effective Sample Size (ESS).

Model	Variable	Mean	Median	SD	MAD	5%	95%	$\hat{R}$	ESS
Catch (Post exp.) start_N /1	N_{recent}/N_0	0.47	0.45	0.16	0.15	0.25	0.75	1.00	4086.99
Catch (Post exp.) start_N /2	N_{recent}/N_0	0.19	0.18	0.08	0.07	0.09	0.34	1.00	3874.09
Catch (Post exp.) start_N /0.5	N_{recent}/N_0	0.66	0.64	0.19	0.19	0.39	0.99	1.00	4133.79
Catch (Post exp.) start_N /1	U_{recent}	0.02	0.01	0.01	0.01	0.00	0.04	1.00	4024.12
Catch (Post exp.) start_N /2	U_{recent}	0.03	0.02	0.01	0.01	0.01	0.05	1.00	3930.20
Catch (Post exp.) start_N /0.5	U_{recent}	0.01	0.01	0.01	0.01	0.00	0.03	1.00	3992.99
Catch (Post exp.) start_N /1	$\log(K)$	17.48	17.35	0.86	0.76	16.31	19.08	1.00	4021.97
Catch (Post exp.) start_N /2	$\log(K)$	17.81	17.74	0.68	0.64	16.79	18.99	1.00	4069.84
Catch (Post exp.) start_N /0.5	$\log(K)$	17.62	17.45	0.95	0.92	16.33	19.39	1.00	3962.46
Catch (Post exp.) start_N /1	q	4.41	4.10	1.65	1.44	2.35	7.45	1.00	4074.09
Catch (Post exp.) start_N /2	q	11.88	11.03	4.86	4.24	5.64	20.98	1.00	4015.21
Catch (Post exp.) start_N /0.5	q	2.90	2.73	0.97	0.85	1.71	4.66	1.00	4016.86

10.2.3 Length-based spatial risk assessment

Table 6: Estimates and associated uncertainty for model parameters and derived quantities for the base model of the hybrid length-based spatial risk assessment. SD: Standard deviation, MAD: median absolute deviation, credible intervals (5% and 95%), the $\hat{R}$ convergence diagnostic (should be as close as possible to 1.00) and the Effective Sample Size (ESS).

Variable	Mean	Median	SD	MAD	5%	95%	$\hat{R}$	ESS
μ_D	42.3	37.1	22	22.2	16.1	84.9	0.992	546
Q_{LL}	0.000282	0.000228	0.000179	0.000141	9.34e-05	0.000648	1.01	449
ϕ	3.89	3.88	0.0767	0.0745	3.76	4.02	0.997	560
ν	0.8	0.799	0.0195	0.0183	0.771	0.834	1.01	479
Harvest-rate	0.09	0.0894	0.00915	0.00839	0.0757	0.106	0.999	532
Gear-affected area	1.34e+03	1.15e+03	677	730	501	2.6e+03	0.995	526
$Q_{PS-ASSOC}$	5.93	5.92	0.422	0.412	5.29	6.64	1.02	389
$Q_{PS-UNASSOC}$	4.59	4.6	0.421	0.404	3.87	5.25	1	443

Table 7: Estimates of risk for sensitivities run for the the hybrid length-based spatial risk assessment.

Sensitivity	Median F/F_{crash}	$P(F > F_{lim})$	$P(F > F_{crash})$
base (2020)	0.569	0.29	0.147
2018	0.746	0.495	0.276
2019	0.725	0.472	0.261
LF weight x 10	0.574	0.29	0.146
L_∞ x 1.2	1.05	0.8	0.543
$M = 0.2$	0.315	0.0762	0.0421

10.2.4 Model Comparison

Table 8: Estimates of management quantities (stock status as SSB_{recent}/SSB_0, and fishing mortality (F) relative to indicators (F_{MSY}) and possible limit reference points F_{lim}, F_{crash}) across models and subsets within models (diagnostic vs ensemble), arranged by model type. P(>RP) refers to the probability that the metric (status, fishing mortality) is above the respective indicator (B_0, F_{MSY}, F_{lim}, F_{crash}). SS3: Stock Synthesis 3, DSP: Dynamic surplus production, LAM: Length and age based model, SRA: spatial length - based risk assessment.

Model	Subset	Metric	Mean	SD	Median	2.5%	25%	75%	97.5%	P(>RP)
SS3	Ensemble	SSB_{recent}/SSB_0	0.75	0.14	0.77	0.45	0.55	0.90	0.98	0.01
SS3	Ensemble	$F_{recent}/F_{\text{MSY}}$	0.65	0.16	0.63	0.38	0.47	0.84	1.01	0.03
SS3	Ensemble	F_{recent}/F_{lim}	0.44	0.11	0.43	0.26	0.32	0.57	0.69	0.00
SS3	Ensemble	F_{recent}/F_{crash}	0.33	0.08	0.32	0.19	0.24	0.43	0.52	0.00
SS3	Diagnostic	SSB_{recent}/SSB_0	0.76	0.07	0.76	0.63	0.67	0.84	0.89	0.00
SS3	Diagnostic	$F_{recent}/F_{\text{MSY}}$	0.74	0.14	0.73	0.52	0.59	0.90	1.05	0.05
SS3	Diagnostic	F_{recent}/F_{lim}	0.51	0.09	0.50	0.35	0.40	0.61	0.71	0.00
SS3	Diagnostic	F_{recent}/F_{crash}	0.38	0.07	0.37	0.26	0.30	0.46	0.54	0.00
DSP	Ensemble	N_{recent}/N_0	0.44	0.24	0.42	0.10	0.16	0.74	0.96	0.02
DSP	Ensemble	$U_{recent}/U_{\text{MSY}}$	0.54	0.26	0.56	0.06	0.19	0.84	1.01	0.03
DSP	Ensemble	U_{recent}/U_{lim}	0.18	0.09	0.19	0.02	0.06	0.28	0.34	0.00
DSP	Ensemble	U_{recent}/U_{crash}	0.13	0.07	0.14	0.01	0.05	0.21	0.25	0.00
DSP	Diagnostic	N_{recent}/N_0	0.47	0.15	0.45	0.22	0.30	0.64	0.82	0.00
DSP	Diagnostic	$U_{recent}/U_{\text{MSY}}$	0.52	0.24	0.53	0.08	0.21	0.80	0.97	0.02
DSP	Diagnostic	U_{recent}/U_{lim}	0.17	0.08	0.18	0.03	0.07	0.27	0.32	0.00
DSP	Diagnostic	U_{recent}/U_{crash}	0.13	0.06	0.13	0.02	0.05	0.20	0.24	0.00
SRA	Ensemble (All models)	F_{recent}/F_{lim}	1.13	1.13	0.85	0.28	0.47	1.74	3.70	0.39
SRA	Ensemble (All models)	F_{recent}/F_{crash}	0.85	0.85	0.64	0.21	0.35	1.31	2.77	0.23
SRA	Diagnostic (2020)	F_{recent}/F_{lim}	1.12	1.03	0.86	0.42	0.54	1.64	3.49	0.38
SRA	Diagnostic (2020)	F_{recent}/F_{crash}	0.84	0.77	0.65	0.31	0.40	1.23	2.61	0.20
LAM	Ensemble	F_{recent}/F_{lim}	0.07	0.05	0.07	0.01	0.02	0.13	0.17	0.00
LAM	Ensemble	F_{recent}/F_{crash}	0.05	0.03	0.05	0.01	0.01	0.09	0.12	0.00
LAM	Ensemble	$F_{recent}/F_{\text{MSY}}$	0.13	0.08	0.13	0.02	0.04	0.24	0.30	0.00
LAM	Ensemble	SSB_{recent}/SSB_0	0.48	0.28	0.43	0.07	0.17	0.88	1.09	0.06
LAM	Diagnostic (Intermed F_{Init})	F_{recent}/F_{lim}	0.06	0.04	0.05	0.01	0.02	0.10	0.14	0.00
LAM	Diagnostic (Intermed F_{Init})	F_{recent}/F_{crash}	0.04	0.02	0.03	0.01	0.01	0.07	0.10	0.00
LAM	Diagnostic (Intermed F_{Init})	$F_{recent}/F_{\text{MSY}}$	0.11	0.07	0.09	0.02	0.03	0.19	0.26	0.00
LAM	Diagnostic (Intermed F_{Init})	SSB_{recent}/SSB_0	0.47	0.21	0.46	0.12	0.22	0.74	0.92	0.01

Table 9: Estimates of management quantities (stock status as SSB_{recent}/SSB_0, and fishing mortality (F) relative to indicators (F_{MSY}) and possible limit reference points F_{lim}, F_{crash}) across models and subsets within models (diagnostic vs ensemble), arranged by indicator. P(>RP) refers to the probability that the metric (status, fishing mortality) is above the respective indicator (B_0, F_{MSY}, F_{lim}, F_{crash}). SS3: Stock Synthesis 3, DSP: Dynamic surplus production, LAM: Length and age based model, SRA: spatial length - based risk assessment.

Model	Subset	Metric	Mean	SD	Median	2.5%	25%	75%	97.5%	P(>RP)
SS3	Ensemble	SSB_{recent}/SSB_0	0.75	0.14	0.77	0.45	0.55	0.90	0.98	0.01
SS3	Diagnostic	SSB_{recent}/SSB_0	0.76	0.07	0.76	0.63	0.67	0.84	0.89	0.00
DSP	Ensemble	N_{recent}/N_0	0.44	0.24	0.42	0.10	0.16	0.74	0.96	0.02
DSP	Diagnostic	N_{recent}/N_0	0.47	0.15	0.45	0.22	0.30	0.64	0.82	0.00
LAM	Ensemble	SSB_{recent}/SSB_0	0.48	0.28	0.43	0.07	0.17	0.88	1.09	0.06
LAM	Diagnostic (Intermed F_{Init})	SSB_{recent}/SSB_0	0.47	0.21	0.46	0.12	0.22	0.74	0.92	0.01
SS3	Ensemble	$F_{recent}/F_{\text{MSY}}$	0.65	0.16	0.63	0.38	0.47	0.84	1.01	0.03
SS3	Diagnostic	$F_{recent}/F_{\text{MSY}}$	0.74	0.14	0.73	0.52	0.59	0.90	1.05	0.05
DSP	Ensemble	$U_{recent}/U_{\text{MSY}}$	0.54	0.26	0.56	0.06	0.19	0.84	1.01	0.03
DSP	Diagnostic	$U_{recent}/U_{\text{MSY}}$	0.52	0.24	0.53	0.08	0.21	0.80	0.97	0.02
LAM	Ensemble	$F_{recent}/F_{\text{MSY}}$	0.13	0.08	0.13	0.02	0.04	0.24	0.30	0.00
LAM	Diagnostic (Intermed F_{Init})	$F_{recent}/F_{\text{MSY}}$	0.11	0.07	0.09	0.02	0.03	0.19	0.26	0.00
SS3	Ensemble	F_{recent}/F_{crash}	0.33	0.08	0.32	0.19	0.24	0.43	0.52	0.00
SS3	Diagnostic	F_{recent}/F_{crash}	0.38	0.07	0.37	0.26	0.30	0.46	0.54	0.00
DSP	Ensemble	U_{recent}/U_{crash}	0.13	0.07	0.14	0.01	0.05	0.21	0.25	0.00
DSP	Diagnostic	U_{recent}/U_{crash}	0.13	0.06	0.13	0.02	0.05	0.20	0.24	0.00
SRA	Ensemble (All models)	F_{recent}/F_{crash}	0.85	0.85	0.64	0.21	0.35	1.31	2.77	0.23
SRA	Diagnostic (2020)	F_{recent}/F_{crash}	0.84	0.77	0.65	0.31	0.40	1.23	2.61	0.20
LAM	Ensemble	F_{recent}/F_{crash}	0.05	0.03	0.05	0.01	0.01	0.09	0.12	0.00
LAM	Diagnostic (Intermed F_{Init})	F_{recent}/F_{crash}	0.04	0.02	0.03	0.01	0.01	0.07	0.10	0.00
SS3	Ensemble	F_{recent}/F_{lim}	0.44	0.11	0.43	0.26	0.32	0.57	0.69	0.00
SS3	Diagnostic	F_{recent}/F_{lim}	0.51	0.09	0.50	0.35	0.40	0.61	0.71	0.00
DSP	Ensemble	U_{recent}/U_{lim}	0.18	0.09	0.19	0.02	0.06	0.28	0.34	0.00
DSP	Diagnostic	U_{recent}/U_{lim}	0.17	0.08	0.18	0.03	0.07	0.27	0.32	0.00
SRA	Ensemble (All models)	F_{recent}/F_{lim}	1.13	1.13	0.85	0.28	0.47	1.74	3.70	0.39
SRA	Diagnostic (2020)	F_{recent}/F_{lim}	1.12	1.03	0.86	0.42	0.54	1.64	3.49	0.38
LAM	Ensemble	F_{recent}/F_{lim}	0.07	0.05	0.07	0.01	0.02	0.13	0.17	0.00
LAM	Diagnostic (Intermed F_{Init})	F_{recent}/F_{lim}	0.06	0.04	0.05	0.01	0.02	0.10	0.14	0.00

11. FIGURES

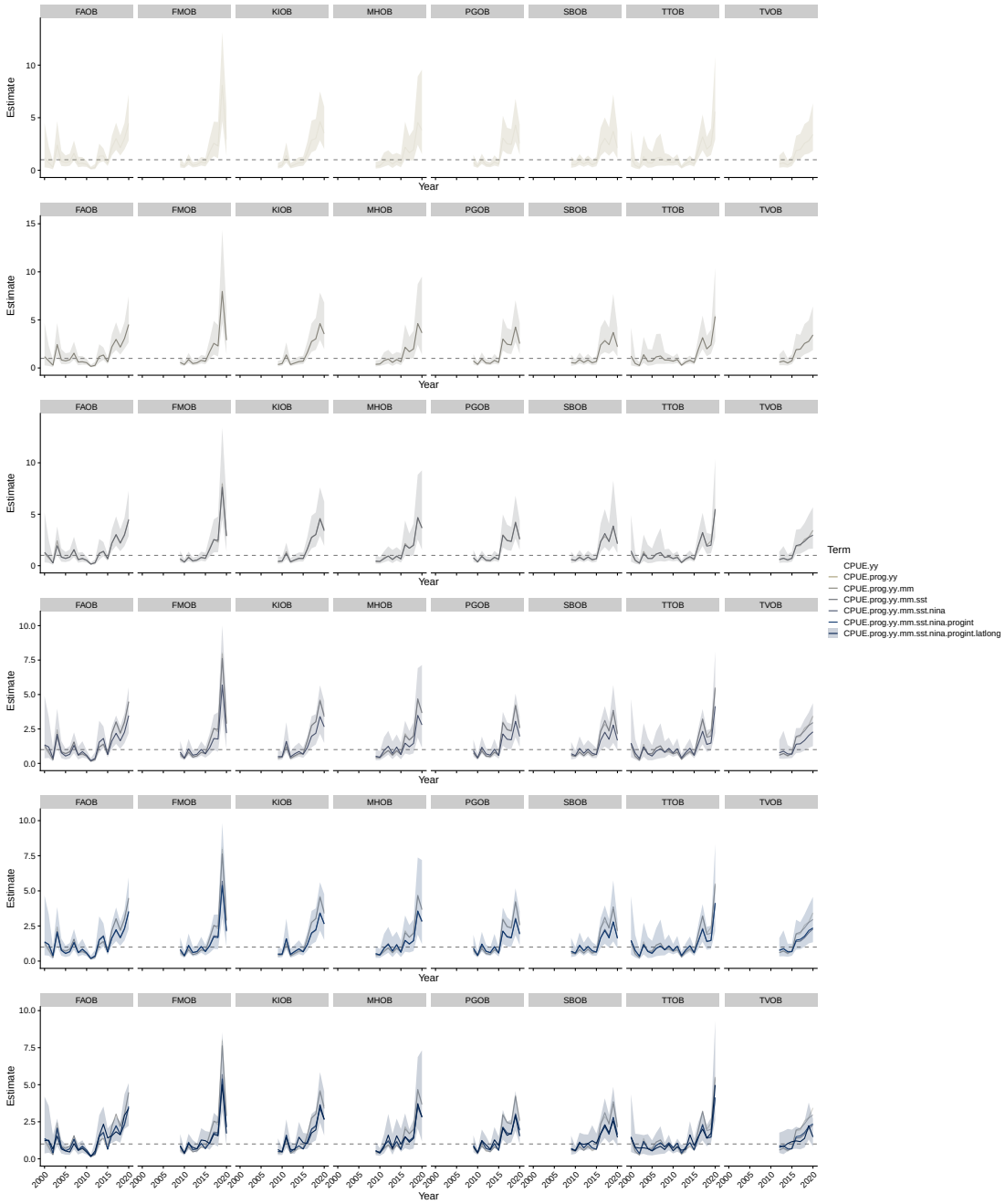

Figure 1: CPUE standardisation effects for free-school purse-seine sets by observer-program. Each row of plots corresponds to the addition of a variable, starting with a model that includes observer-program-year interactions. In each row, the posterior median and credible interval is shown for the updated model, posterior medians for the year effect from sub-models are shown for comparison.

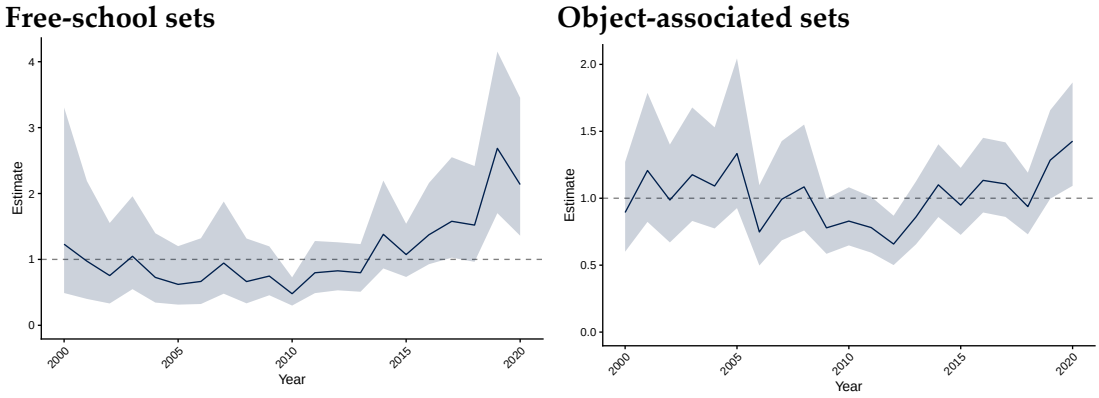

Figure 2: Purse-seine CPUE index by set-type. Shown is the posterior median and 95% credible interval for the year effect, standardised for regional trends and environmental variables.

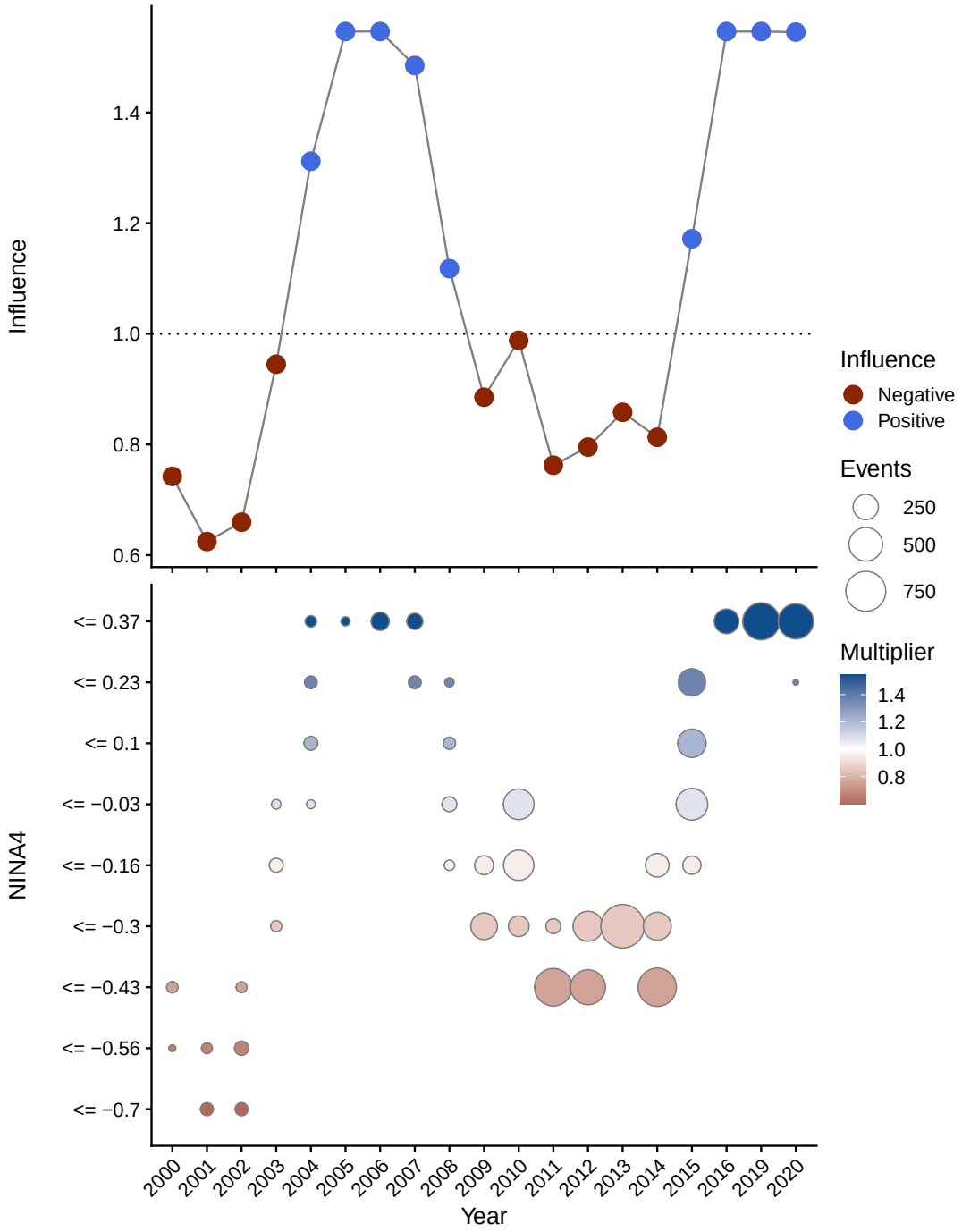

Figure 3: Influence of NINA4 (miev2) index on catch-rates in observed free-school purse-seine sets, with positive influence showing years where the over-all catch-rate in the model was standardised downward by the corresponding amount to account for influences of environmental conditions. Influence is shown in colour as a multiplier on average catch rates, with circle size corresponding to the amount of effort entering the model.

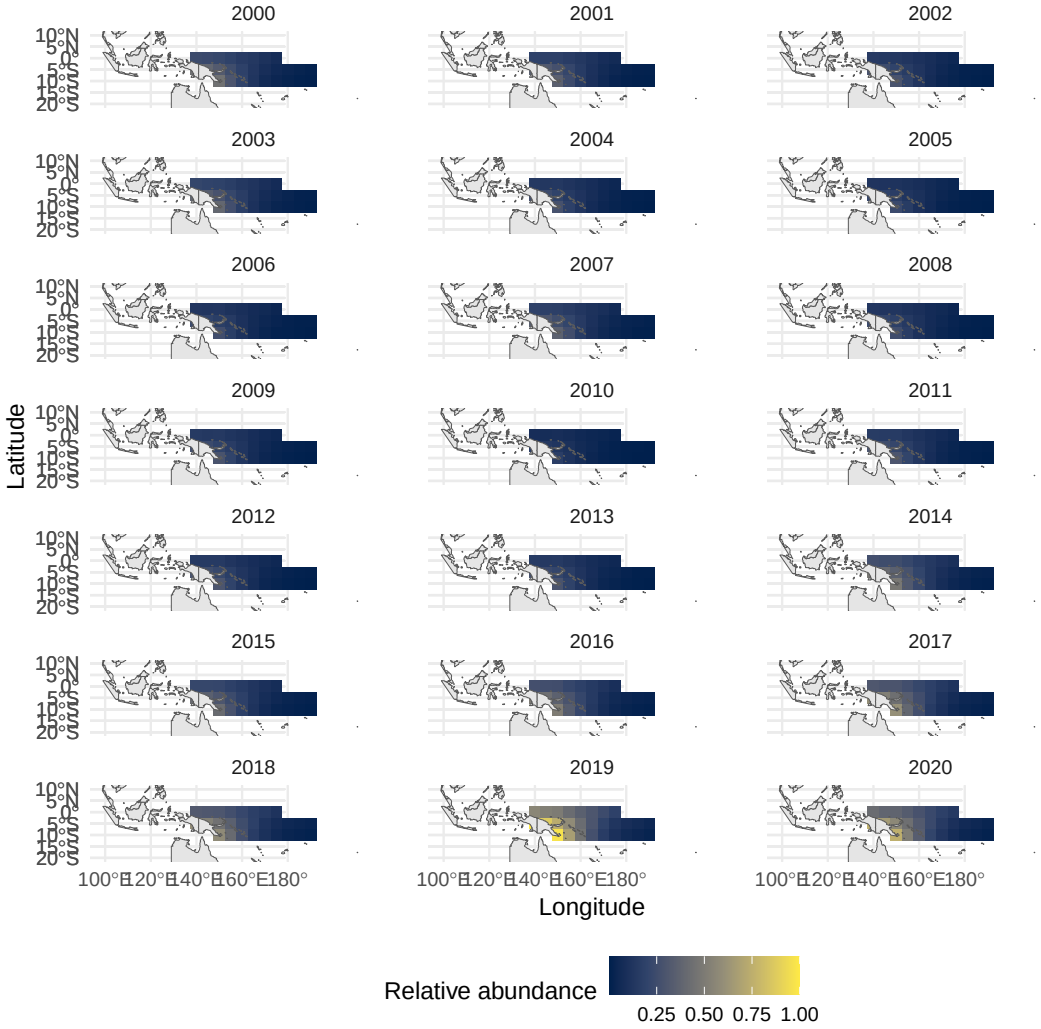

Figure 4: Spatial predictions from the spatio-temporal CPUE derived from a CPUE standardisation model for silky shark including a spatio-temporal spline over longitude, latitude and year. The spatio temporal index is derived by predicting across a consistent domain.

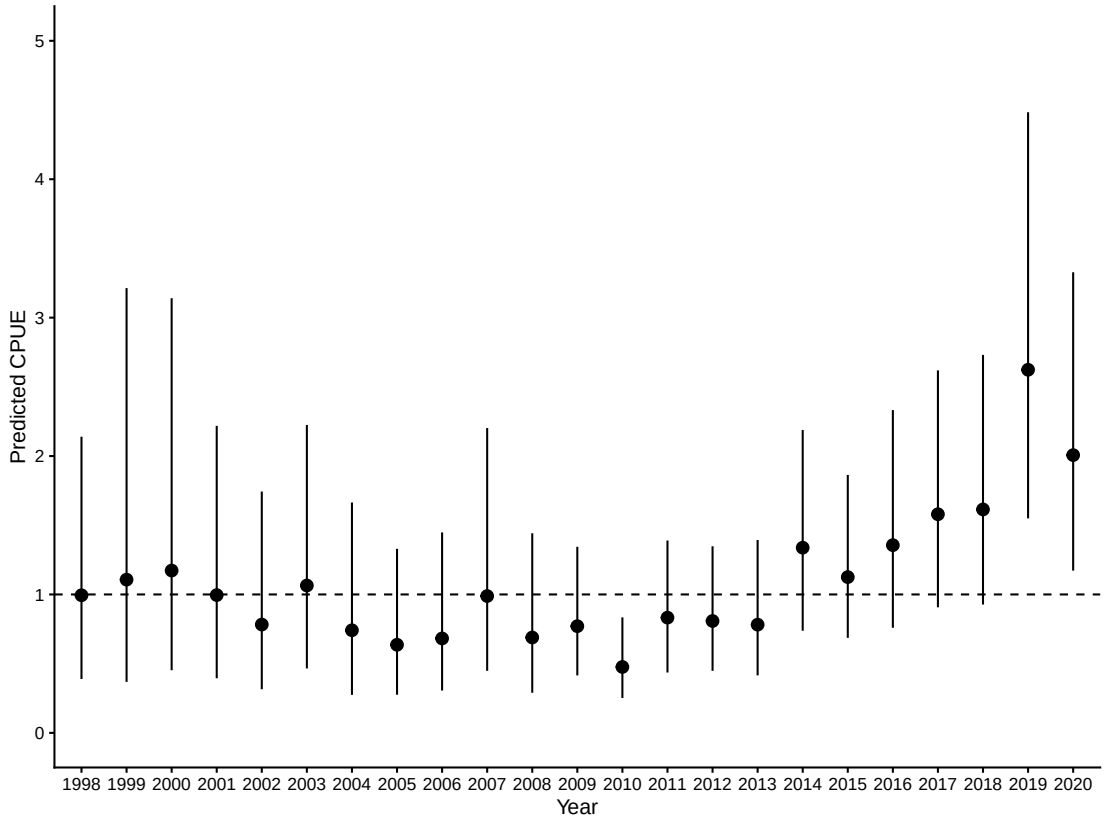

Figure 5: Spatio-temporal CPUE derived from a CPUE standardisation model for silky shark including a spatio-temporal spline over longitude, latitude and year. The spatio temporal index is derived by predicting across a consistent domain.

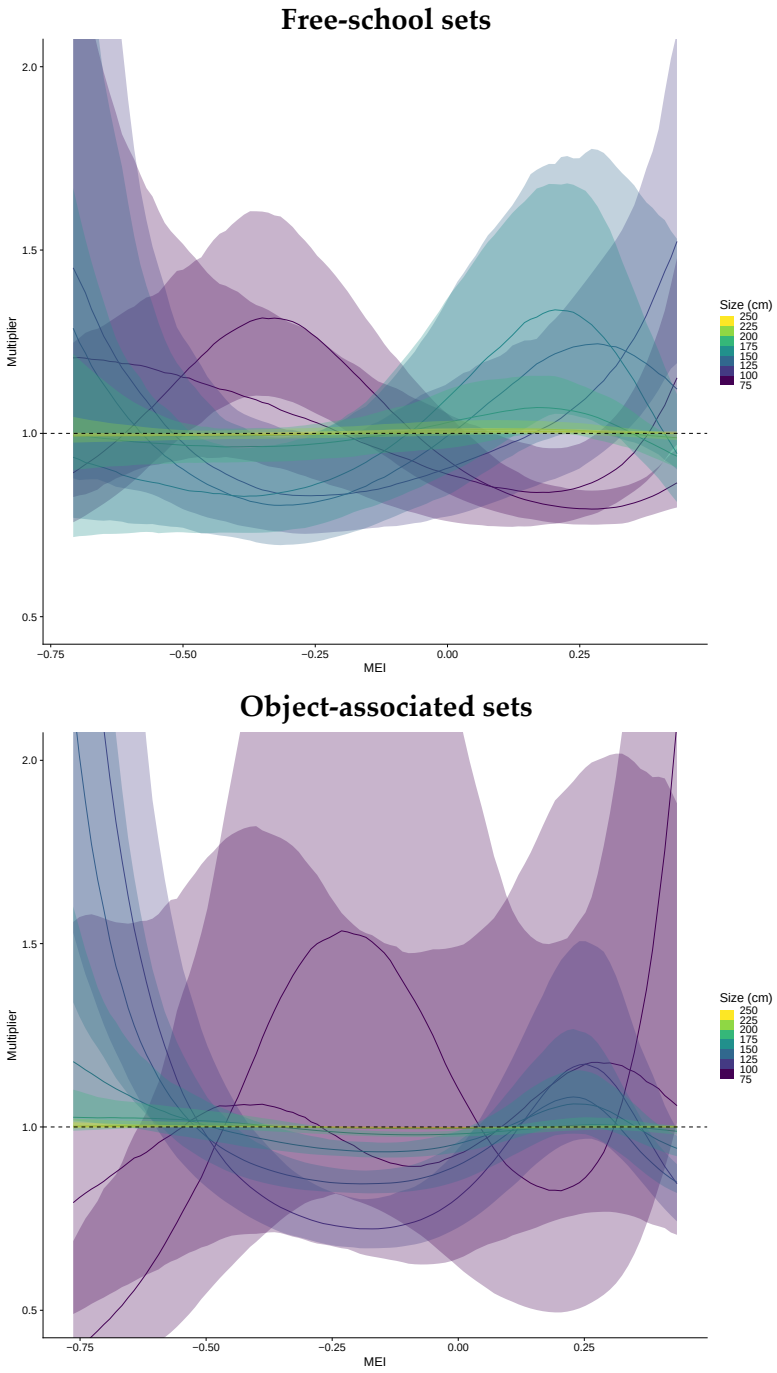

Figure 6: Presence of size classes in the purse-seine catch for free-school and object-associated schools as a function of the multivariate ENSO index (meiv2).

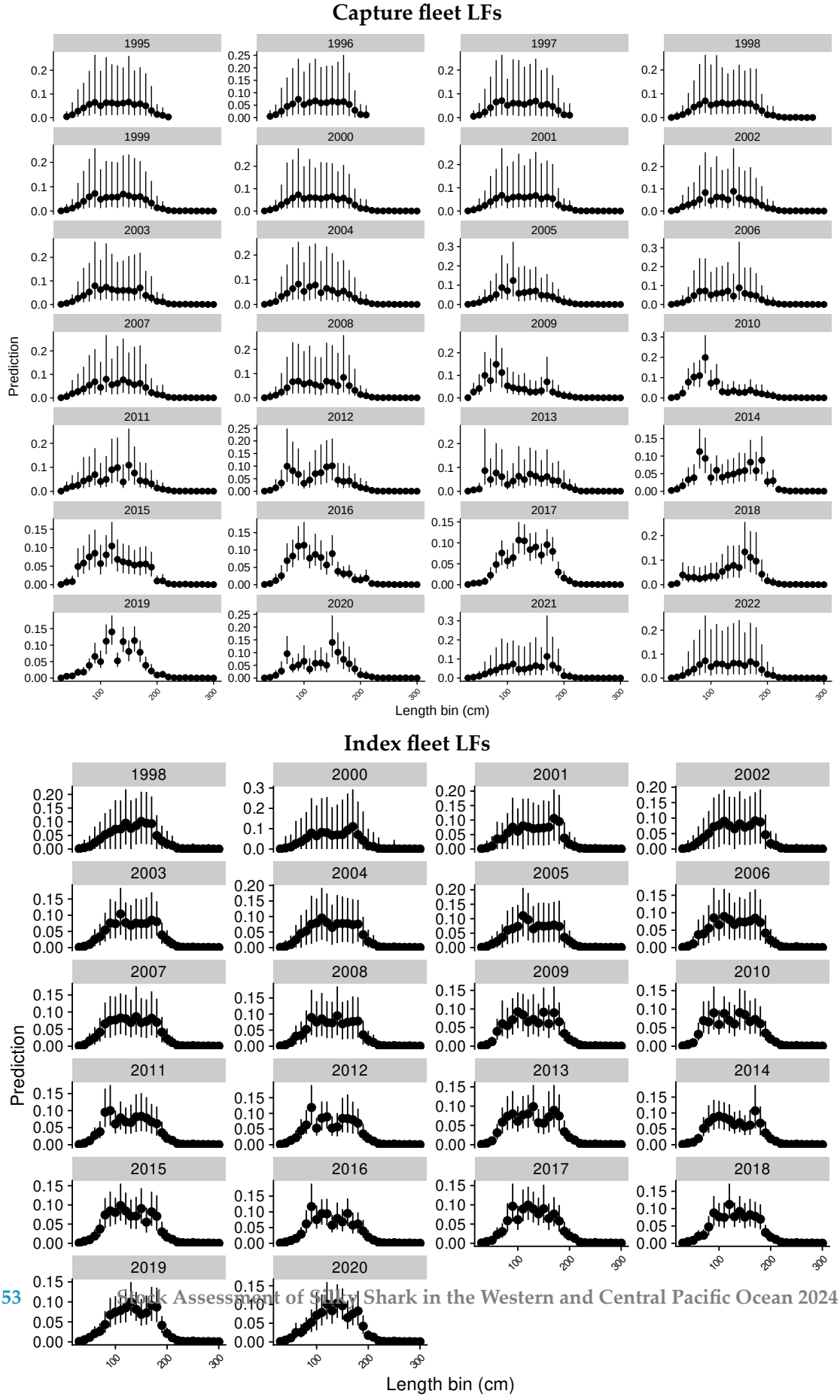

Figure 7: Comparing length frequencies (LFs) for catch (top) and the CPUE index (bottom) for free-school purse-seine.

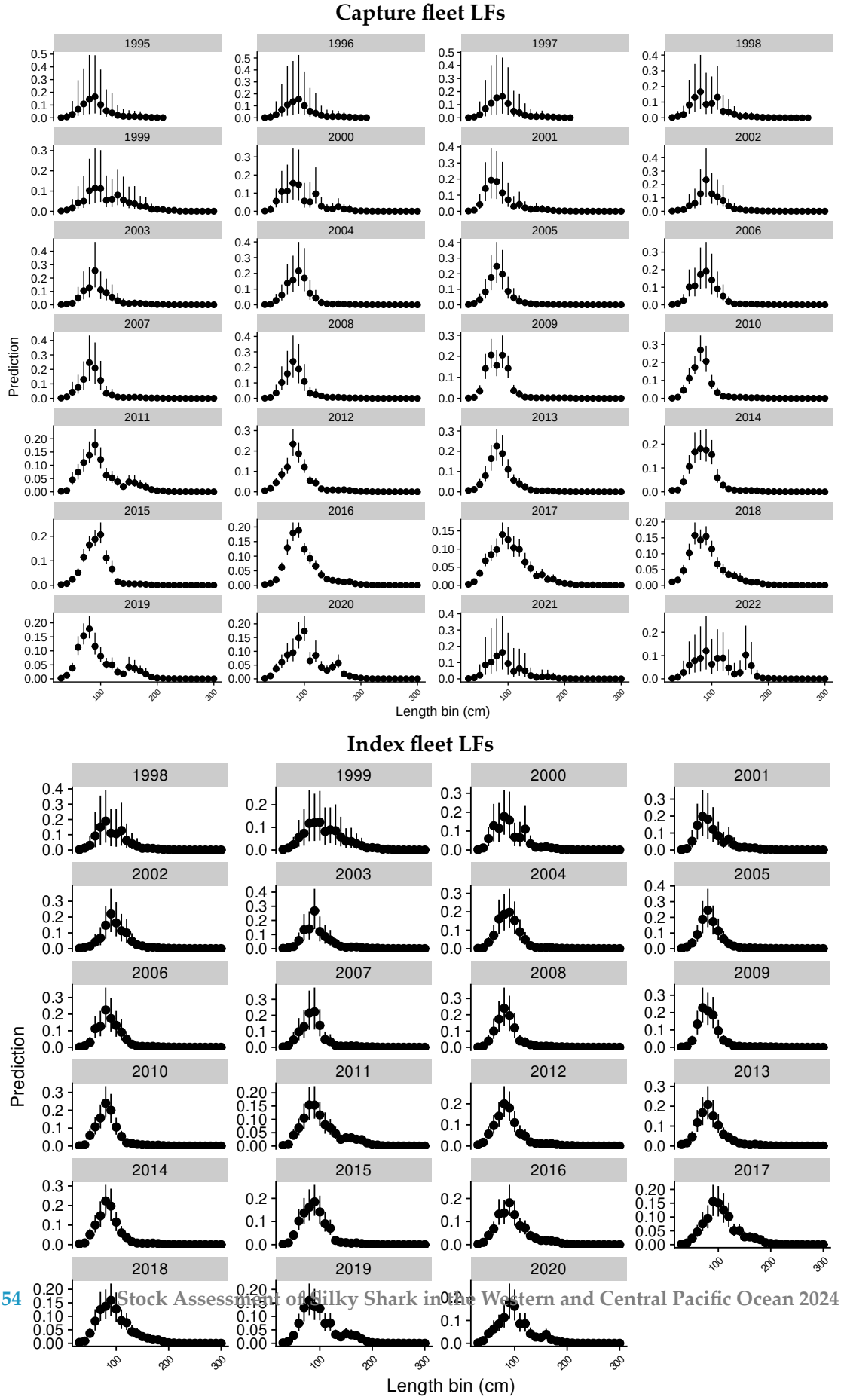

Figure 8: Comparing length frequencies (LFs) for catch (top) and the CPUE index (bottom) for object associated purse-seine.

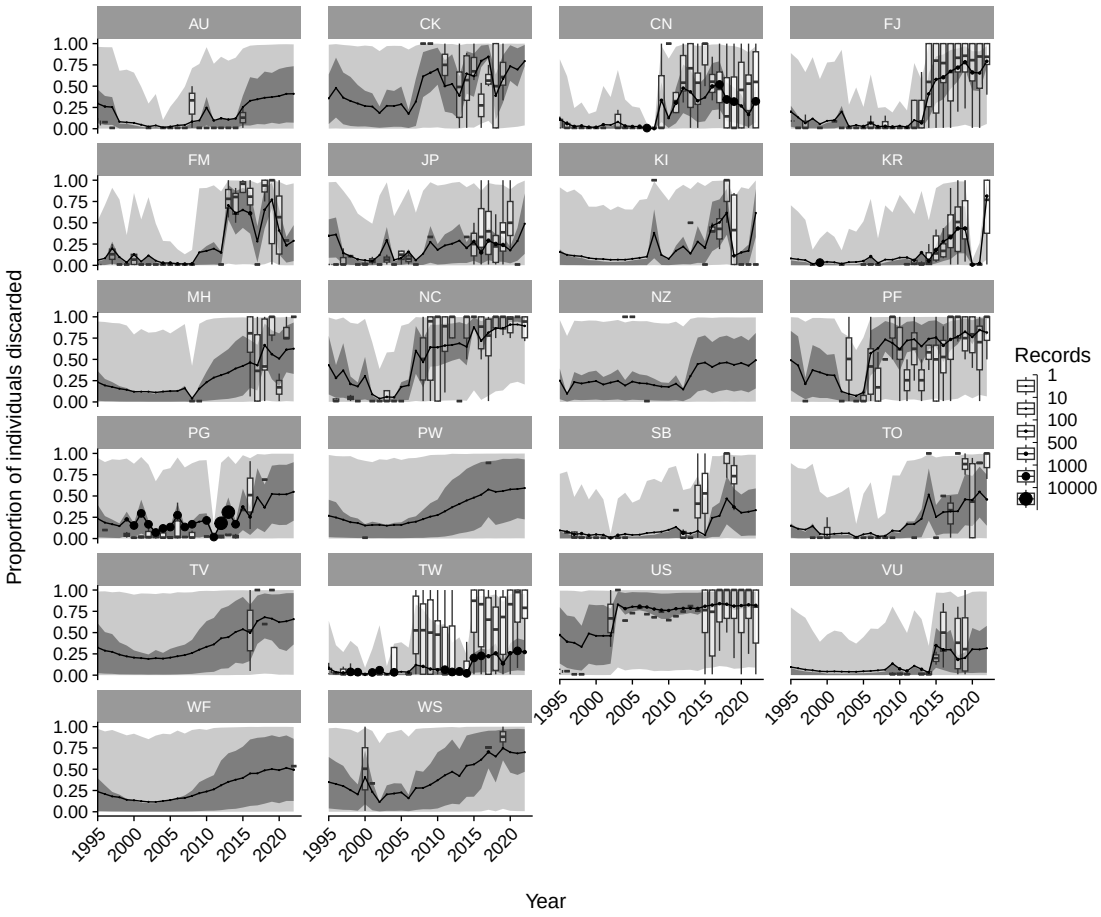

Figure 9: Observed (boxplots for within-flag variability within year) and predicted (posterior mean line and 75% (dark shade) and 95% (light shade) credible intervals) discard rates by flag for longline interactions with silky shark. The size of the points on the line indicates the number of records, with lines without representing model predictions

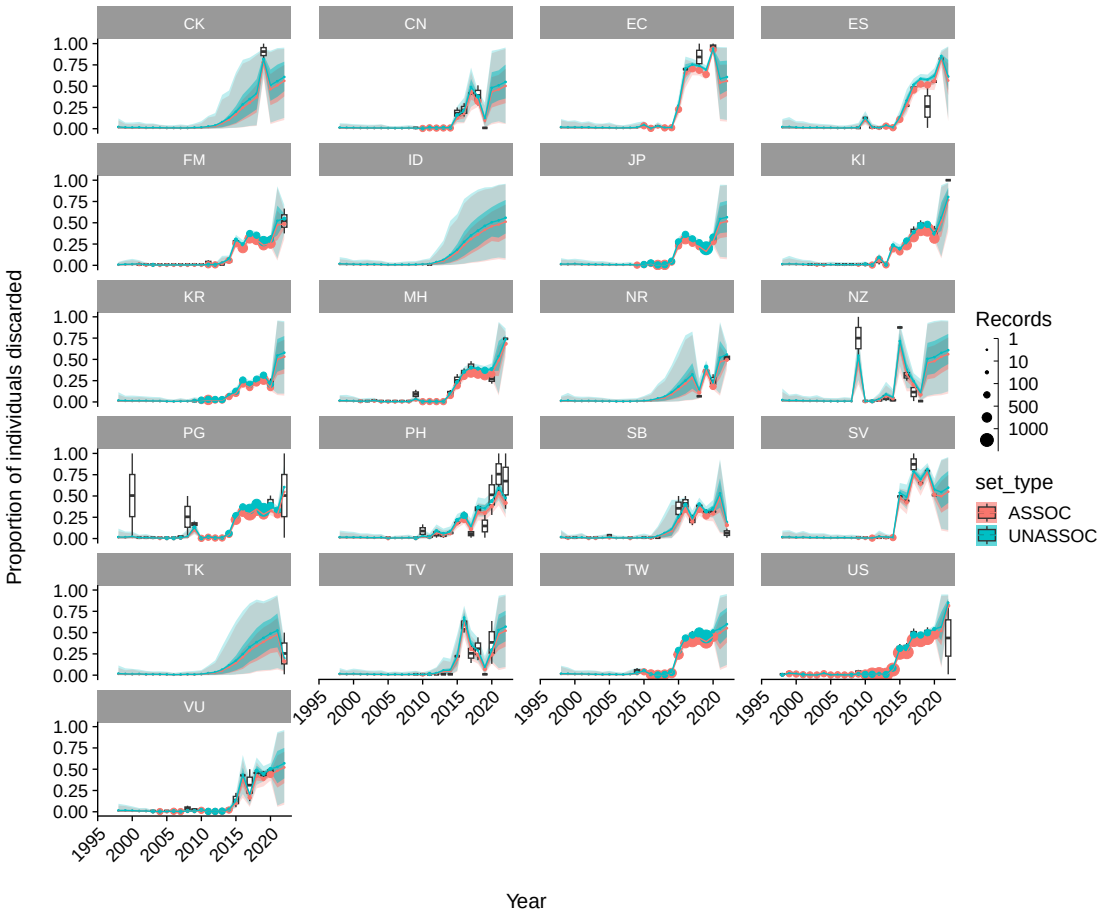

Figure 10: Observed (boxplots for within-flag variability within year) and predicted (posterior mean line and 75% (dark shade) and 95% (light shade) credible intervals) discard rates by flag and set-type for purse-seine interactions with silky shark. The size of the points on the line indicates the number of records, with lines without representing model predictions

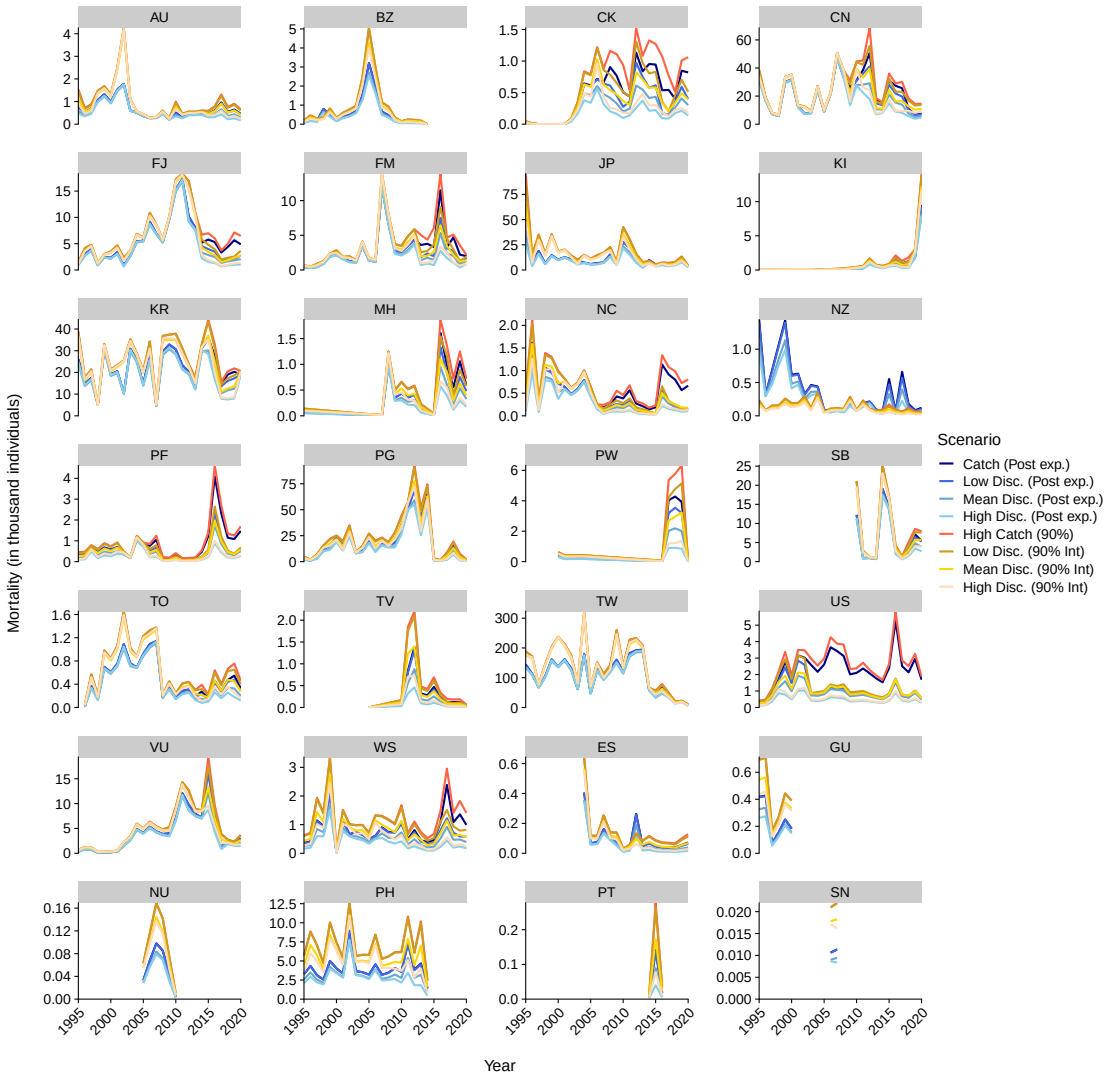

Figure 11: Predicted total fishing related mortality from longline fisheries by flag, including 15% post release mortality for live-discarded silky shark. Interactions refer to the posterior median (50%) and 90^{th} percentile (90%) of the predicted catch from the observer catch rate model. Low, median and high discard scenarios refer to the 25%, 50% (median) and 75% discard estimates.

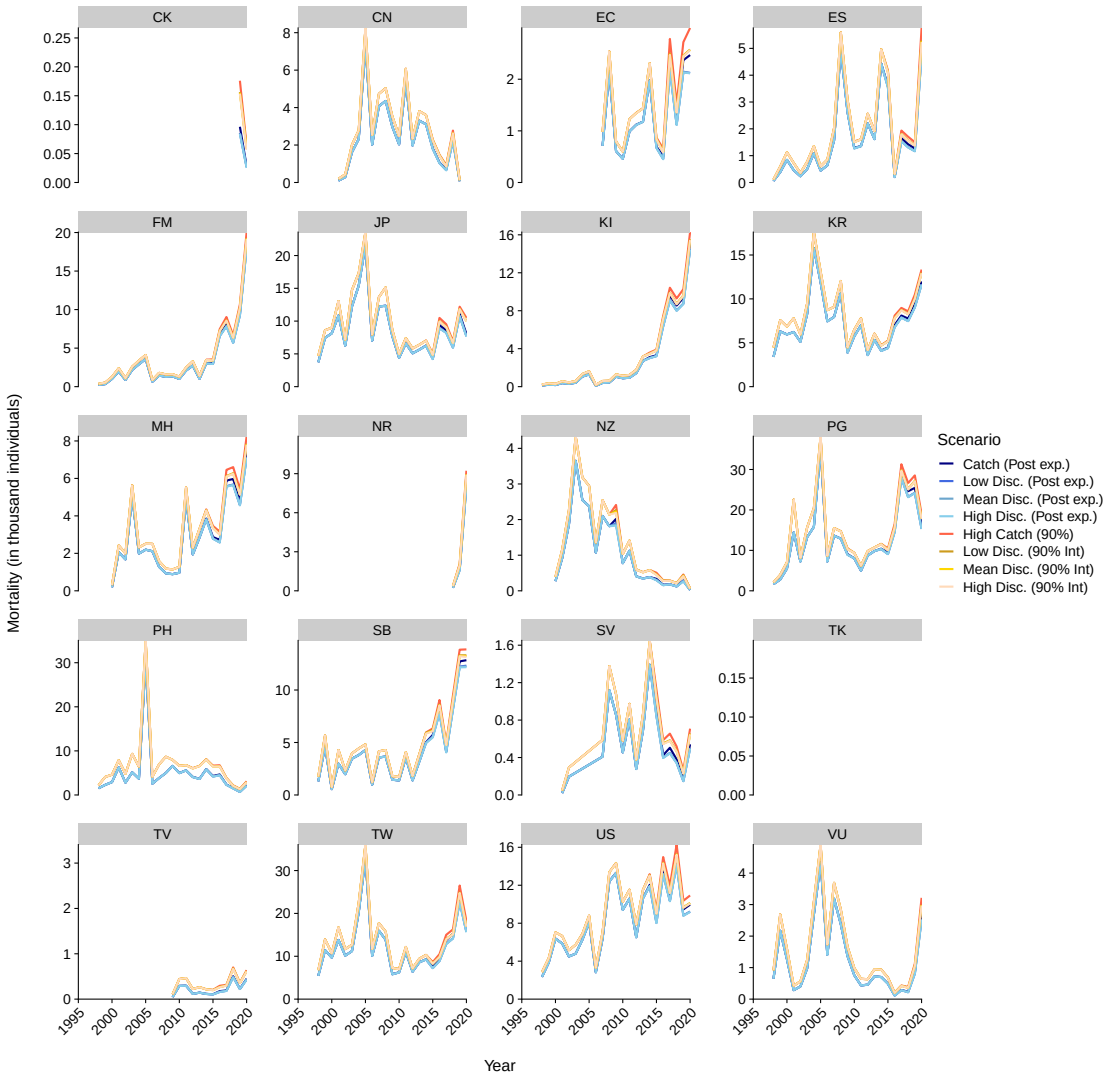

Figure 12: Predicted total fishing related mortality from purse-seine fisheries by flag, including 85% post release mortality for live-discarded silky shark. Interactions refer to the posterior median (50%) and 90^{th} percentile (90%) of the predicted catch from the observer catch rate model. Low, median and high discard scenarios refer to the 25%, 50% (median) and 75% discard estimates.

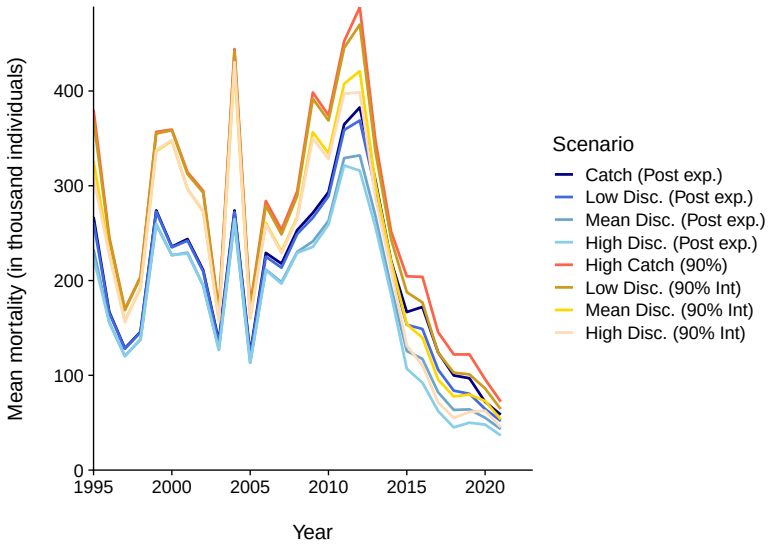

Figure 13: Predicted total fishing related mortality from longline, including 15% post release mortality for live-discarded silky sharks. Interactions refer to the posterior median (50%) and 90^{th} percentile (90%) of the predicted catch from the observer catch rate model. Low, median and high discard scenarios refer to the 25%, 50% (median) and 75% discard estimates. All discard estimates were applied at flag and latitudinal stratum level to overall interactions.

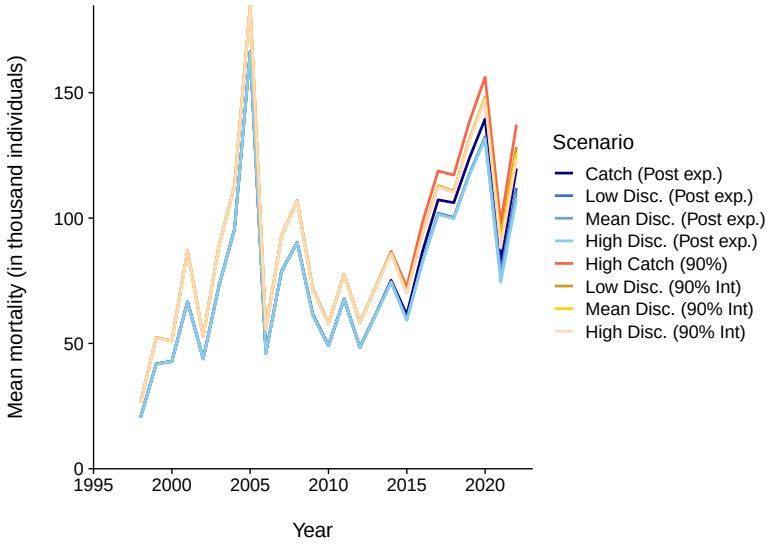

Figure 14: Predicted total fishing related mortality from purse-seine, including 15% post release mortality for live-discarded silky sharks. Interactions refer to the posterior median (50%) and 90^{th} percentile (90%) of the predicted catch from the observer catch rate model. Low, median and high discard scenarios refer to the 25%, 50% (median) and 75% discard estimates. All discard estimates were applied at flag and latitudinal stratum level to overall interactions.

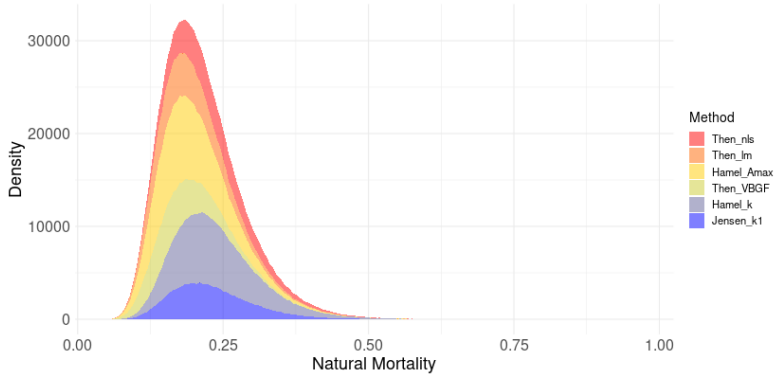

Figure 15: Meta-analytic prior for M using an assumed input CV of 30%, with colours representing individual life-history based estimators of natural mortality (Cope and Hamel 2022).

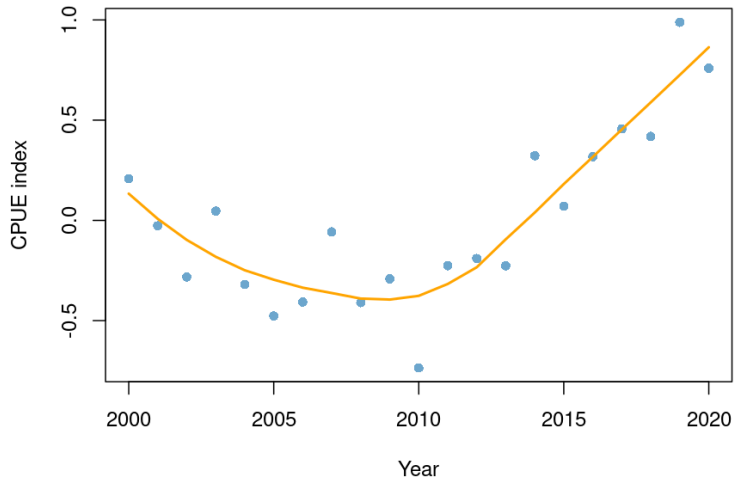

Figure 16: Fitted LOESS smoother with a span of 0.7, resulting in a residual SD of 0.17.

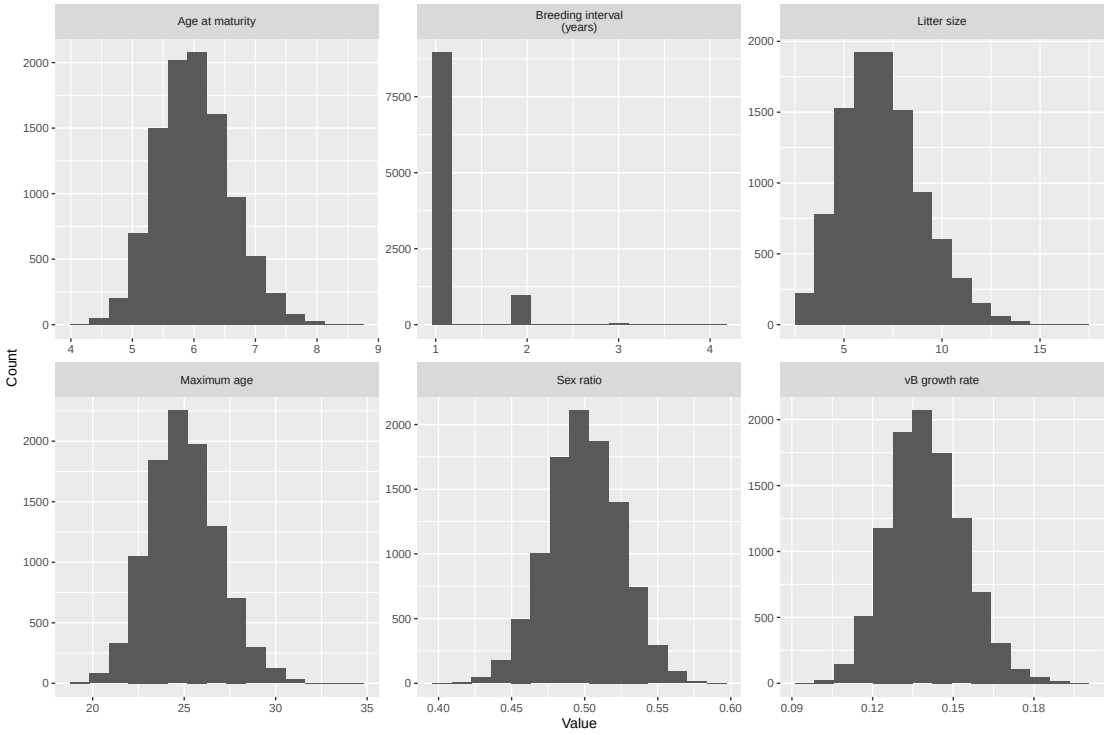

Figure 17: Input values for R_{max} simulations for silky shark, based on parameter values reported in the literature (vB, von Bertalanffy).

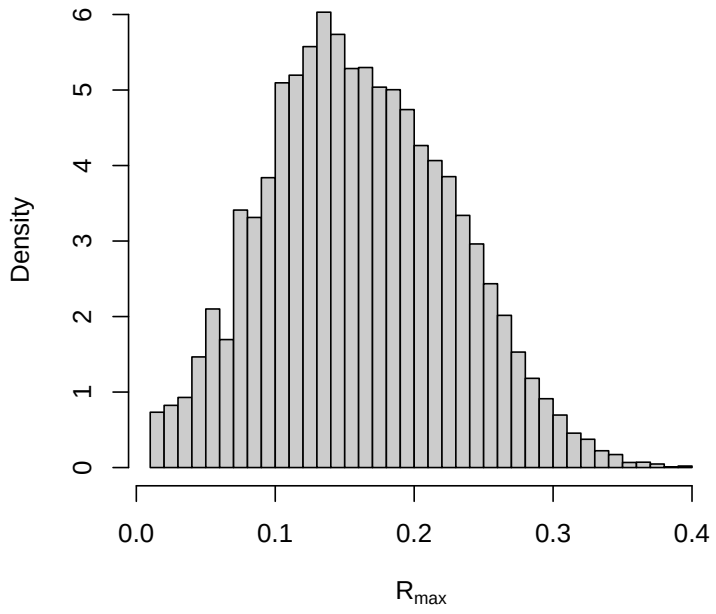

Figure 18: Simulated distribution over R_{max} for silky shark using distributions over input parameters shown in Figure 17.

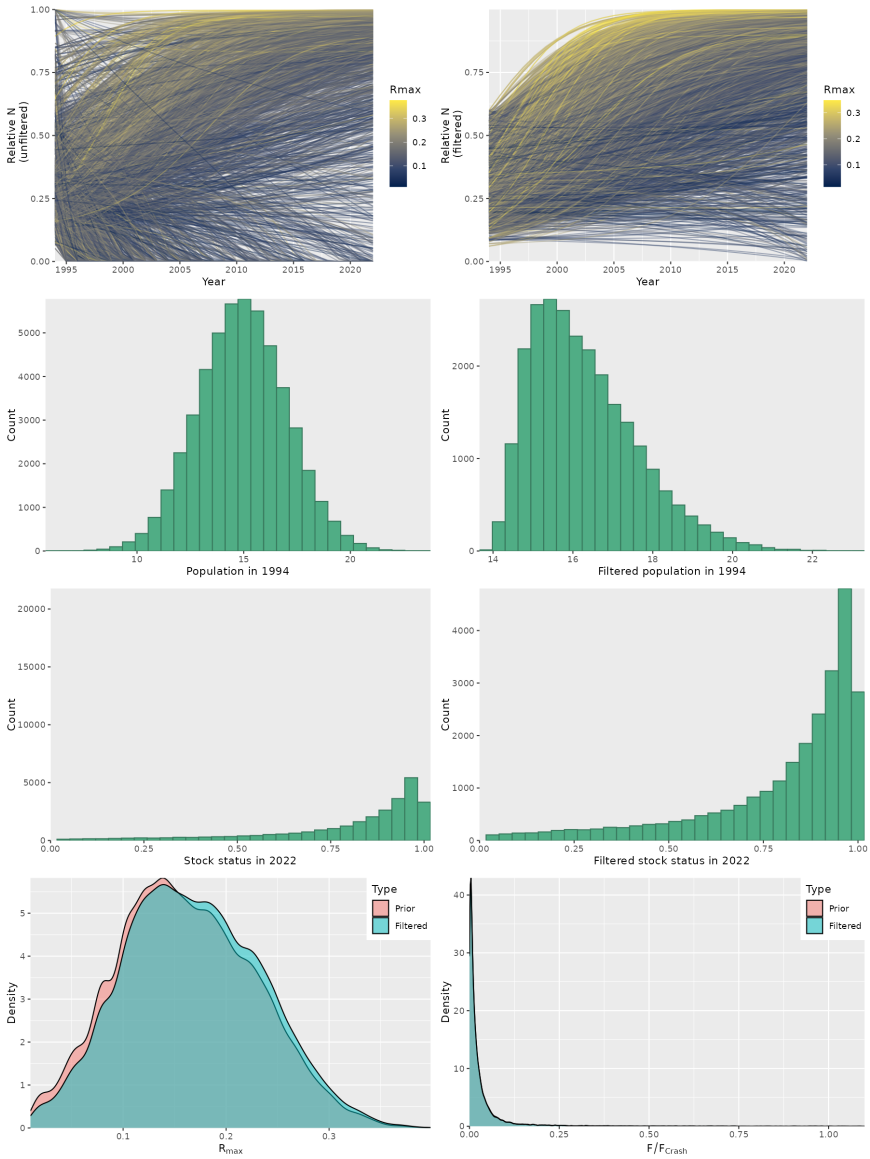

Figure 19: Summary of prior predictive simulations for silky shark shark. Top row: Simulated population trajectories (in terms of relative abundance N_t/K) coloured by the value of the draw from the prior distribution of R_{max}. For each simulation trajectory, a set of values for carrying capacity, initial depletion, and R_{max} were drawn from their prior distribution, and the median estimated catch from the catch reconstruction was applied. A subset of 1000 trajectories is shown on the left hand side, and a subset of 1000 trajectories from the filtered set (after applying constraints on current depletion relative to 1994). The corresponding draws from the prior distribution of stock size in 1994 are shown (2nd row) for the original prior and the constrained (filtered) prior. The prior distribution over stock status corresponding to the unconstrained prior (left) and the constrained prior (right) is shown in the third row. The constrained prior can be thought of as a joint Bayesian prior over parameters and current stock status in the simple surplus production model, and therefore implies a constrained prior for R_{max} and overfishing risk (last row; overfishing risk in terms of $F_{curr}/F_{crash} = F_{curr}/R_{max}$).

11.1 Stock synthesis assessment

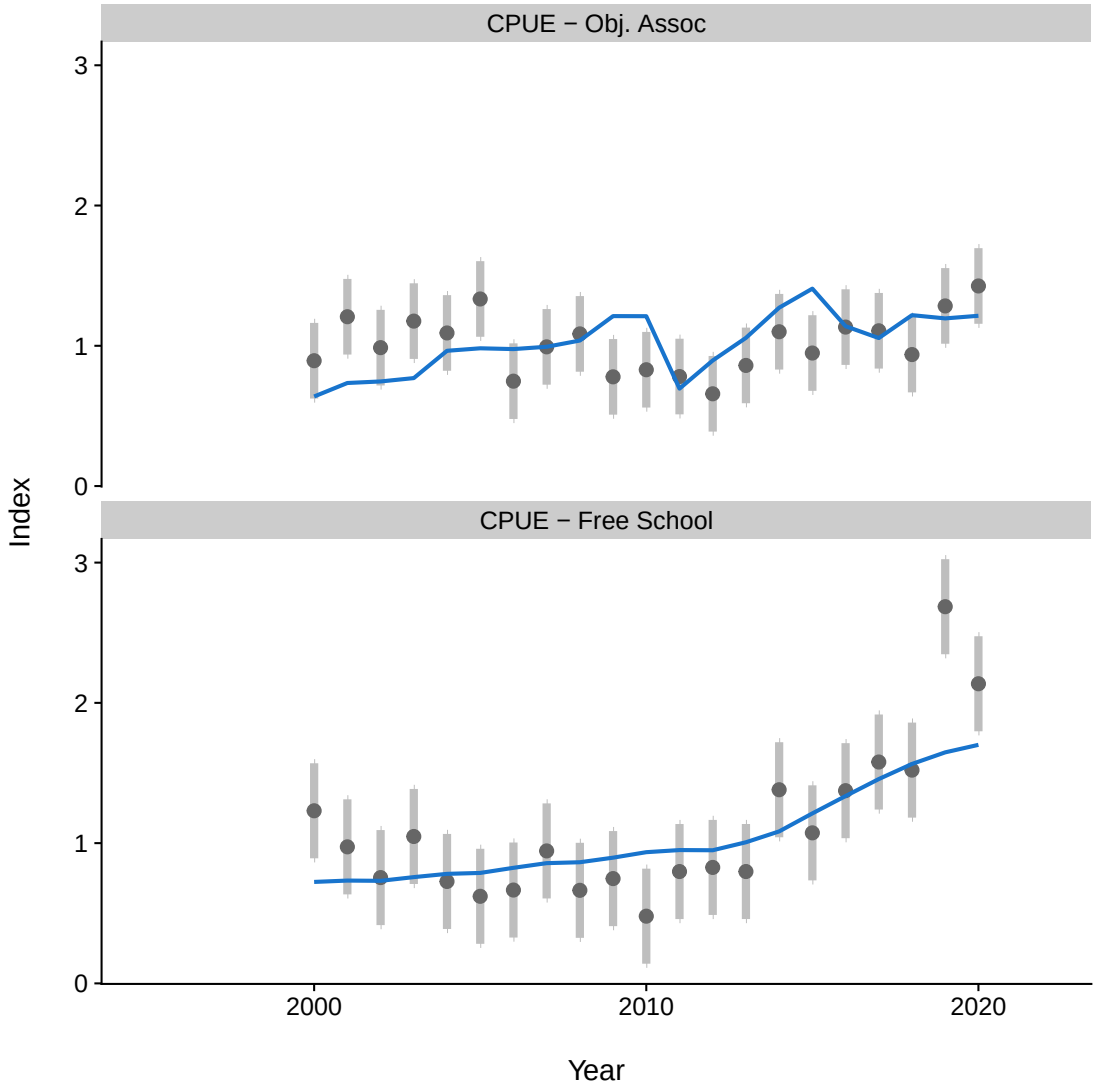

Figure 20: Observed (grey dots) vs. predicted (blue line) CPUE on the log-scale for index longline fleets under the diagnostic case, with vertical light grey bands showing the 95% credible interval for each year index.

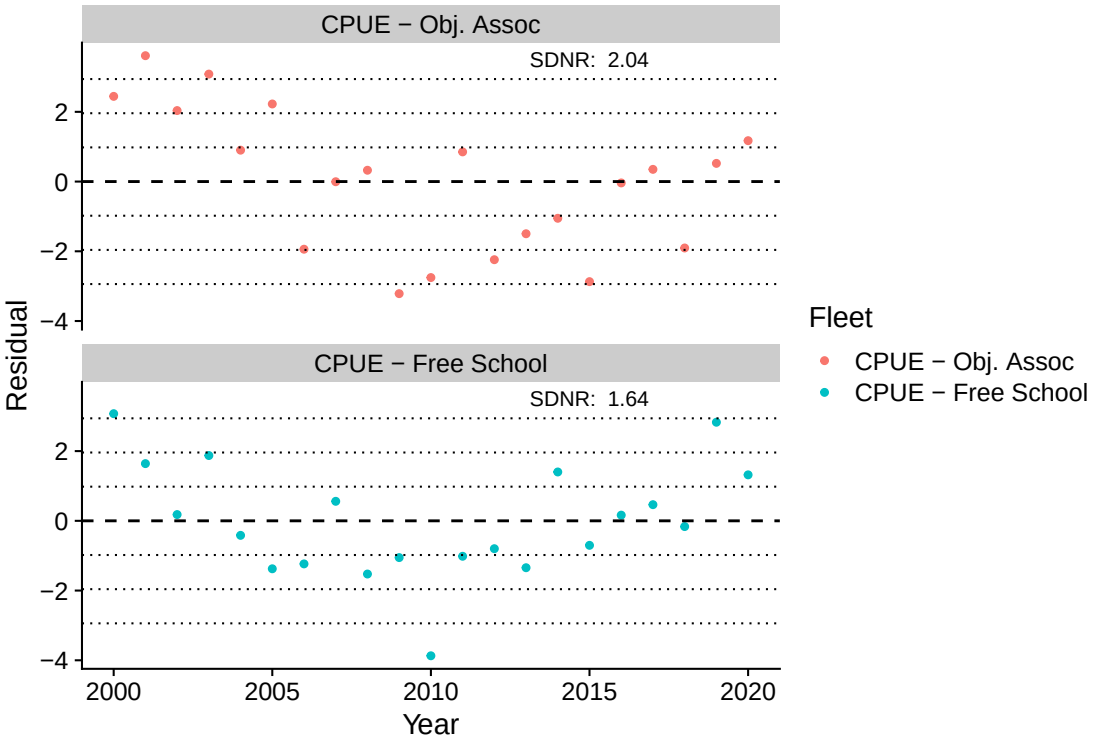

Figure 21: Residuals for CPUE indices from two longline fleets under the diagnostic case.

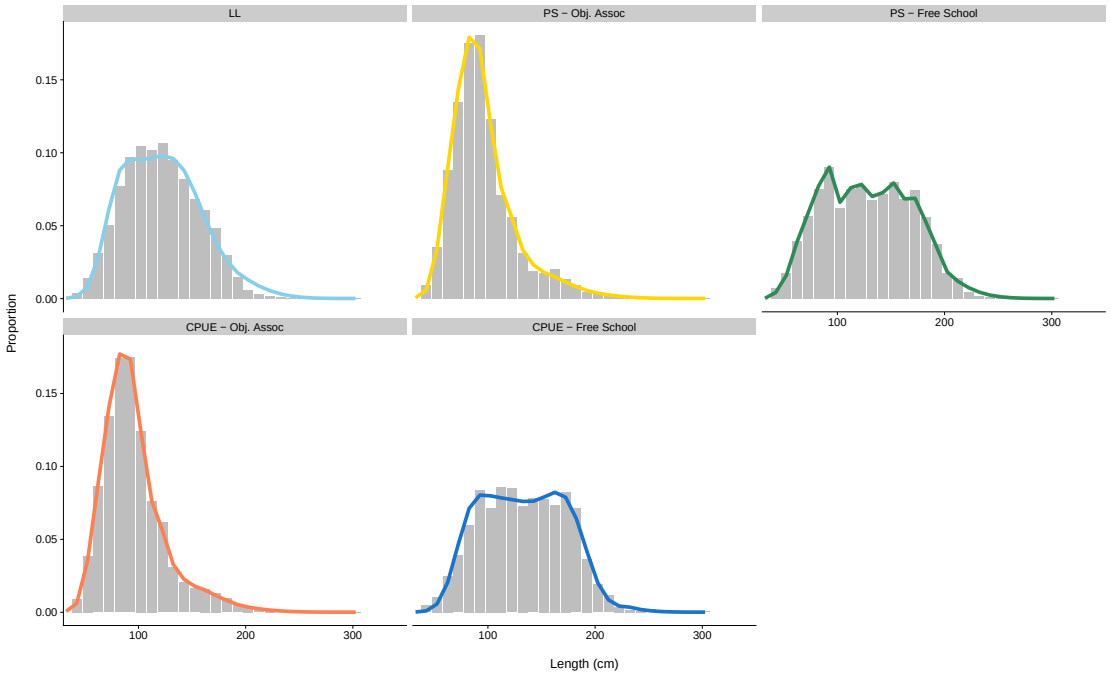

Figure 22: Observed (grey bars) vs. predicted (coloured line) catch-at-length for each fleet aggregated over all years for the diagnostic case.

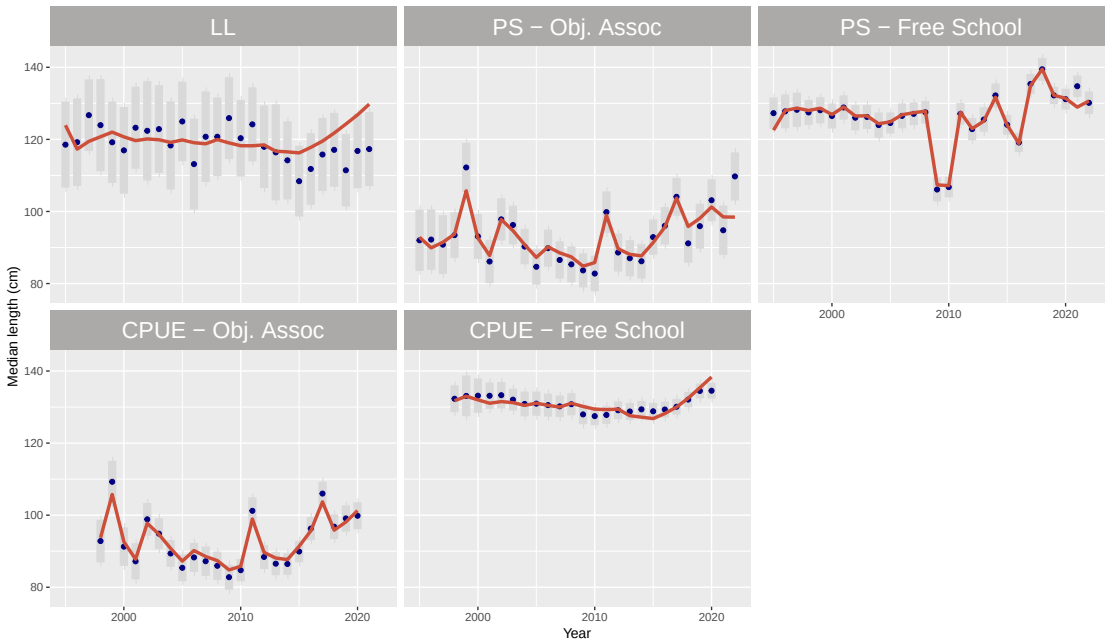

Figure 23: Temporal trend in the observed (navy points) vs. predicted (red line) catch-at-length for each fleet for the diagnostic case. The grey bands cover the 95% quantile range for the observations.

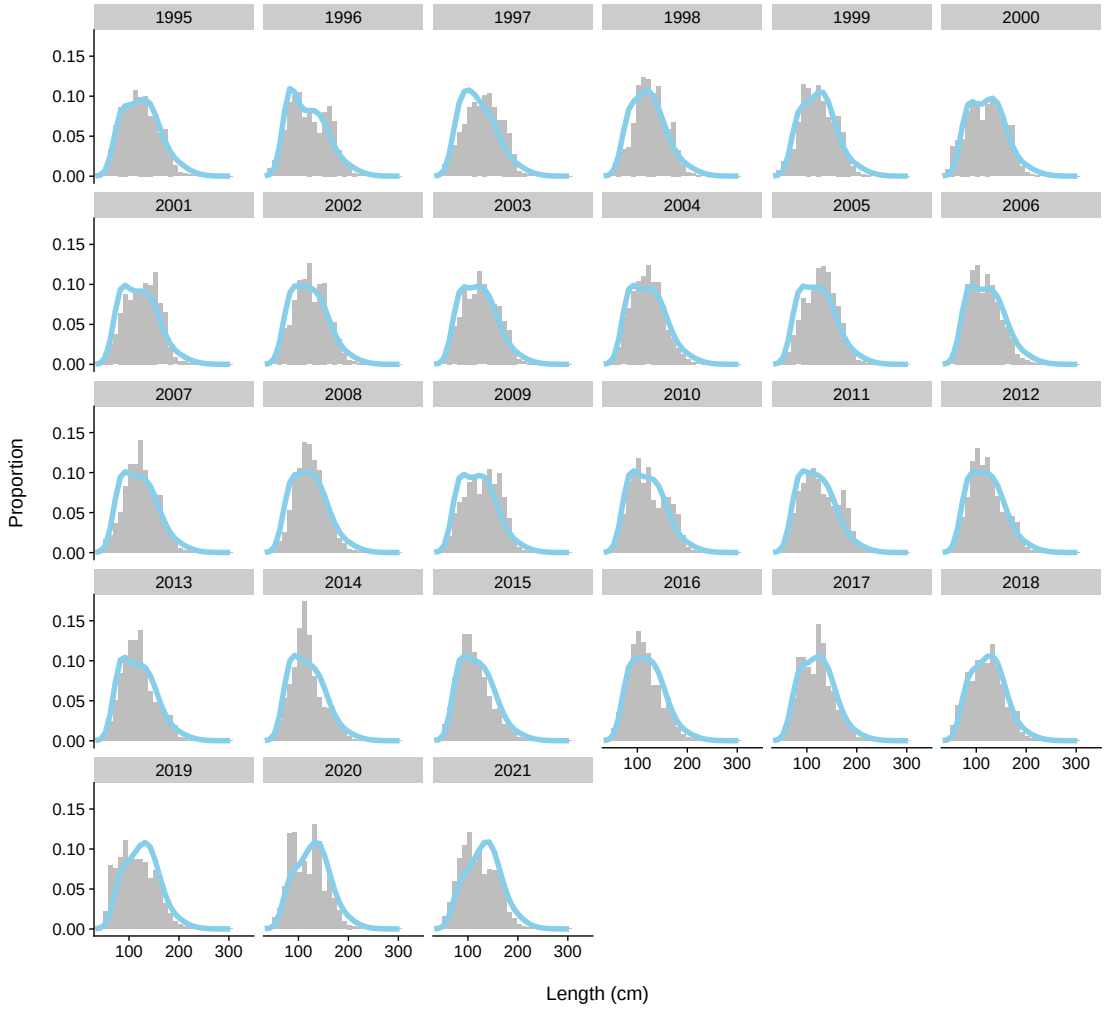

Figure 24: Observed (grey bars) vs. predicted (coloured line) catch-at-length by year for the longline capture fleet in the diagnostic case.

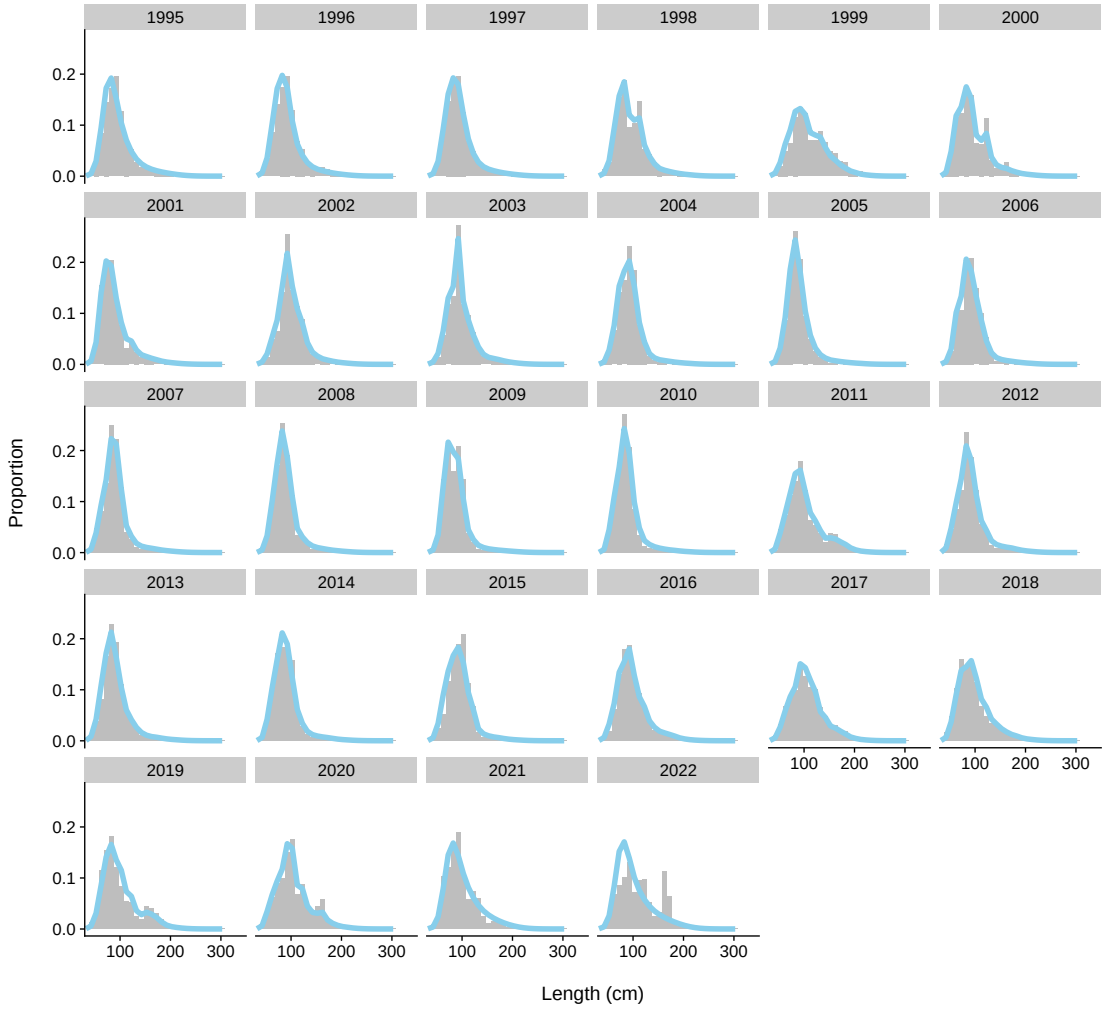

Figure 25: Observed (grey bars) vs. predicted (coloured line) catch-at-length by year for the object-associated purse-seine capture fleet in the diagnostic case.

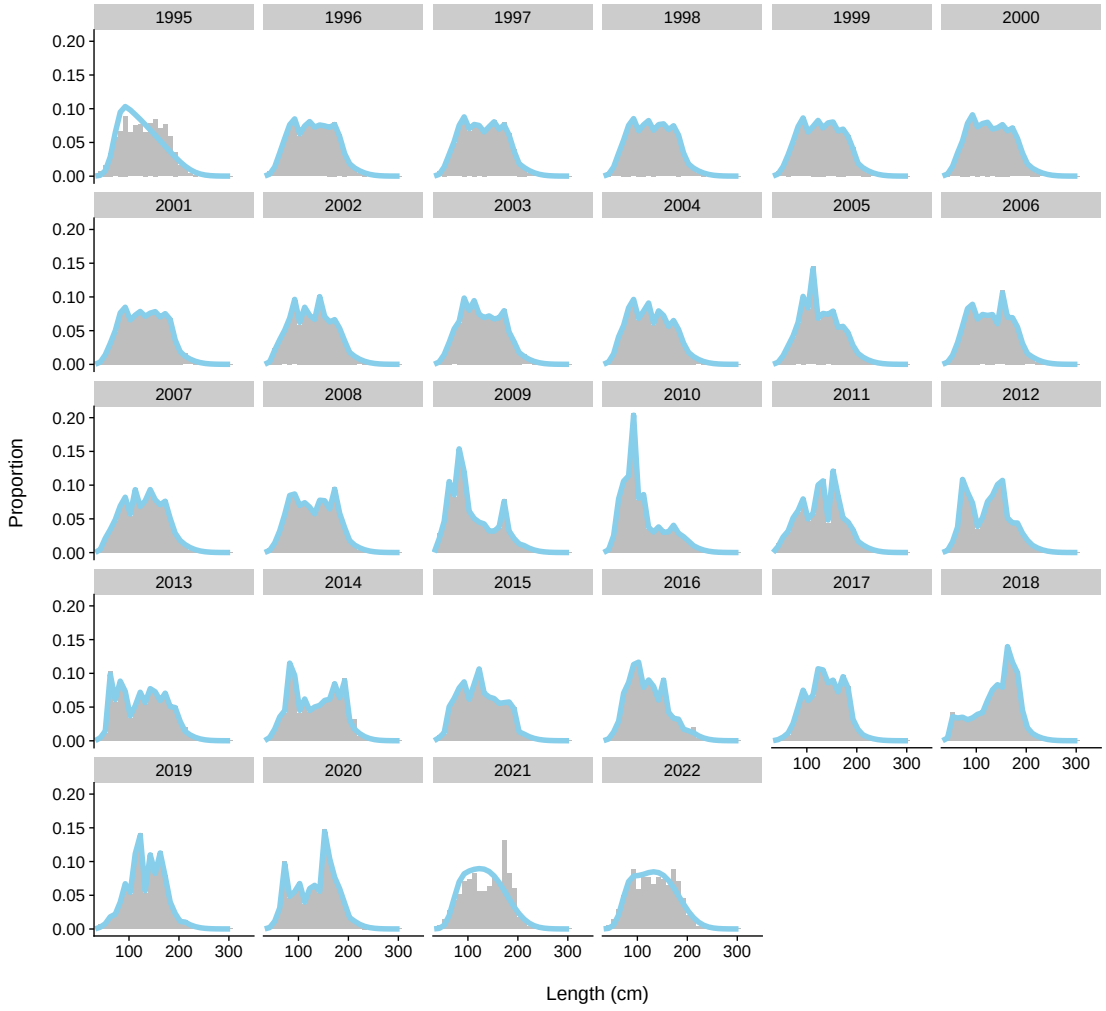

Figure 26: Observed (grey bars) vs. predicted (coloured line) catch-at-length by year for the free-school purse-seine capture fleet in the diagnostic case.

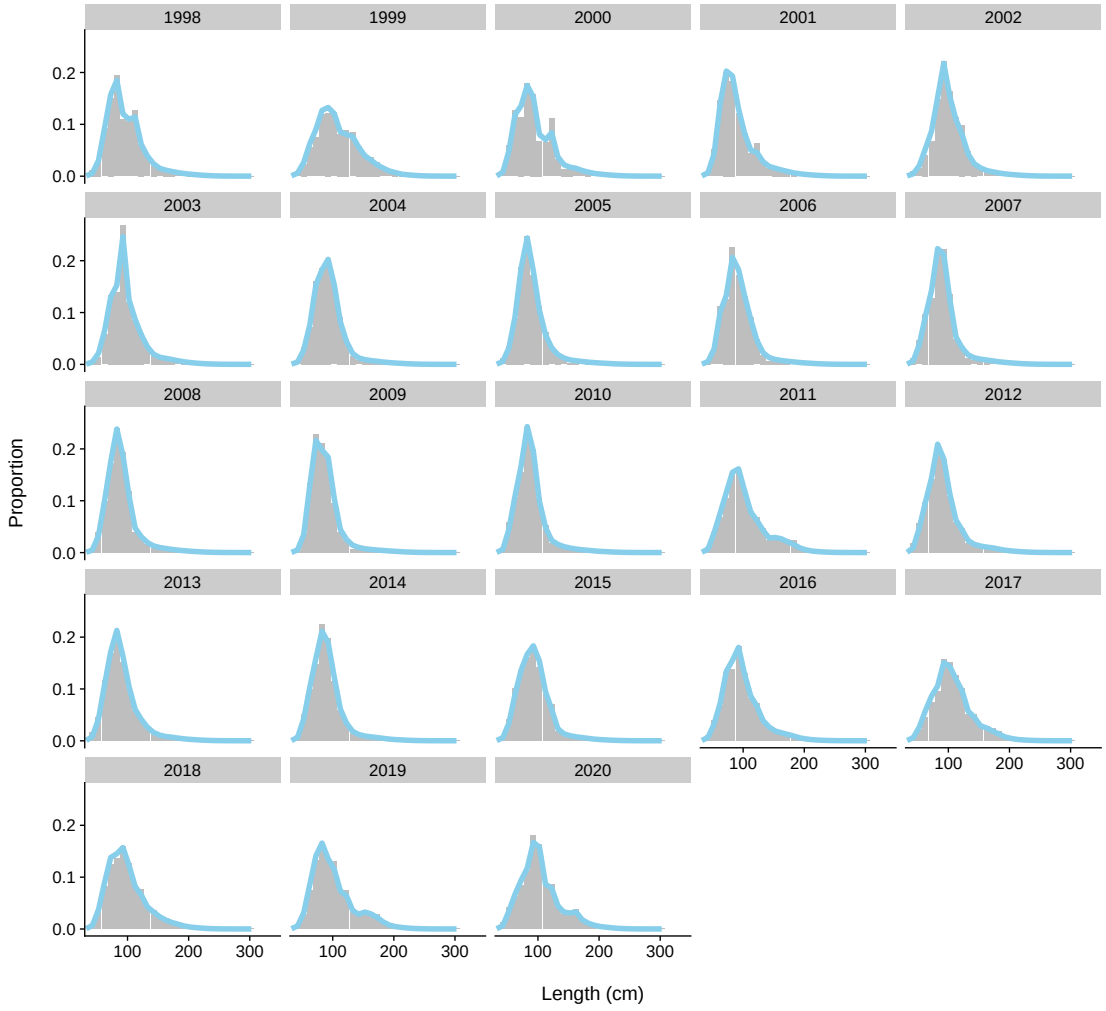

Figure 27: Observed (grey bars) vs. predicted (coloured line) catch-at-length by year for the object-associated purse-seine CPUE index fleet in the diagnostic case.

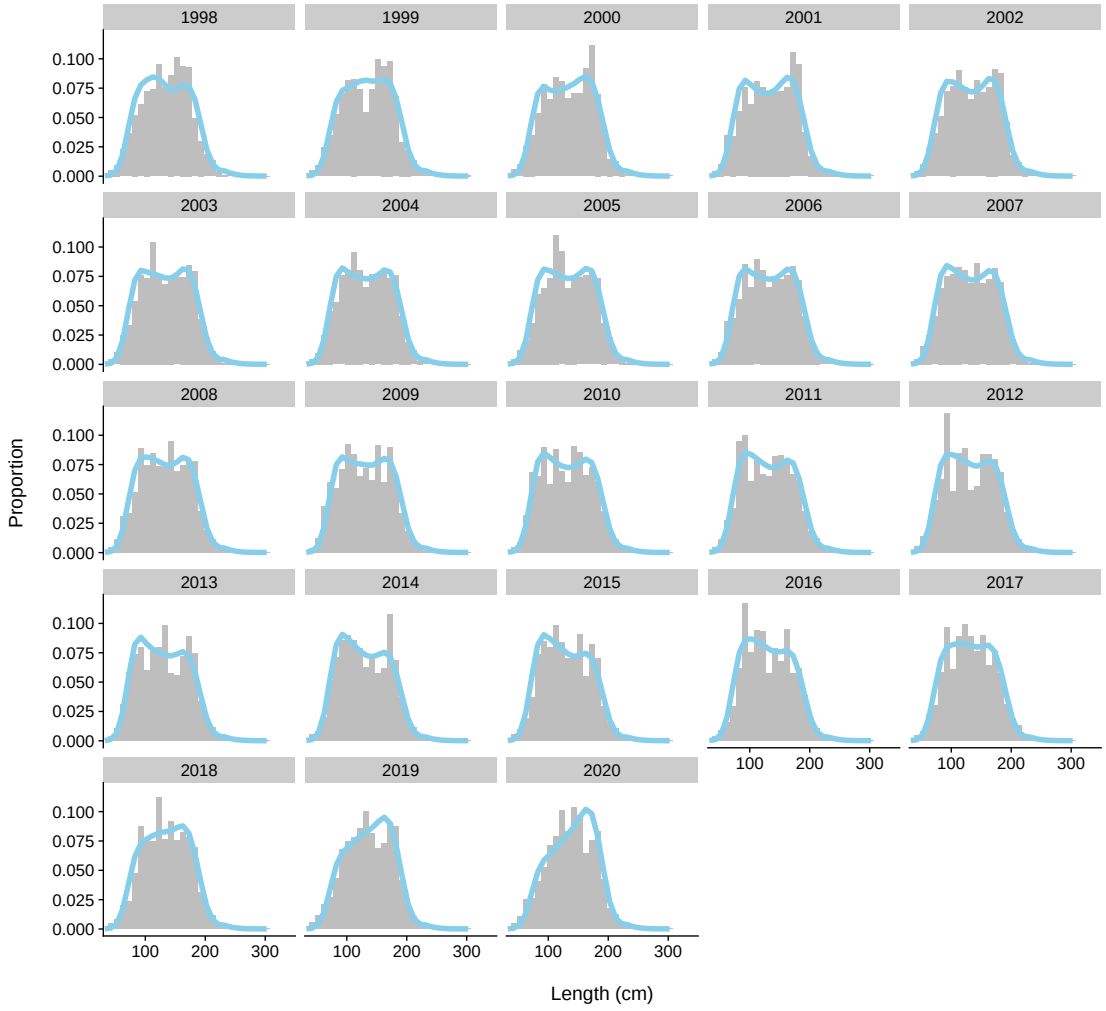

Figure 28: Observed (grey bars) vs. predicted (coloured line) catch-at-length by year for the free-school purse-seine CPUE index fleet in the diagnostic case.

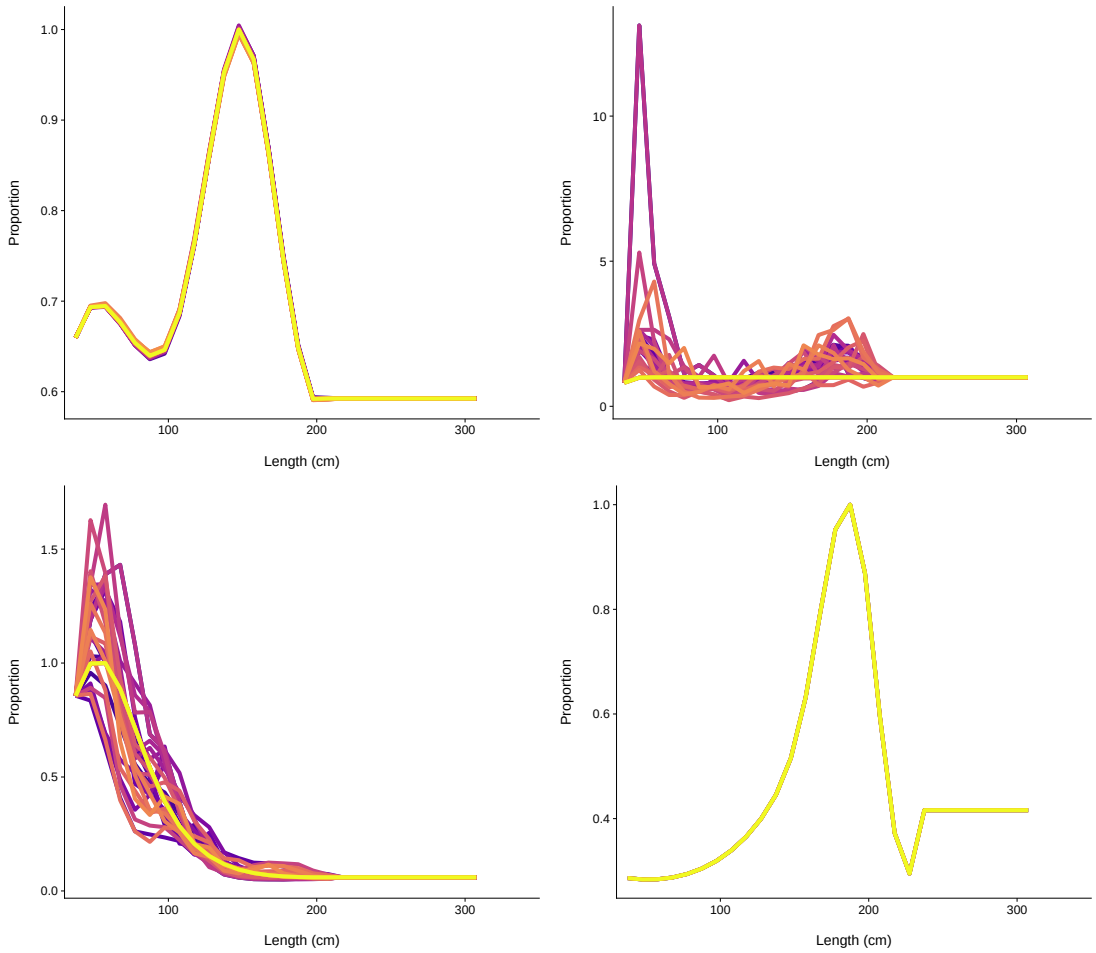

Figure 29: Mean estimated (or fixed) selectivity (yellow) and annual deviation estimated by a two-dimensional auto-regressive process for the longline capture fleet (top-left), free-school purse-seine capture fleet (top-right), object-associated purse-seine (shared selectivity for capture and index fleets; bottom left), and free-school purse-seine CPUE index fleet (bottom-right).

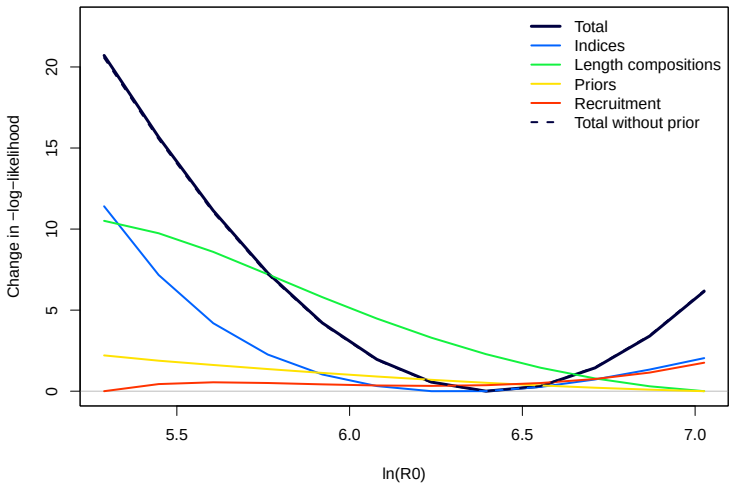

Figure 30: Relative change in log-likelihood for different values of $LN(R_0)$, for the total likelihood and contribution by each component.

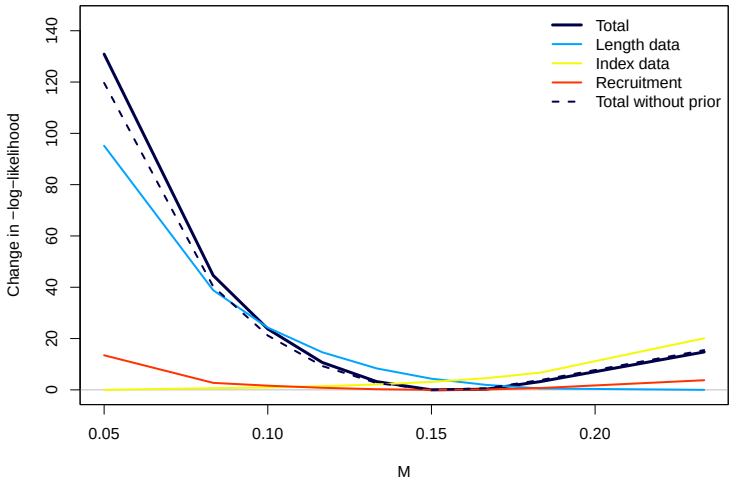

Figure 31: Relative change in log-likelihood for different values of M, for the total likelihood and contribution by each component.

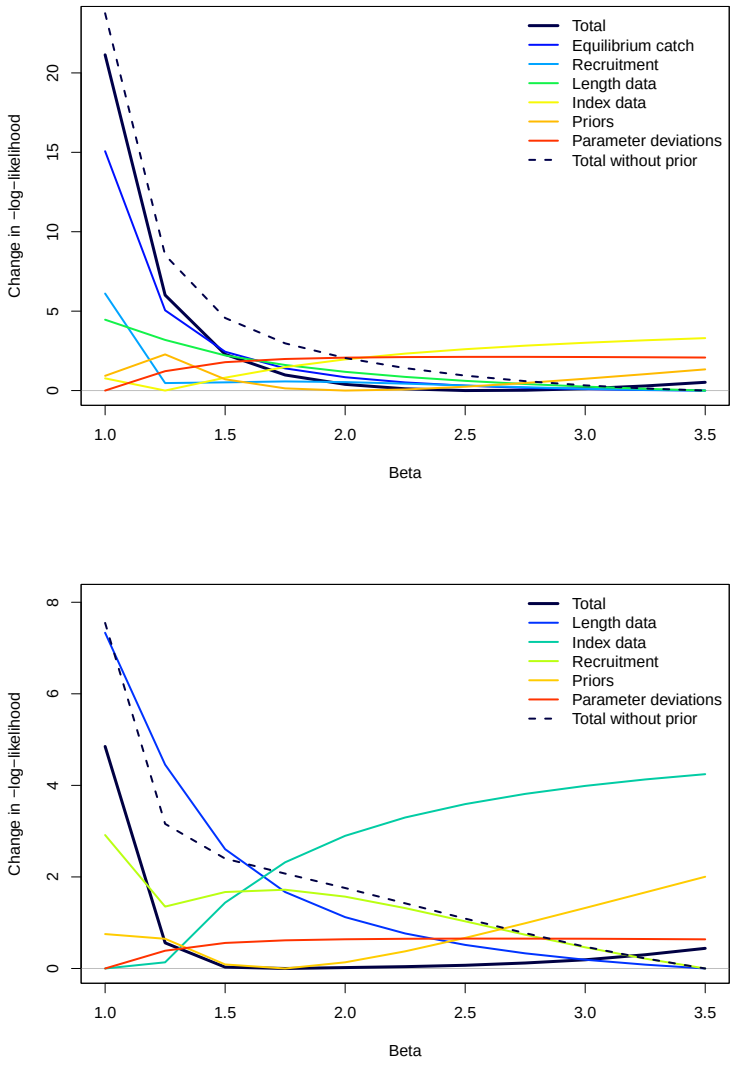

Figure 32: Relative change in log-likelihood for different values of $beta$, for the total likelihood and contribution by each component.

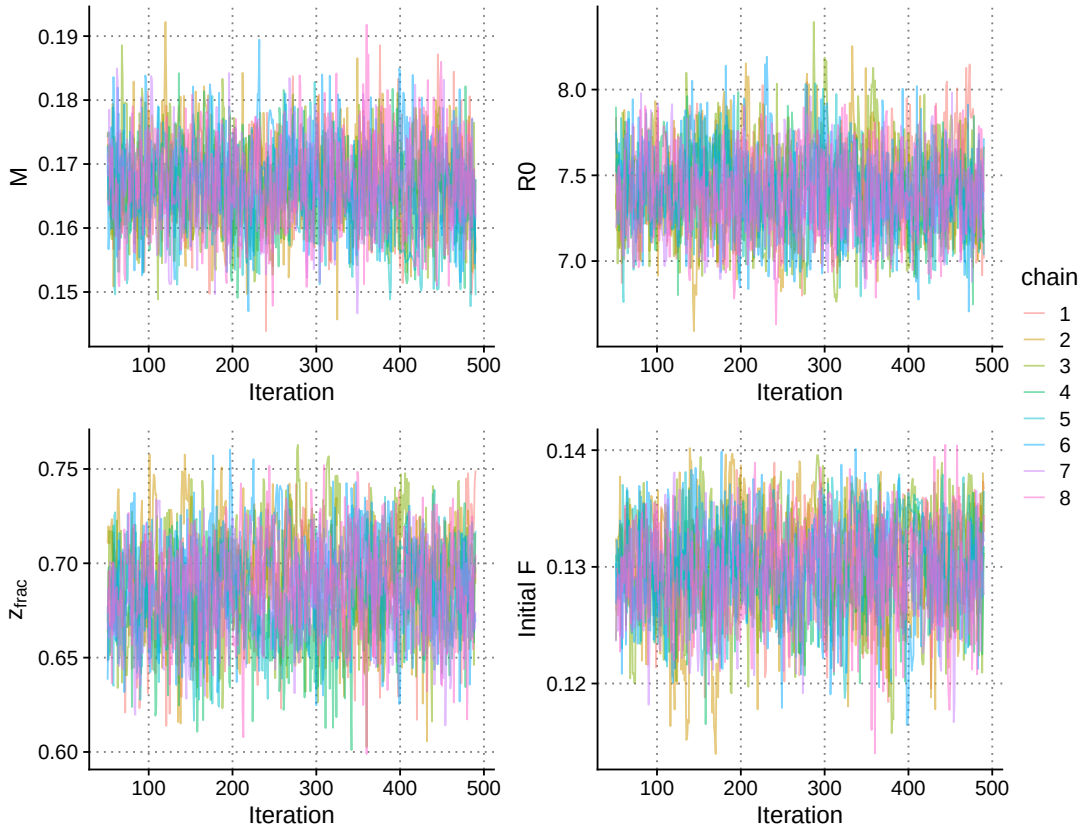

Figure 33: Posterior MCMC traces for R_O and natural mortality (M), the stock-recruit parameter z_{frac}, and initial fishing mortality F, derived from 8 independent MCMC chains (coloured lines).

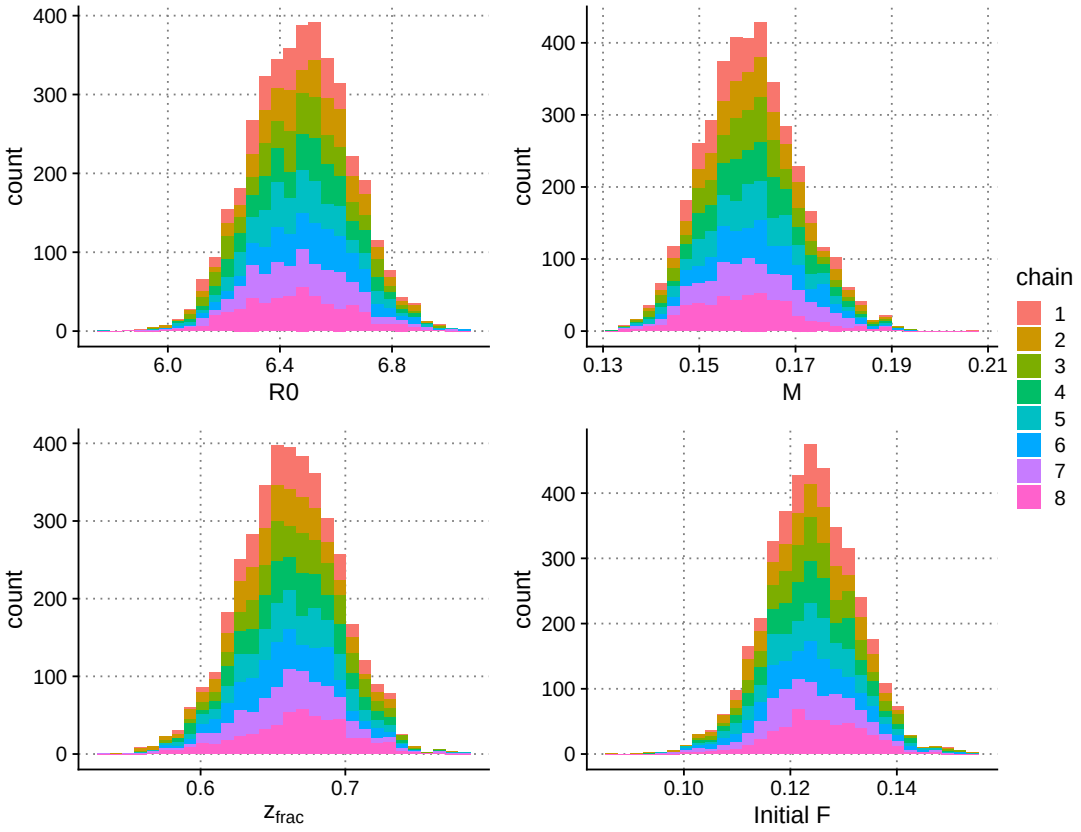

Figure 34: Posterior densities of R_O and natural mortality (M), the stock-recruit parameter z_{frac}, and initial fishing mortality F, derived from 8 independent MCMC chains (coloured bars).

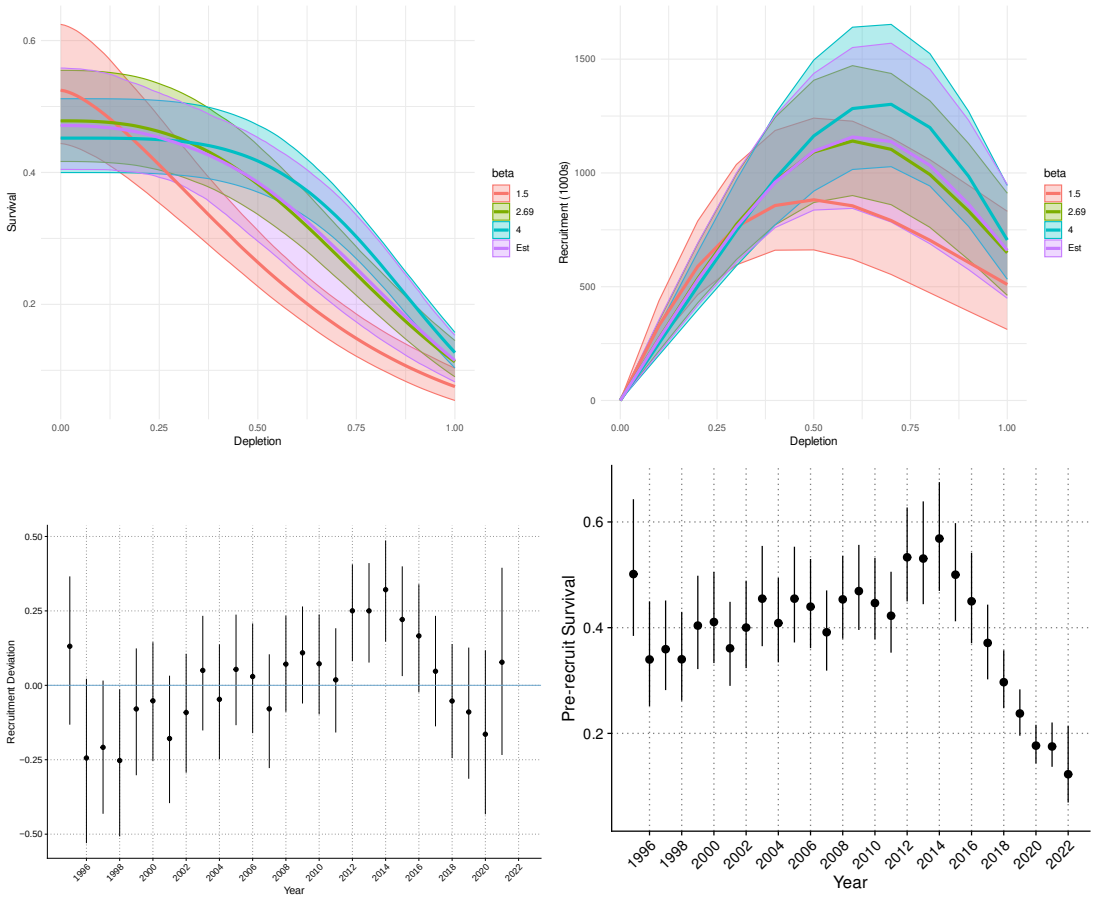

Figure 35: Estimated stock recruit relationship at different levels of fixed $beta$: Expected pre-recruit-survival (top left) and expected recruitment (top right) with associated 95% credible intervals; recruitment deviations and realised pre-recruit survival in the diagnostic case with 95% credible intervals estimated by MCMC.

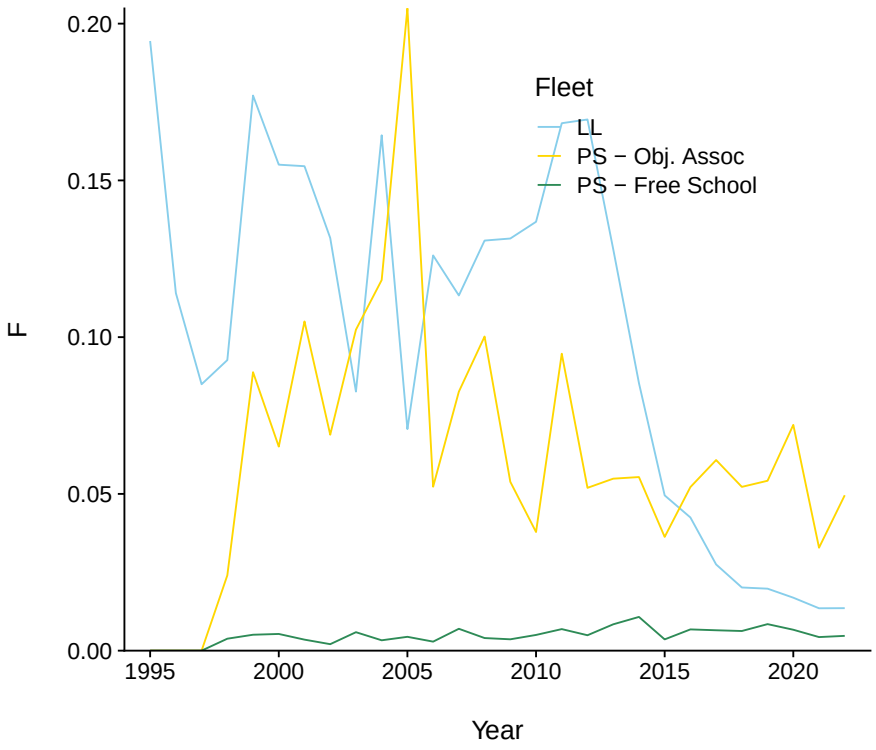

Figure 36: Fishing mortality by fleet estimated for the diagnostic case over the time-span of the assessment.

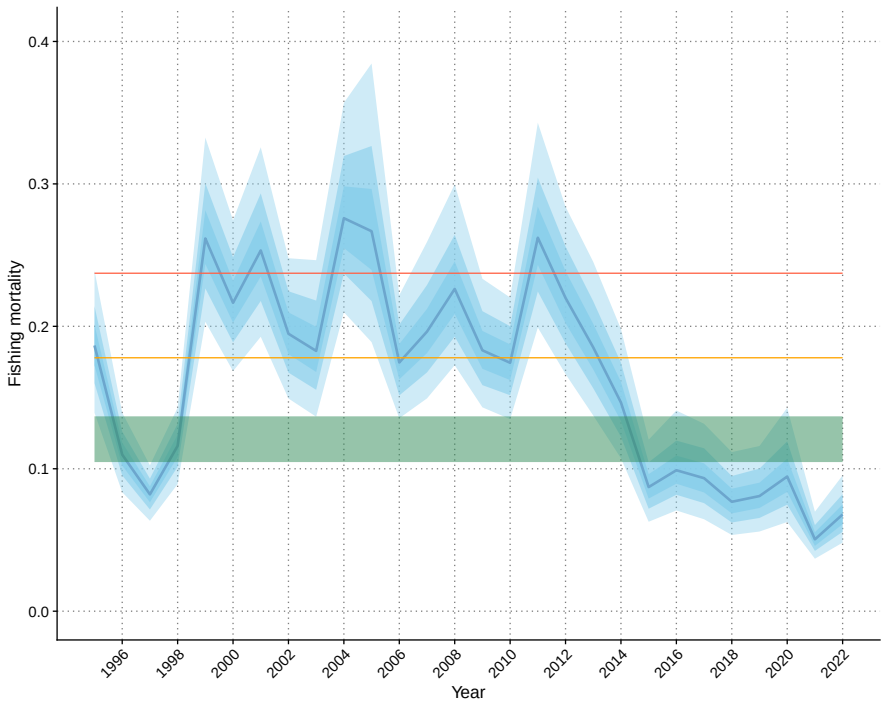

Figure 37: Posterior densities of Fishing mortality F, with posterior percentiles indicated by the colour fill. The posterior distribution of fishing mortality at MSY (F_{MSY}) is shown in green, point estimates of F_{lim} and F_{crash} are given in orange and red, respectively.

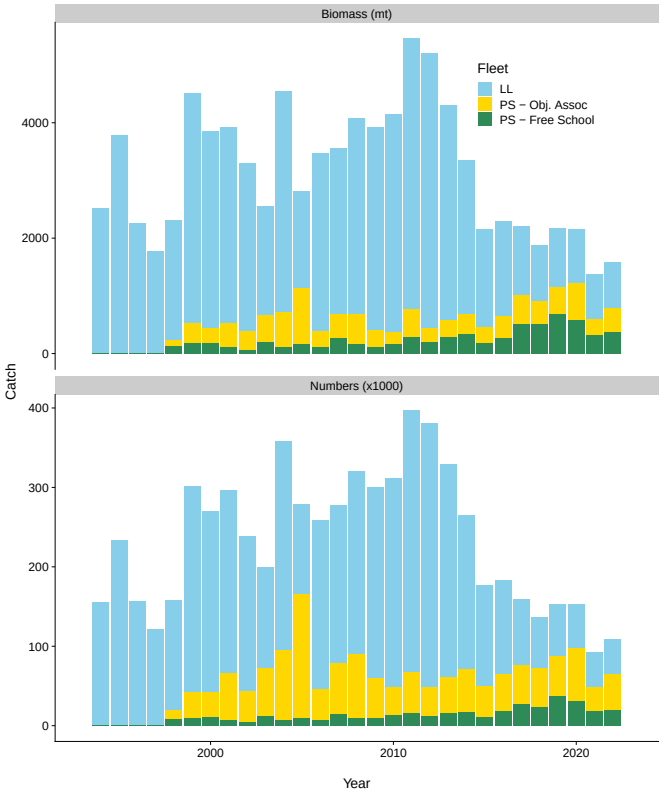

Figure 38: Retained catch by fleet in biomass and numbers.

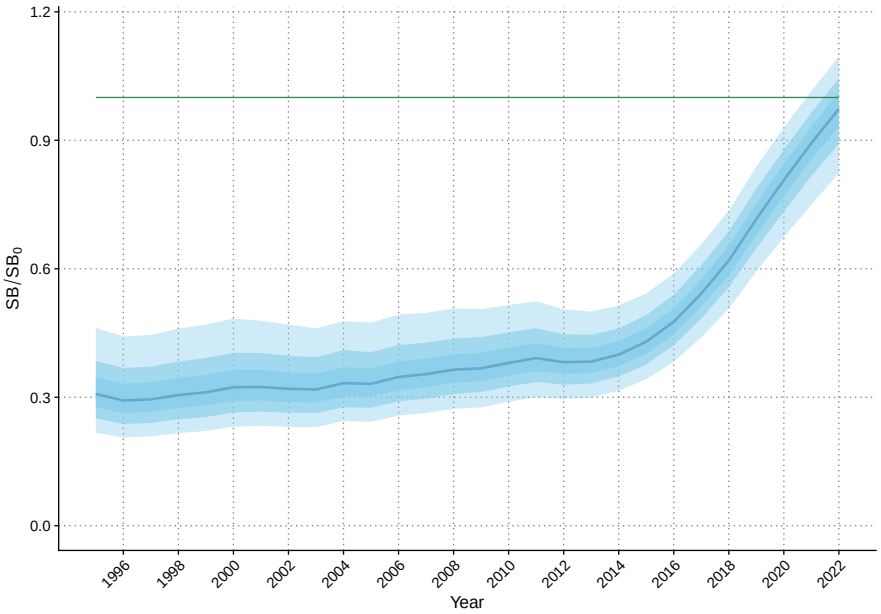

Figure 39: Posterior densities of stock status (SB/SB_O), with posterior percentiles (90%, 95% and 99%) indicated by the colour fill.

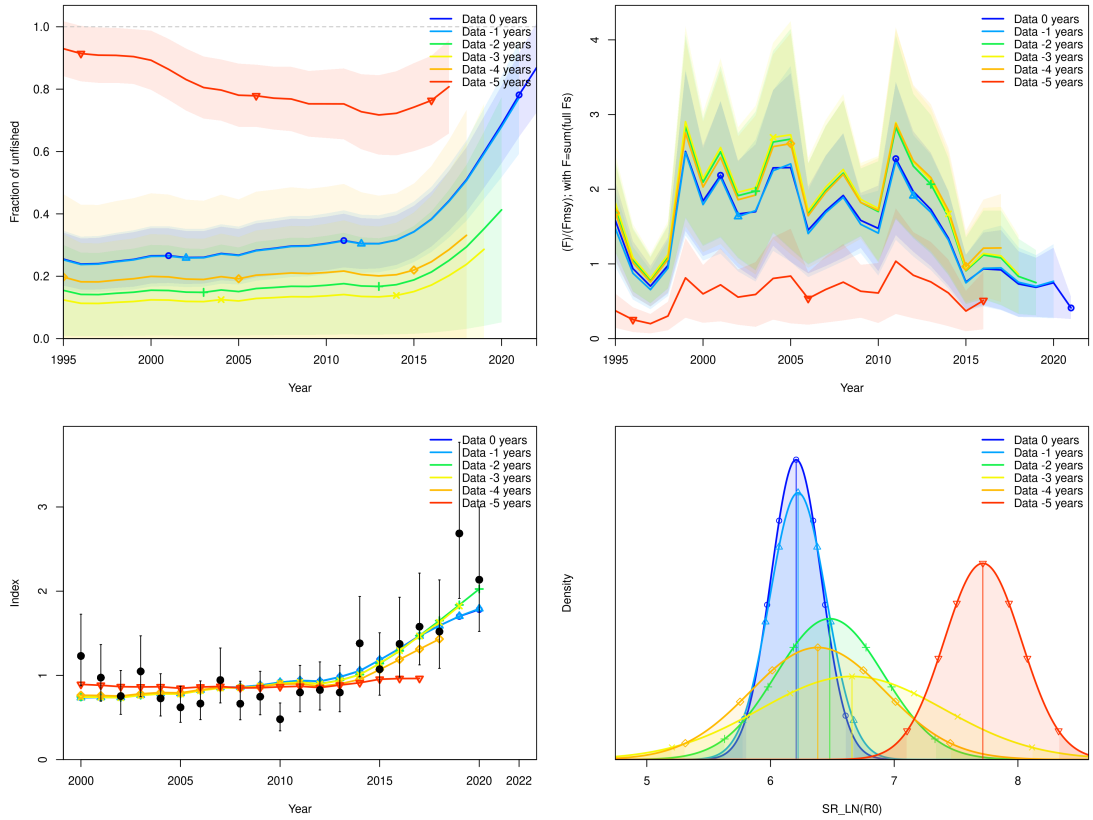

Figure 40: Retrospective patterns of relative spawning biomass, fishing mortality, CPUE fits and unfished biomass with estimated uncertainty levels.

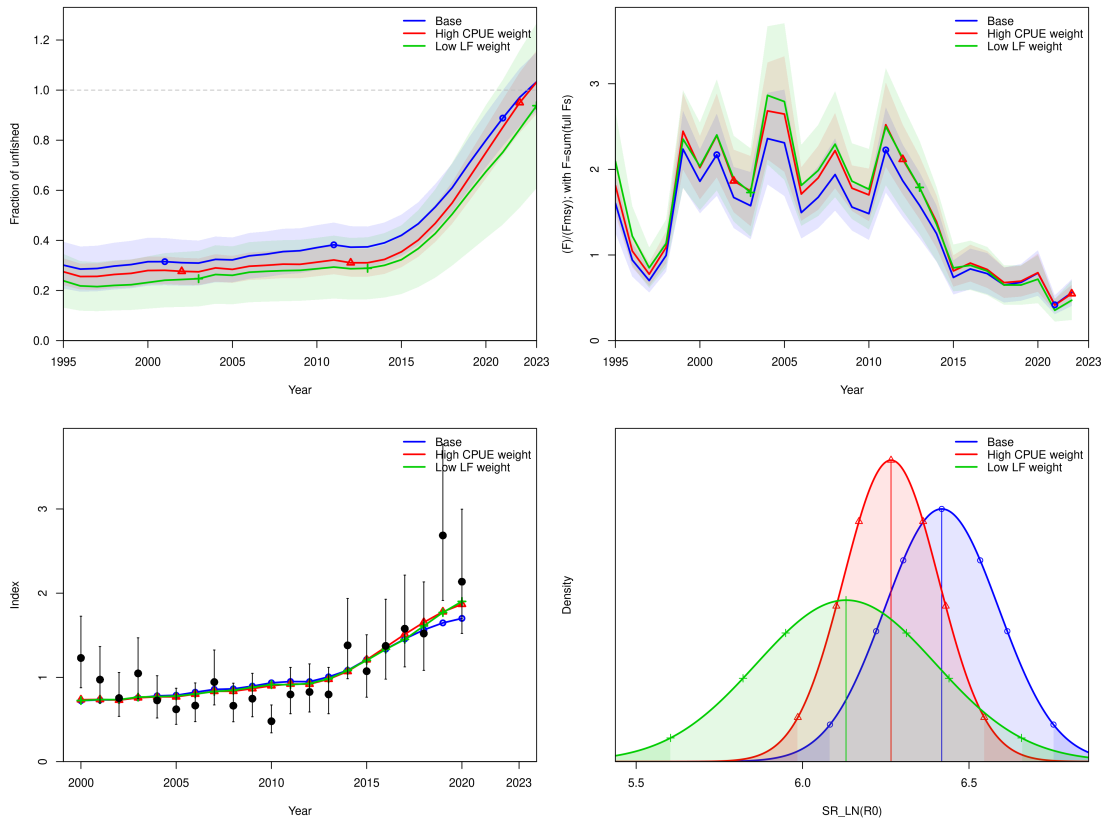

Figure 41: Comparison of relative spawning biomass, fishing mortality, CPUE fits and unfished biomass size for the 2024 diagnostic case and alternative data weighting options, with estimated uncertainty levels from stock synthesis.

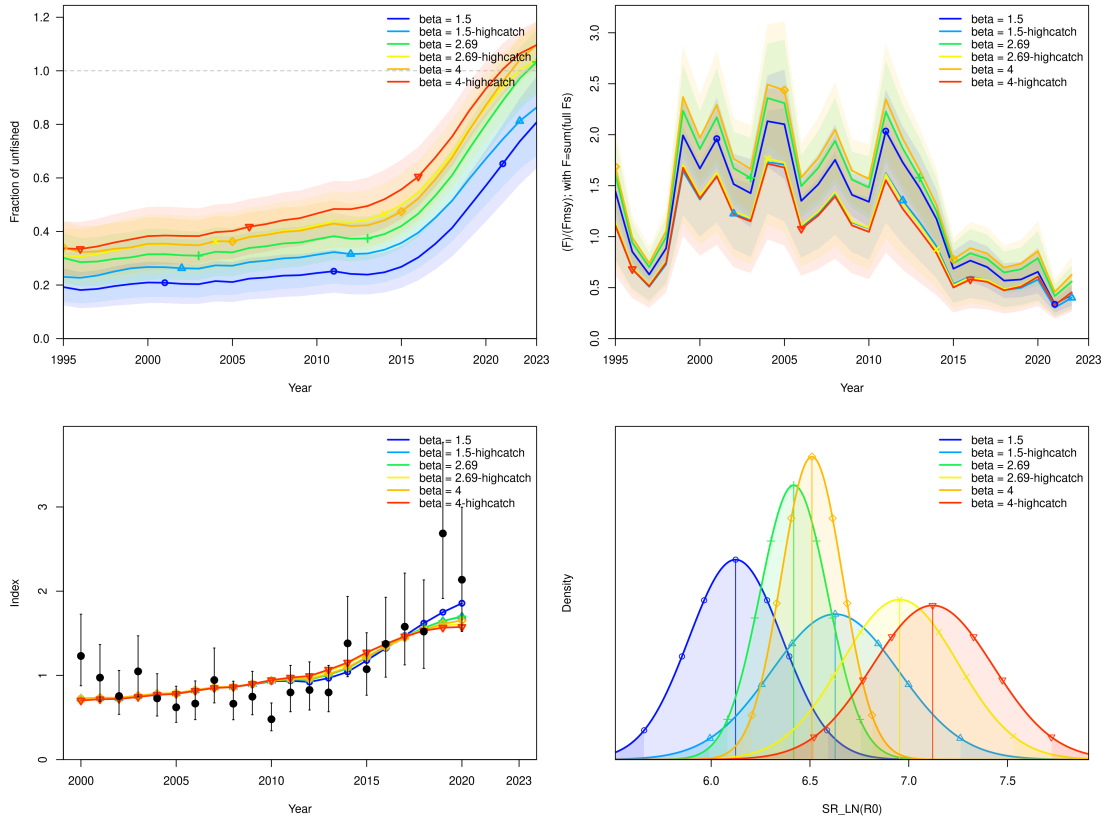

Figure 42: Comparison of relative spawning biomass, fishing mortality, CPUE fits and unfished biomass size for the 2024 diagnostic case and alternative options for $beta$ (stock recruit shape) and initial catch, with estimated uncertainty levels from stock synthesis.

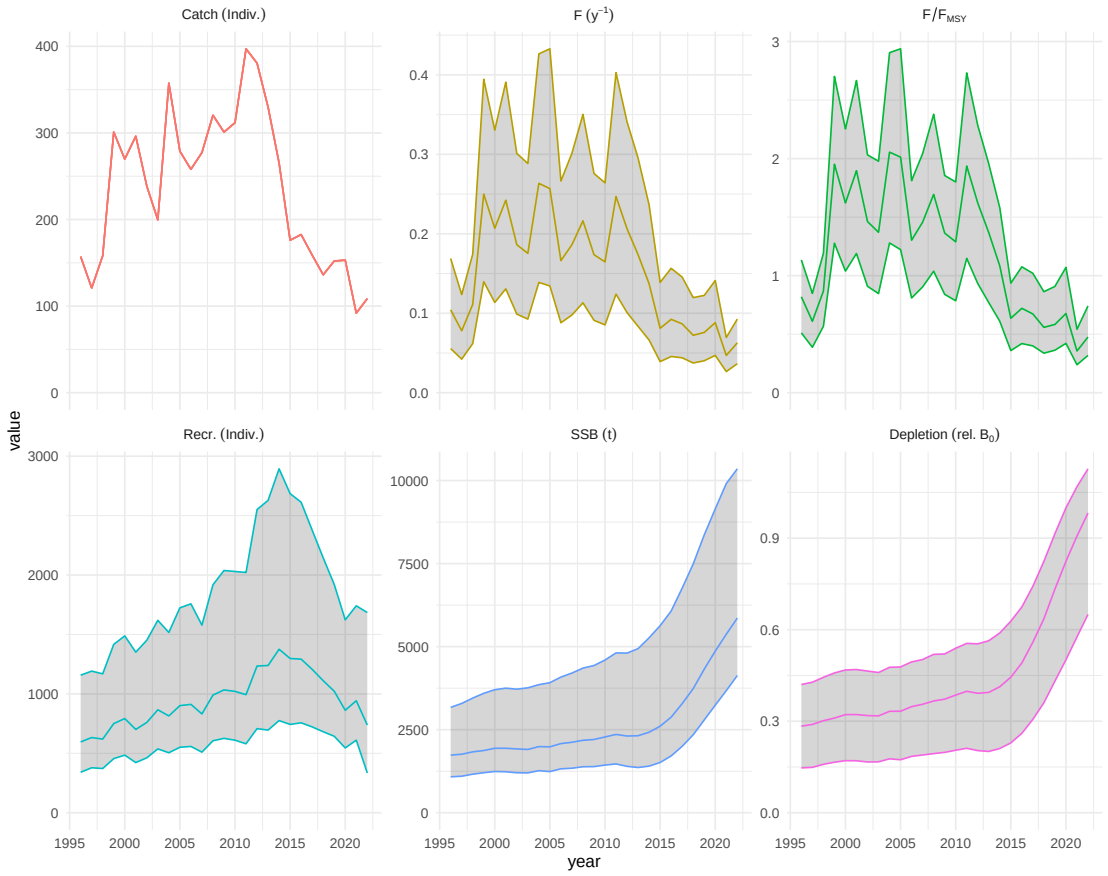

Figure 43: Catch, fishing mortality, recruitment, spawning biomass and depletion trajectories for an ensemble formed by models over an (unweighted) grid of fixed $beta$ options and initial catch, with uncertainty estimated using Monte Carlo draws from a multivariate log-normal based on the Hessian matrix estimated in SS3.

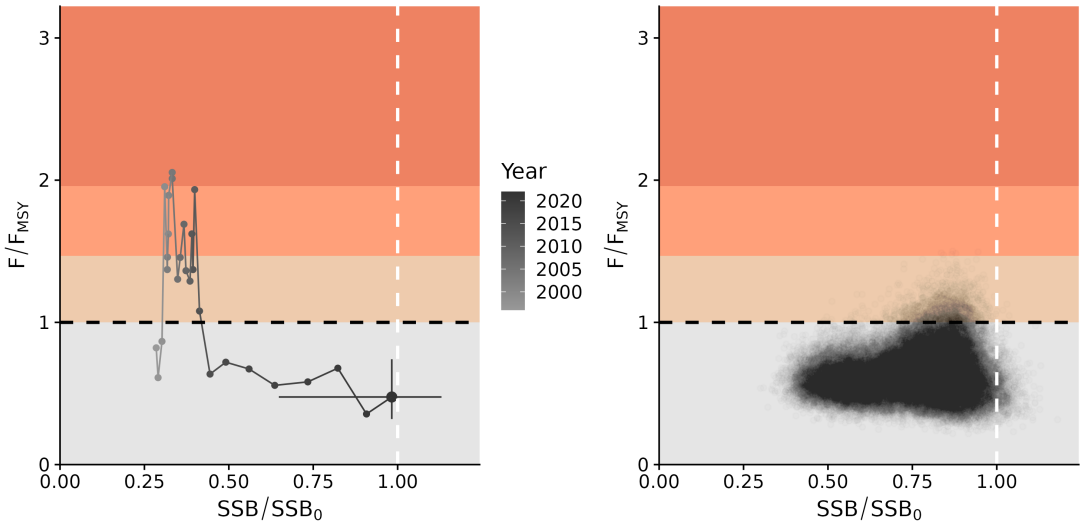

Figure 44: Majuro plots for recent (2019–2020) stock status based on an ensemble formed by SS3 models for silky shark over an (unweighted) grid of fixed $beta$ options and initial catch in the WCPFC. The top row shows outcomes for the base scenario, whereas the bottom row shows the outcomes across all three assumptions of initial depletion. Left hand plots show the stock trajectory, with uncertainty shown for the most recent year in the analysis (2022), whereas the plot on the right-hand side show individual draws from the posterior distribution(s) for recent (2019–2020) years with CPUE.

11.2 Alternative assessments

11.2.1 Length and age structured assessment model

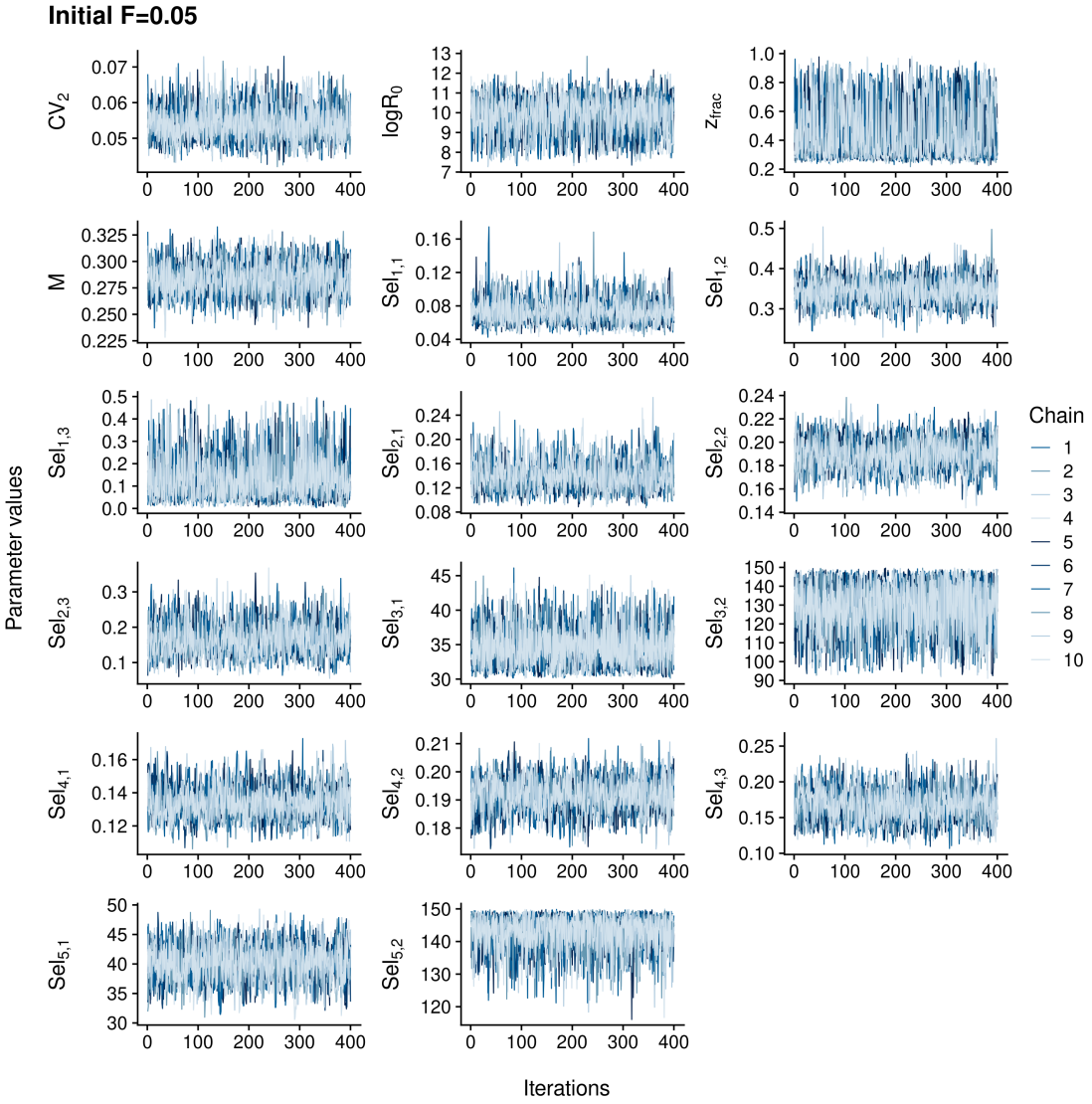

Figure 45: MCMC trace plots for biological and selectivity parameters from a length and age-structured model with an initial fishing mortality rate ($F_{init} = 0.05$). $\text{Sel}_{x,x}$ denotes selectivity parameters (not selectivity values for each length bin). The first subscript indicates the fleet type, and the second denotes the parameter. For example, $\text{Sel}_{1,1}$ is the first parameter of selectivity for the longline fleet, which is p_1 of the exponential logistic (see Equations (2) and (3) for more details about the parameters). The order of the fleet types and parameters are the same as those in Figure 57 and Table 3.

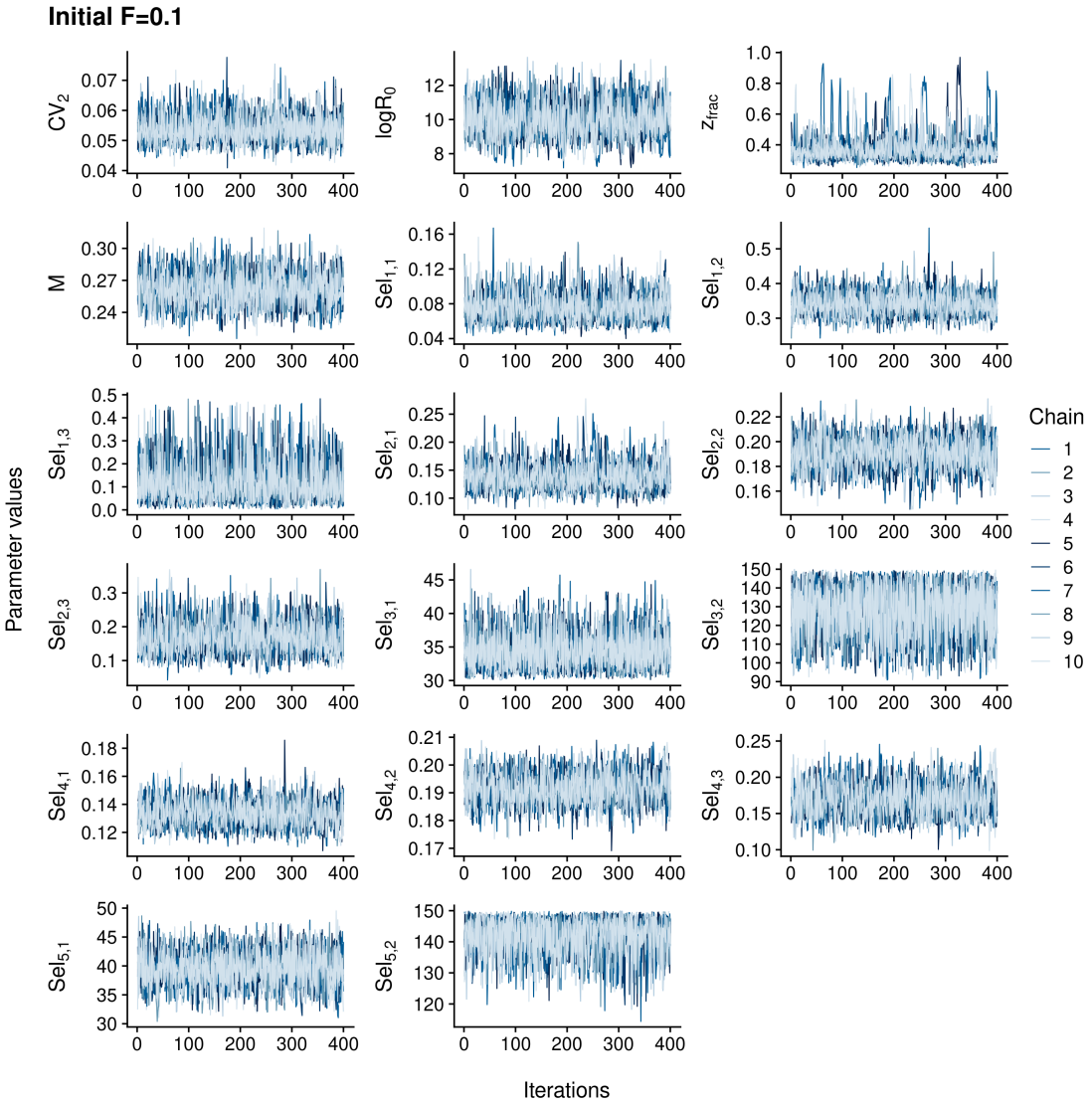

Figure 46: MCMC trace plots for biological and selectivity parameters from a length and age-structured model with an initial fishing mortality rate ($F_{init} = 0.1$). $\text{Sel}_{x,x}$ denotes selectivity parameters (not selectivity values for each length bin). The first subscript indicates the fleet type, and the second denotes the parameter. For example, $\text{Sel}_{1,1}$ is the first parameter of selectivity for the longline fleet, which is p_1 of the exponential logistic (see Equations (2) and (3) for more details about the parameters). The order of the fleet types and parameters are the same as those in Figure 57 and Table 3.

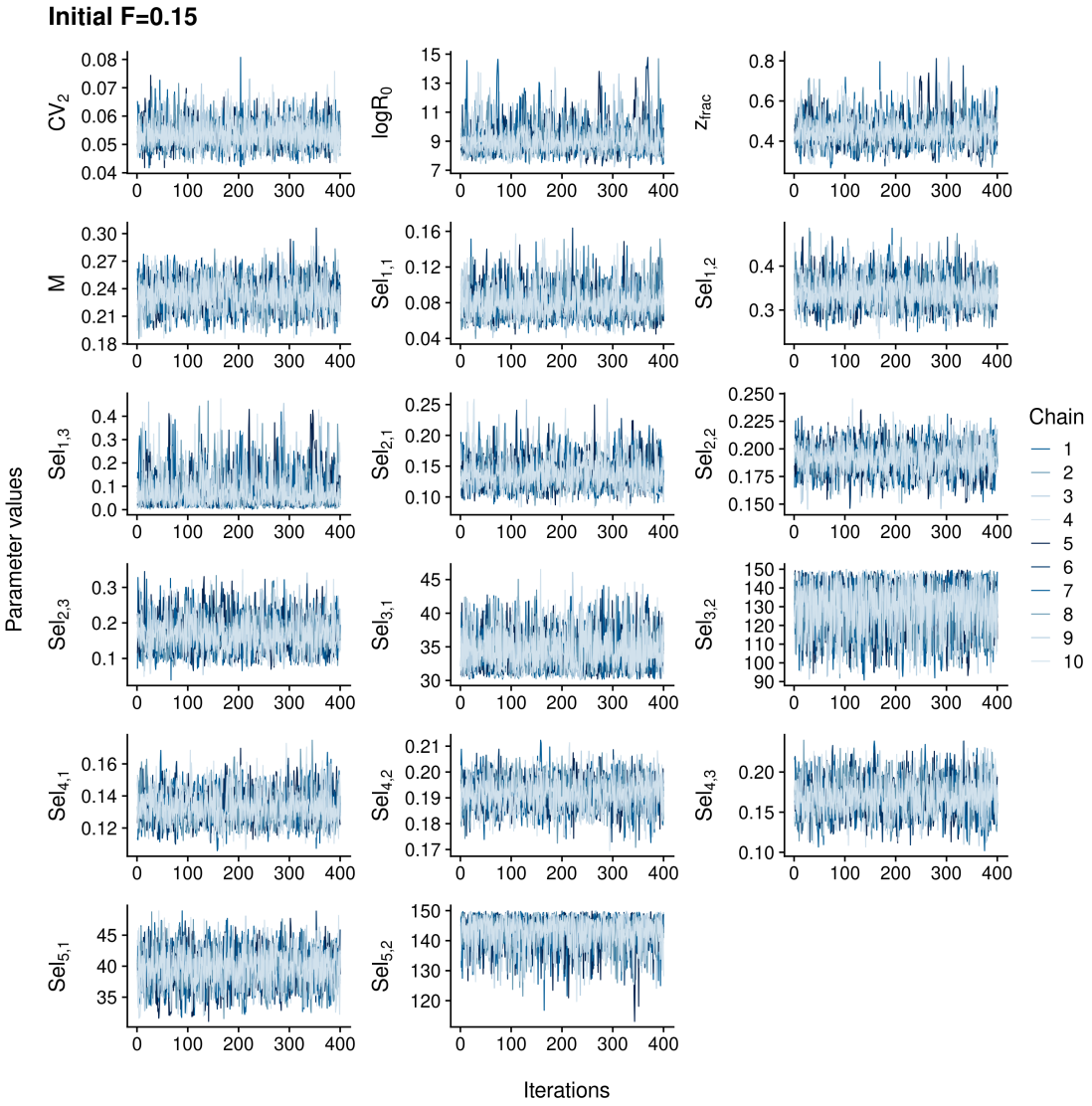

Figure 47: MCMC trace plots for biological and selectivity parameters from a length and age-structured model with an initial fishing mortality rate ($F_{init} = 0.15$). $\text{Sel}_{x,x}$ denotes selectivity parameters (not selectivity values for each length bin). The first subscript indicates the fleet type, and the second denotes the parameter. For example, $\text{Sel}_{1,1}$ is the first parameter of selectivity for the longline fleet, which is p_1 of the exponential logistic (see Equations (2) and (3) for more details about the parameters). The order of the fleet types and parameters are the same as those in Figure 57 and Table 3.

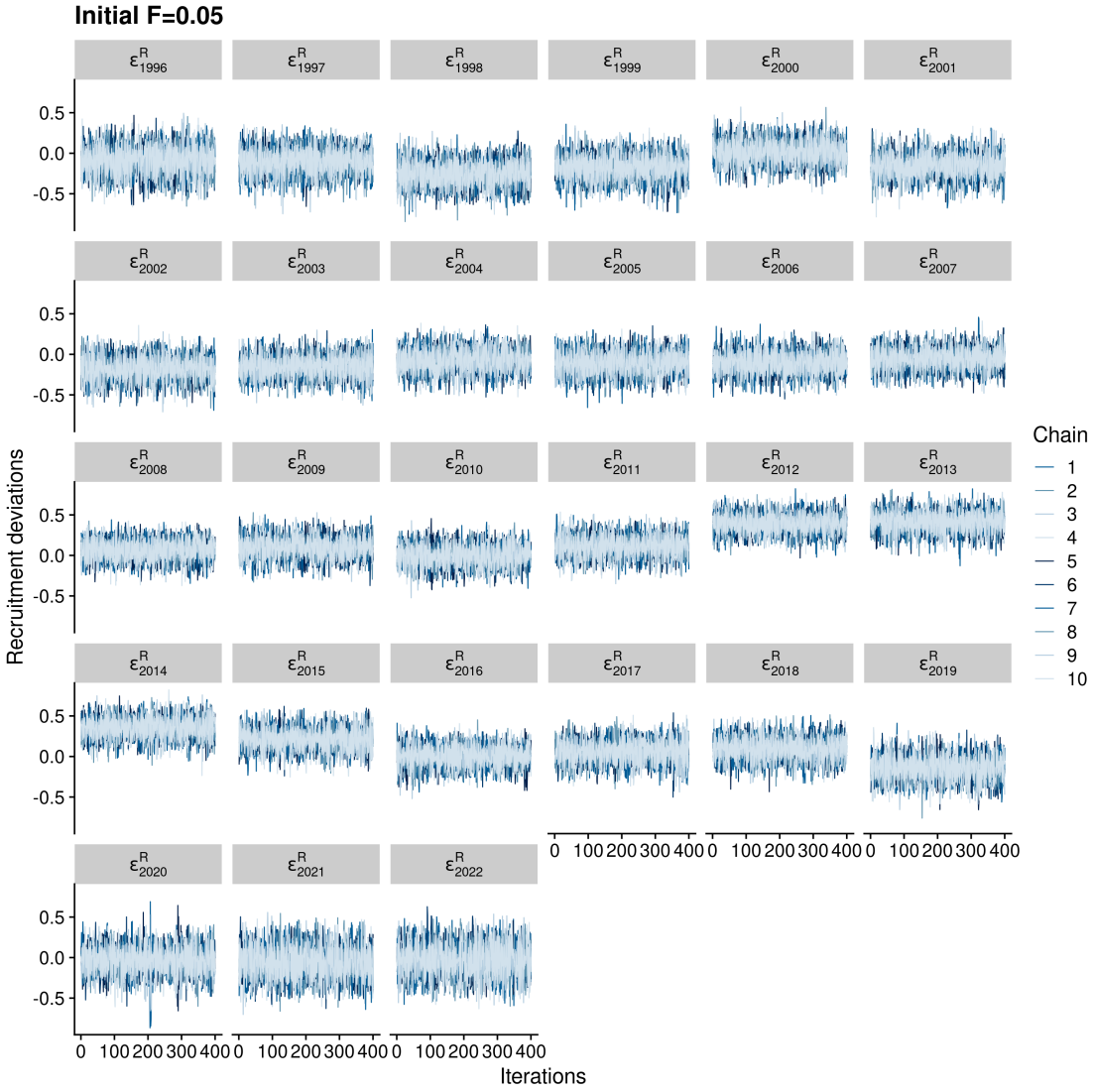

Figure 48: MCMC trace plots for recruitment deviaitions from a length and age - structured model with an initial fishing mortality rate ($F_{init} = 0.05$).

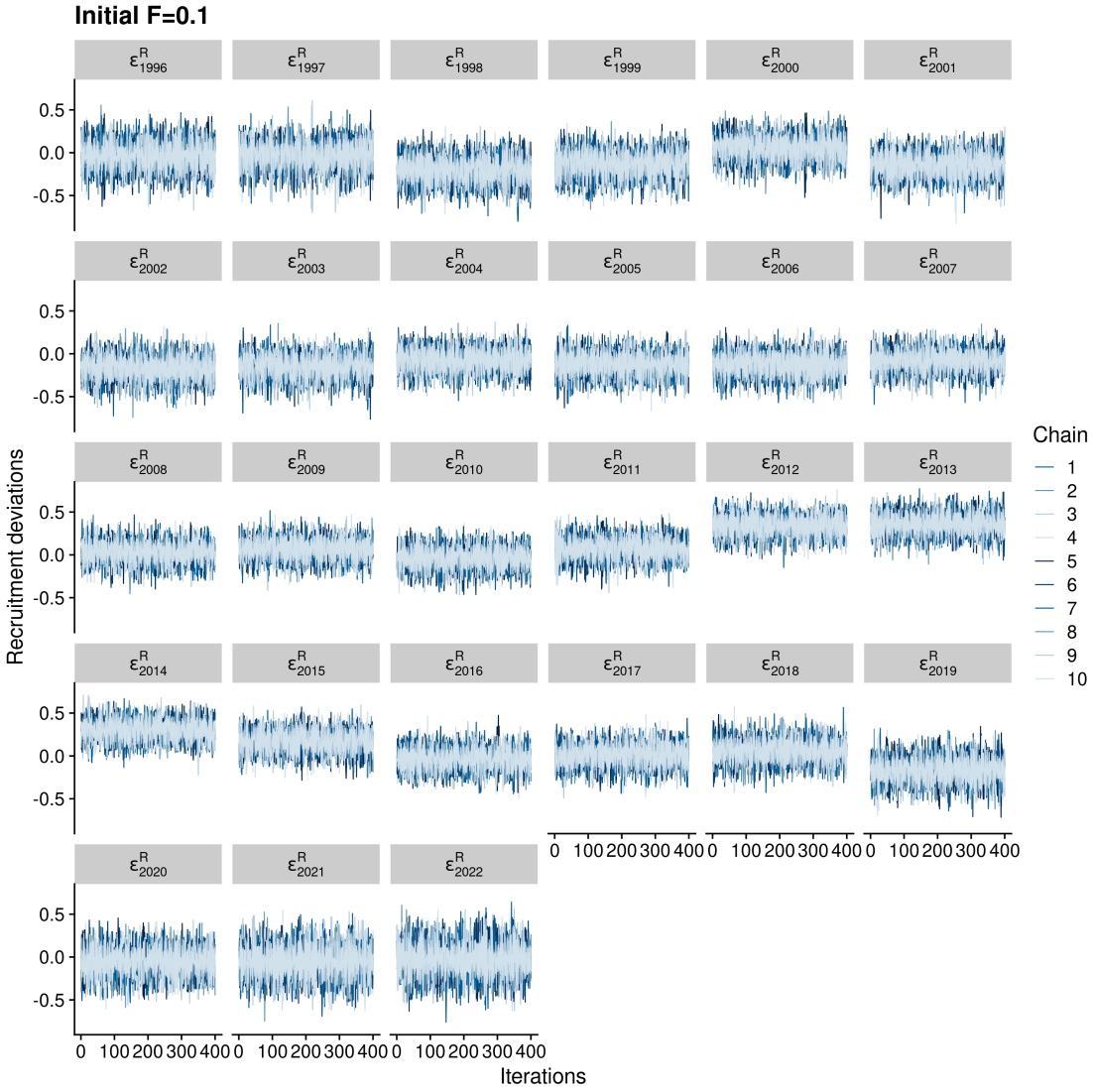

Figure 49: MCMC trace plots for recruitment deviaitions from a length and age - structured model with an initial fishing mortality rate ($F_{init} = 0.1$).

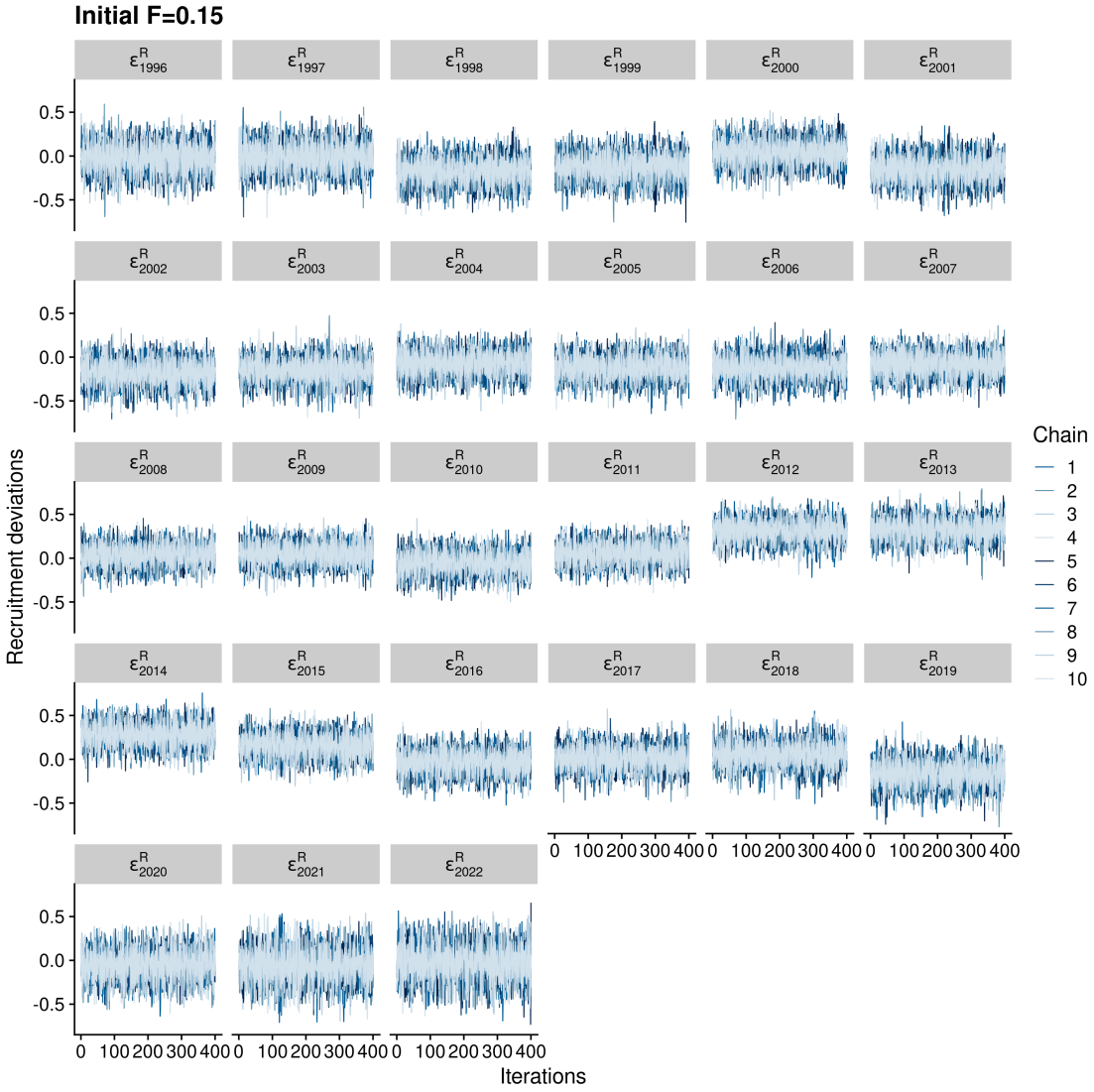

Figure 50: MCMC trace plots for recruitment deviaitions from a length and age - structured model with an initial fishing mortality rate ($F_{init} = 0.15$).

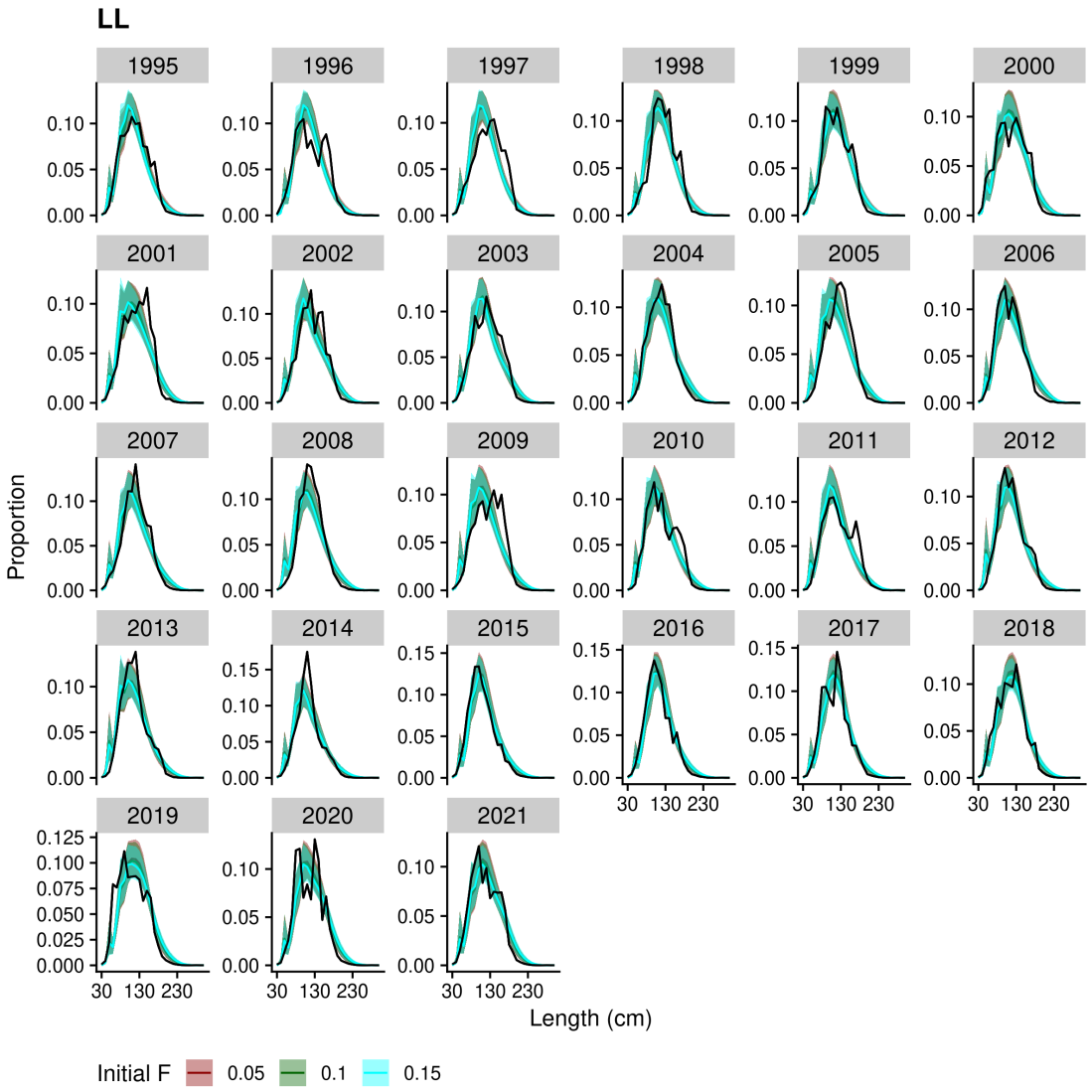

Figure 51: Fitted results for length frequency distributions in proportion for the longline capture fleet from 1995 to 2021. The black line represents the observed data. Each color indicates the sensitivity analysis results for different initial fishing mortality rates ($F_{init} = 0.05$, 0.1, and 0.15). Shades represent 95% credible intervals.

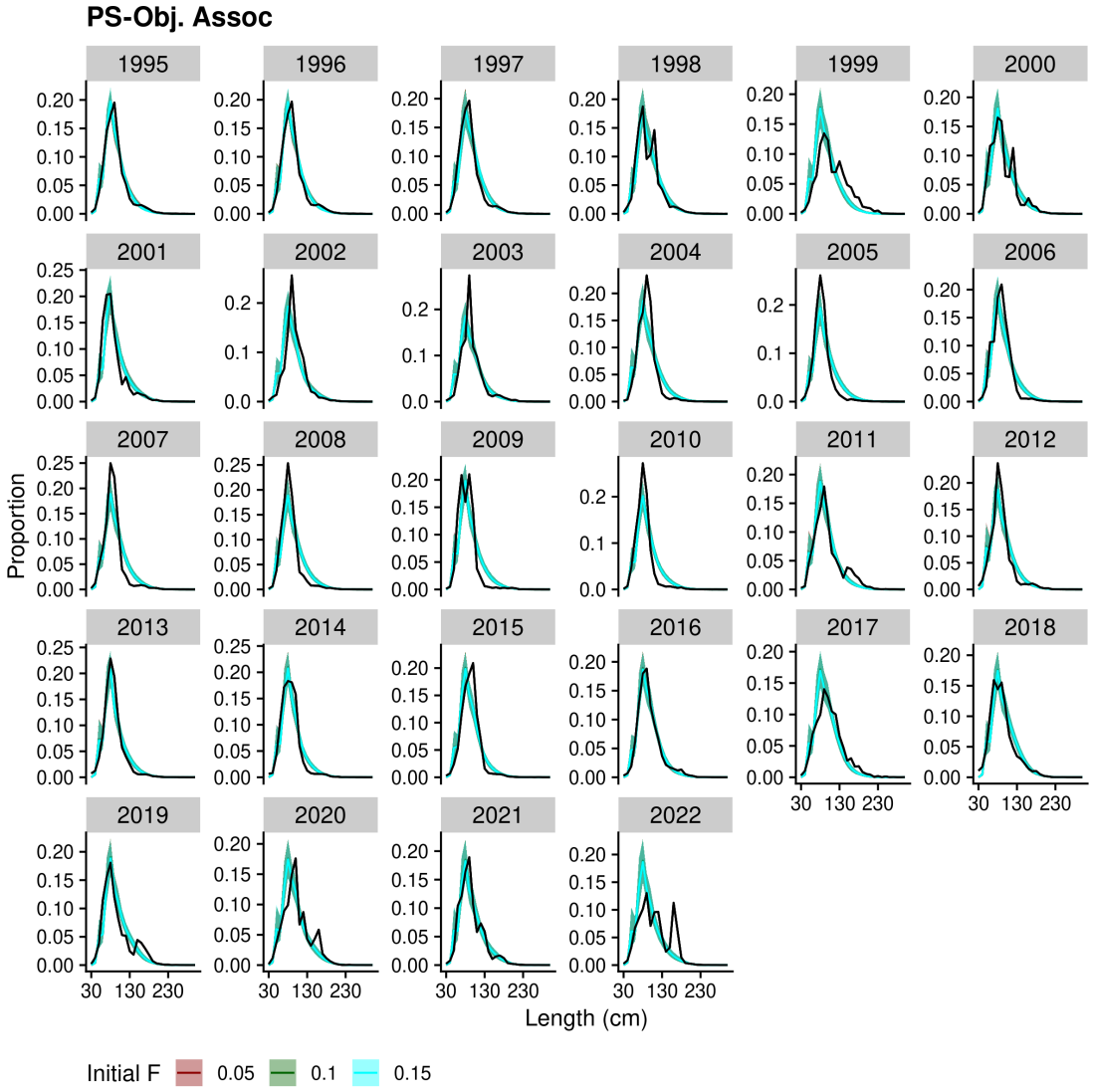

Figure 52: Fitted results for length frequency distributions in proportion for the object-associated purse-seine (PS-Obj. Assoc.) fleet from 1995 to 2022. The black line represents the observed data. Each color indicates the sensitivity analysis results for different initial fishing mortality rates ($F_{init} = 0.05, 0.1,$ and 0.15). Shades represent 95% credible intervals.

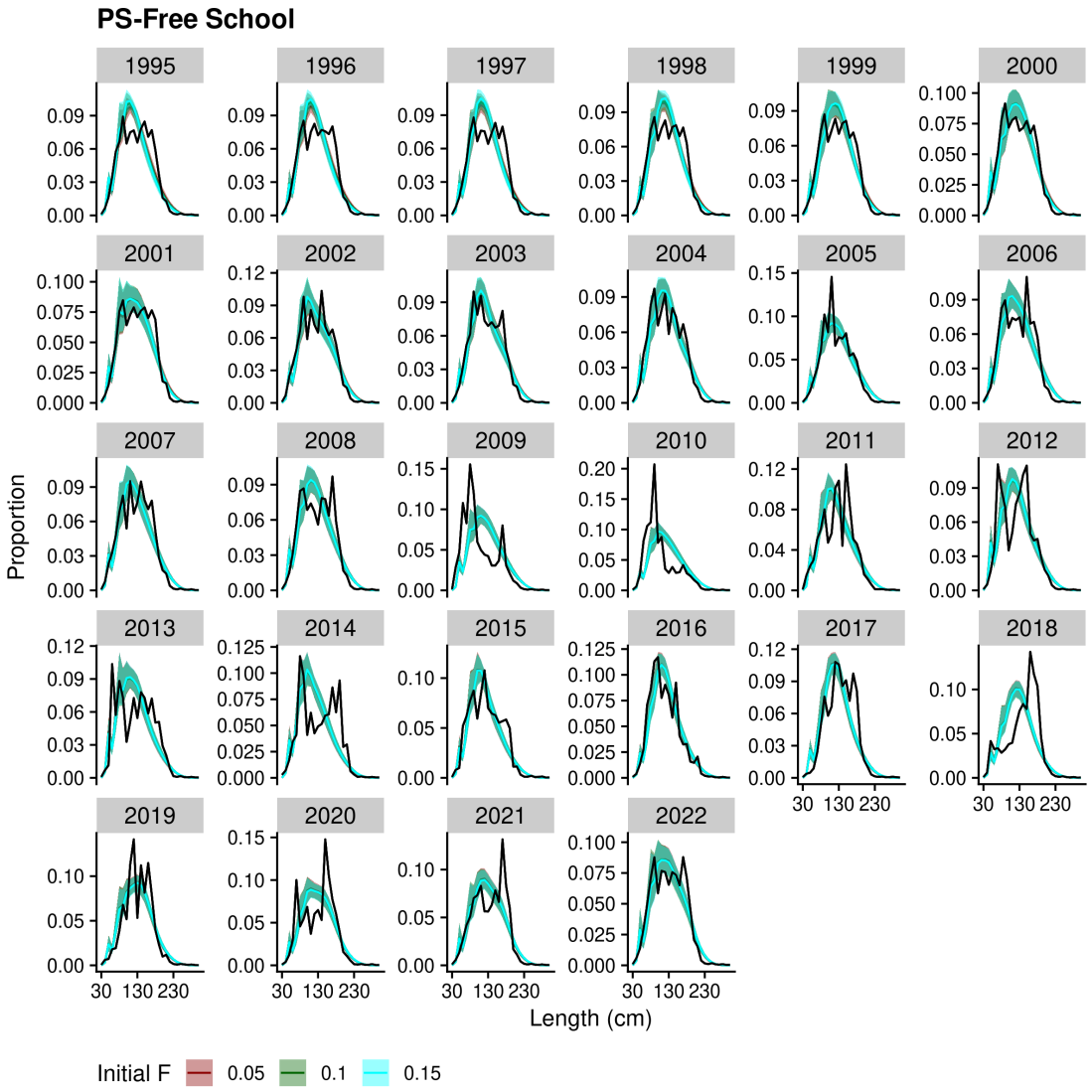

Figure 53: Fitted results for length frequency distributions in proportion for the free-school purse-seine (PS-Free School) fleet from 1995 to 2022. The black line represents the observed data. Each color indicates the sensitivity analysis results for different initial fishing mortality rates ($F_{init} = 0.05$, 0.1, and 0.15). Shades represent 95% credible intervals.

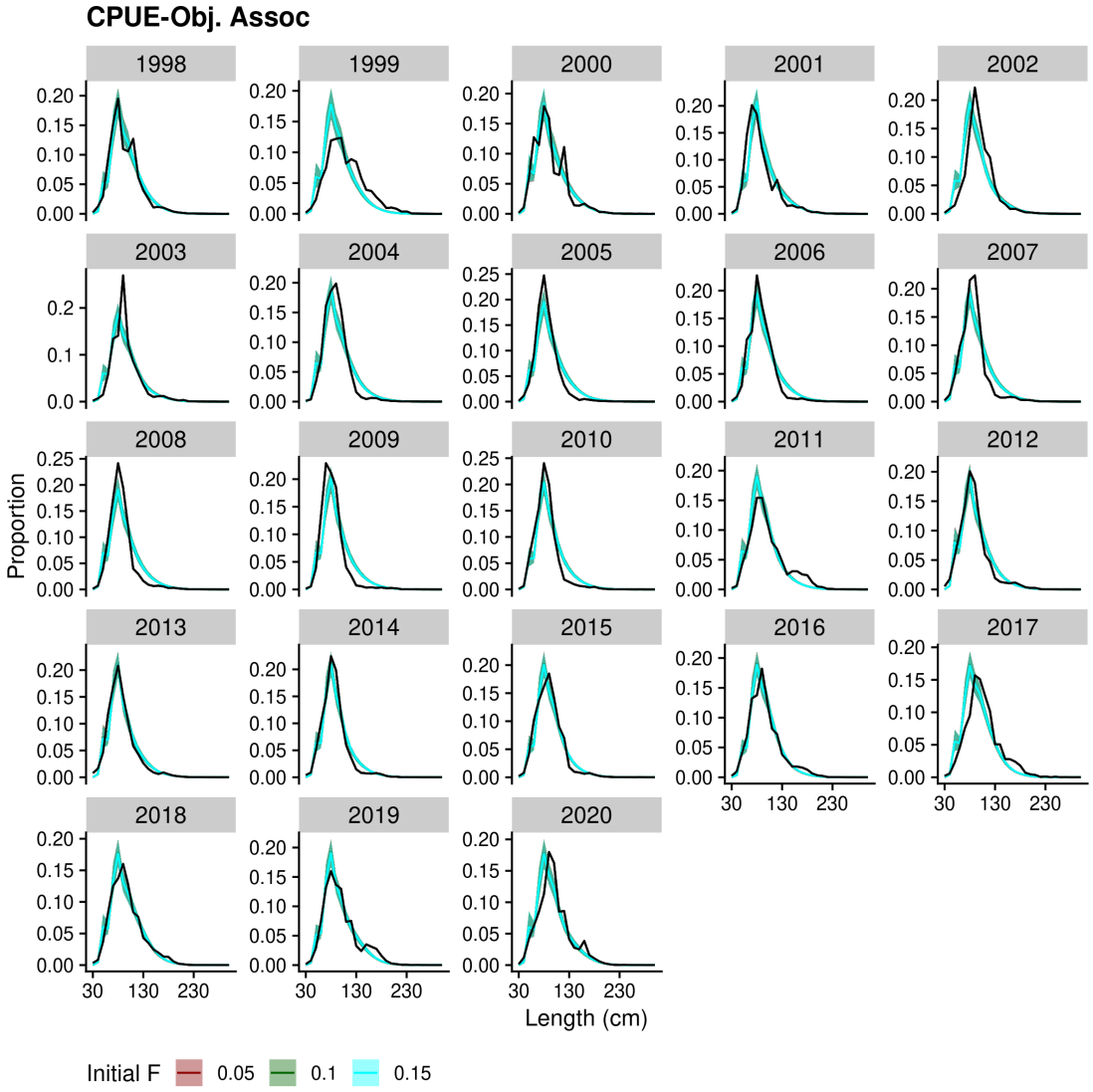

Figure 54: Fitted results for length frequency distributions in proportion for the object-associated index fleet (CPUE-Obj. Assoc.) from 1998 to 2020. The black line represents the observed data. Each color indicates the sensitivity analysis results for different initial fishing mortality rates ($F_{init} = 0.05, 0.1,$ and 0.15). Shades represent 95% credible intervals.

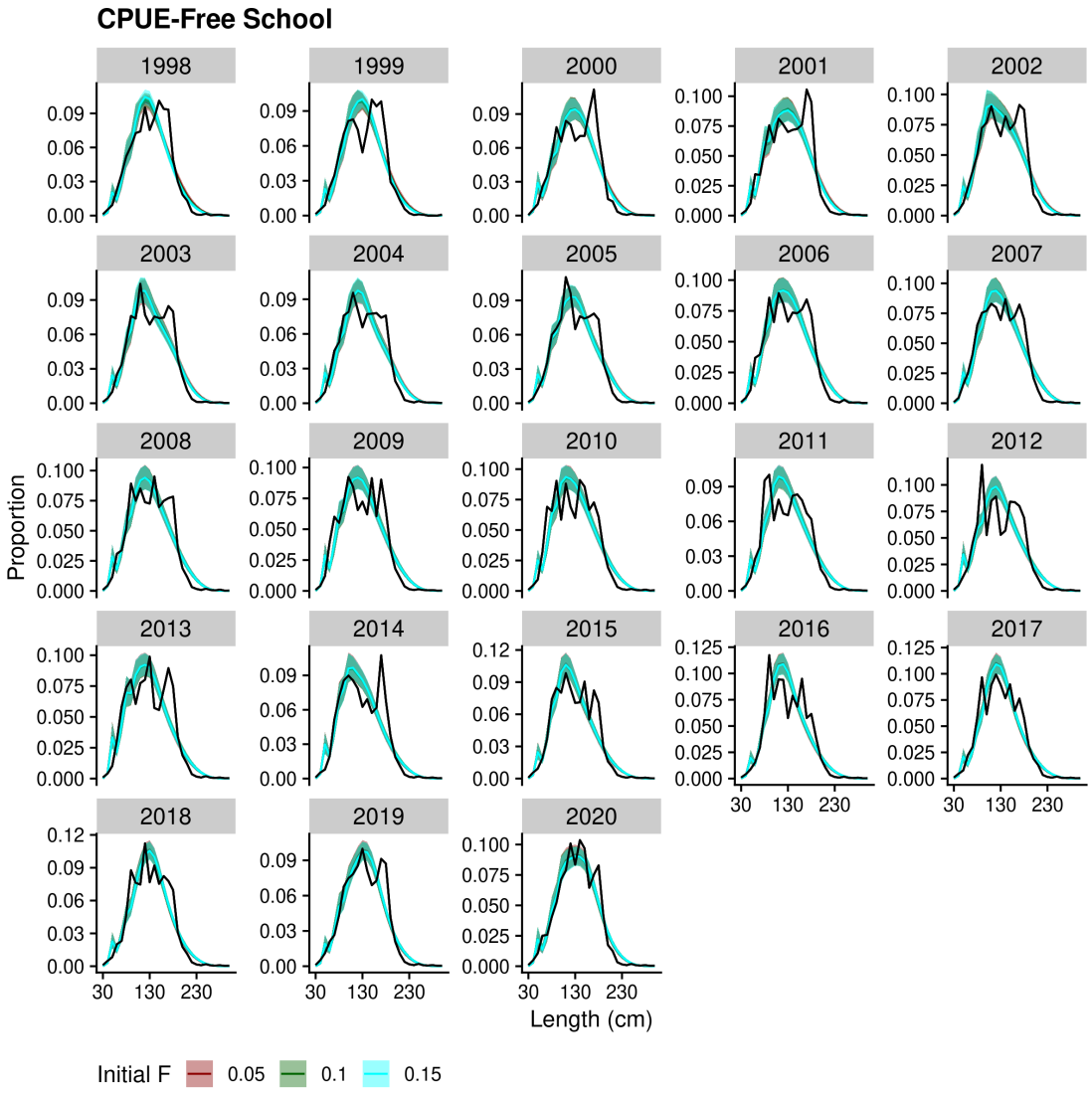

Figure 55: Fitted results for length frequency distributions in proportion for the free - school index fleet (CPUE - Free School) from 1998 to 2020. The black line represents the observed data. Each color indicates the sensitivity analysis results for different initial fishing mortality rates ($F_{init} = 0.05, 0.1,$ and 0.15). Shades represent 95% credible intervals.

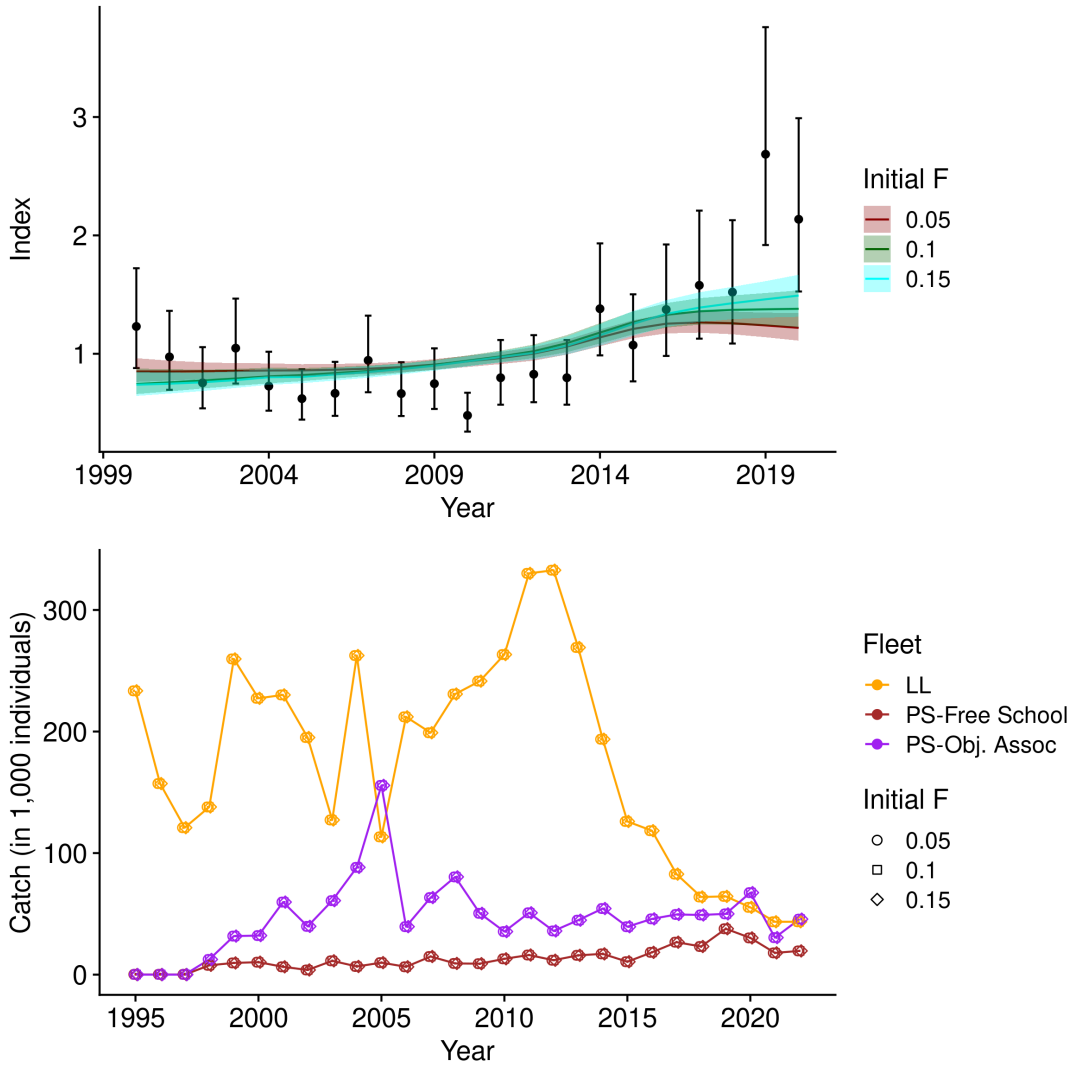

Figure 56: Fitted results to CPUE and catch using a length and age-structured model with sensitivity analysis on initial F. The top panel shows the index of abundance with error bars indicating 95% uncertainty intervals, and the fitted results of sensitivity analysis for different initial fishing mortality rates ($F = 0.05, 0.1,$ and 0.15) represented by lines and shaded areas (95% credible intervals). The bottom panel depicts the actual catch (in 1,000 individuals) by fleet: Longline (LL), free-school purse-seine (PS-Free School), and object-associated purse-seine (PS-Obj. Assoc.). Different markers indicate model-predicted catches from models with different initial F values (circle for 0.05, square for 0.1, and diamond for 0.15), assuming no error in catch.

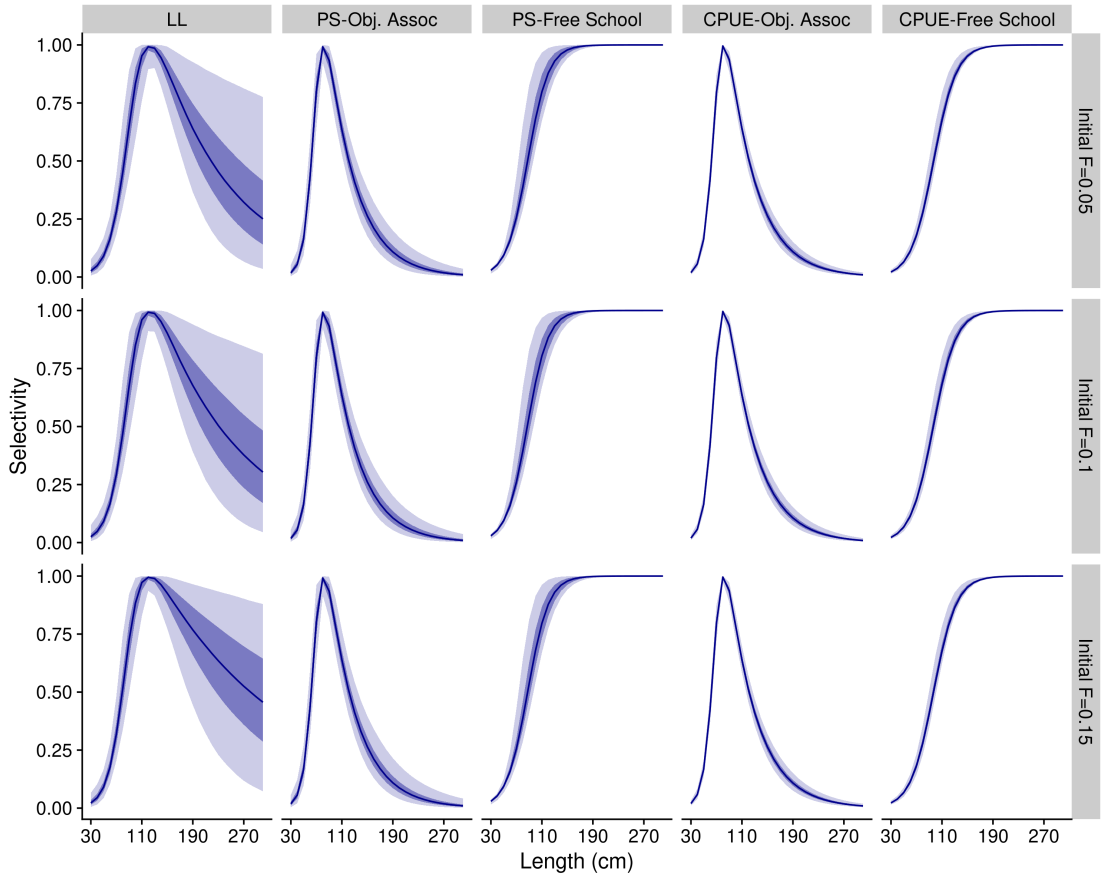

Figure 57: Selectivity curves for different fleets and initial fishing mortality rates ($F_{init} = 0.05, 0.1,$ and 0.15) using a length and age-structured model. The columns represent different length frequency data the model fitted to: Longline capture fleet (LL), object-associated purse-seine capture fleet (PS-Obj. Assoc), free-school purse-seine fleet (PS-Free School), object-associated index fleet (CPUE-Obj. Assoc), and free-school index fleet (CPUE-Free School). The rows represent different initial fishing mortality rates. The solid lines represent the median selectivity, and the shaded areas represent the 50% (darker shade) and 95% (lighter shade) credible intervals.

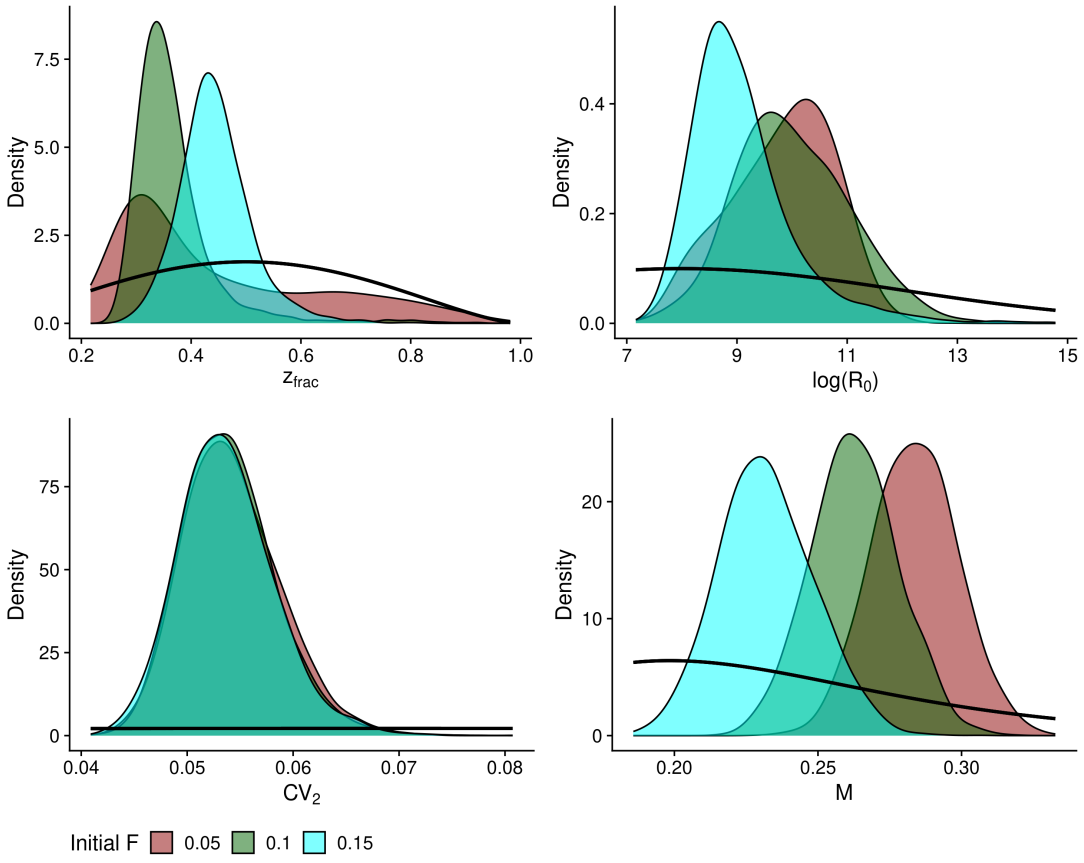

Figure 58: Marginal posterior density distributions for key parameters from a length and age-structured model with different initial fishing mortality rates ($F_{init} = 0.05, 0.1,$ and 0.15). Each color represents a different initial fishing mortality rate. The black line represents the prior distribution.

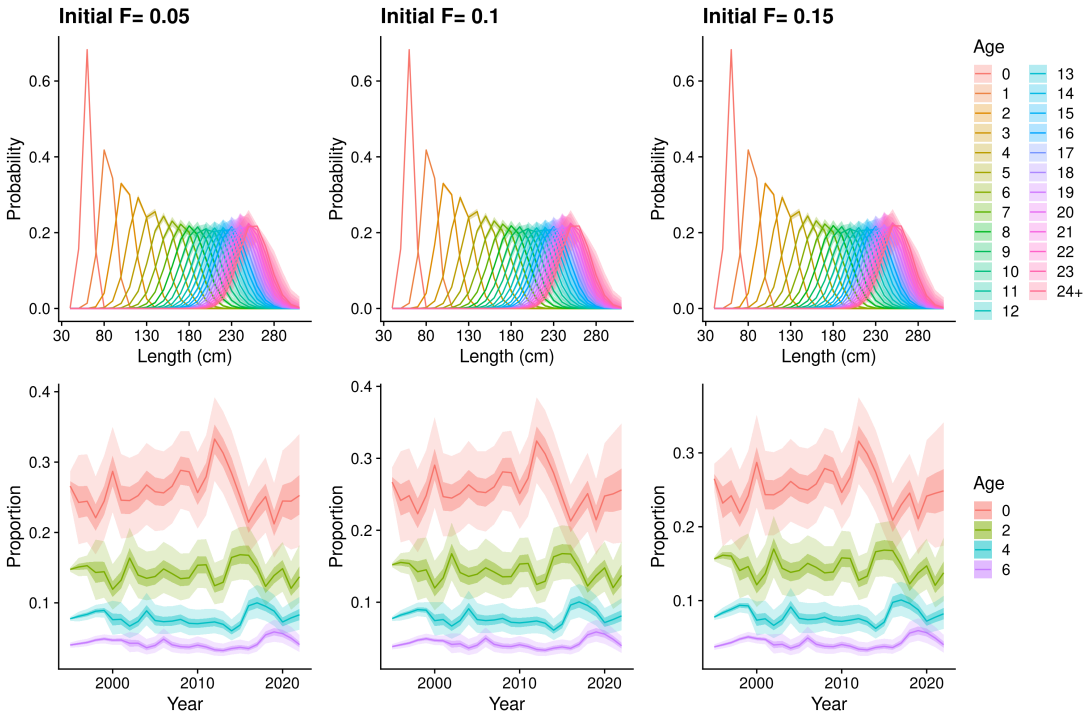

Figure 59: Probability and proportion distributions by length and age with sensitivities on initial fishing mortality rates ($F_{init} = 0.05, 0.1$, and 0.15) estimated using a length and age-structured model. The top row shows the probability of length at age, with different colors representing different ages from 0 to 24+. The bottom row shows the proportion of different age groups over time, with shaded areas representing the 50% (darker shade) and 95% (lighter shade) credible intervals.

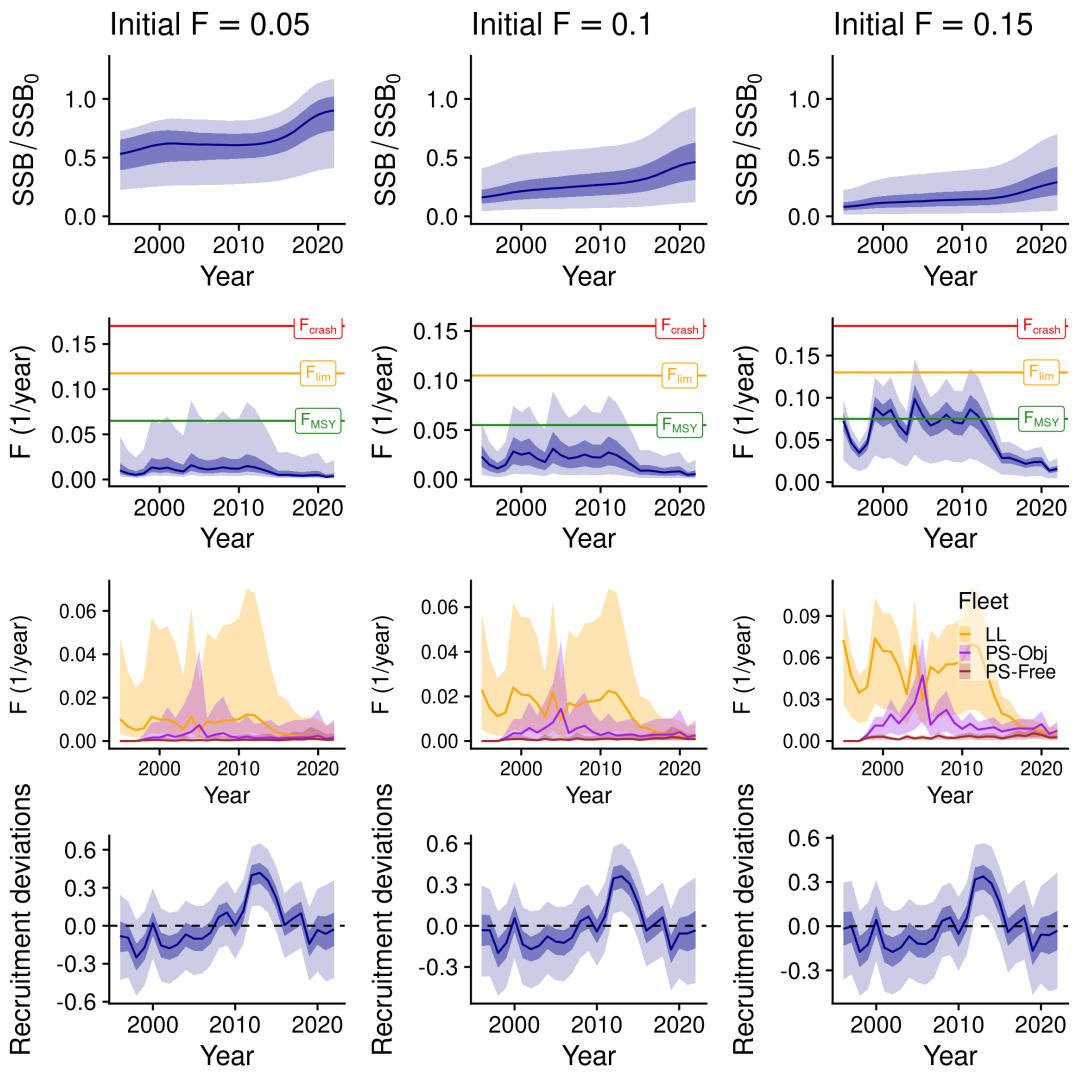

Figure 60: Time series plots illustrating the sensitivity analysis of different initial fishing mortality rates ($F_{init} = 0.05, 0.1,$ and 0.15) on the Spawning Stock Biomass (SSB / SSB_0), fishing mortality (F / year), fleet-specific fishing mortality (F / year), and recruitment deviations. The top row shows the relative SSB, the second row shows the overall fishing mortality with reference points F_{crash}, F_{lim}, and F_{MSY}. The third row illustrates fishing mortality rates by fleet: Longline (LL), object-associated purse-seine (PS-Obj), and free-school purse-seine (PS-Free). The bottom row depicts the recruitment deviations. Shaded areas represent 50% (darker shade) and 95% (lighter shade) credible intervals.

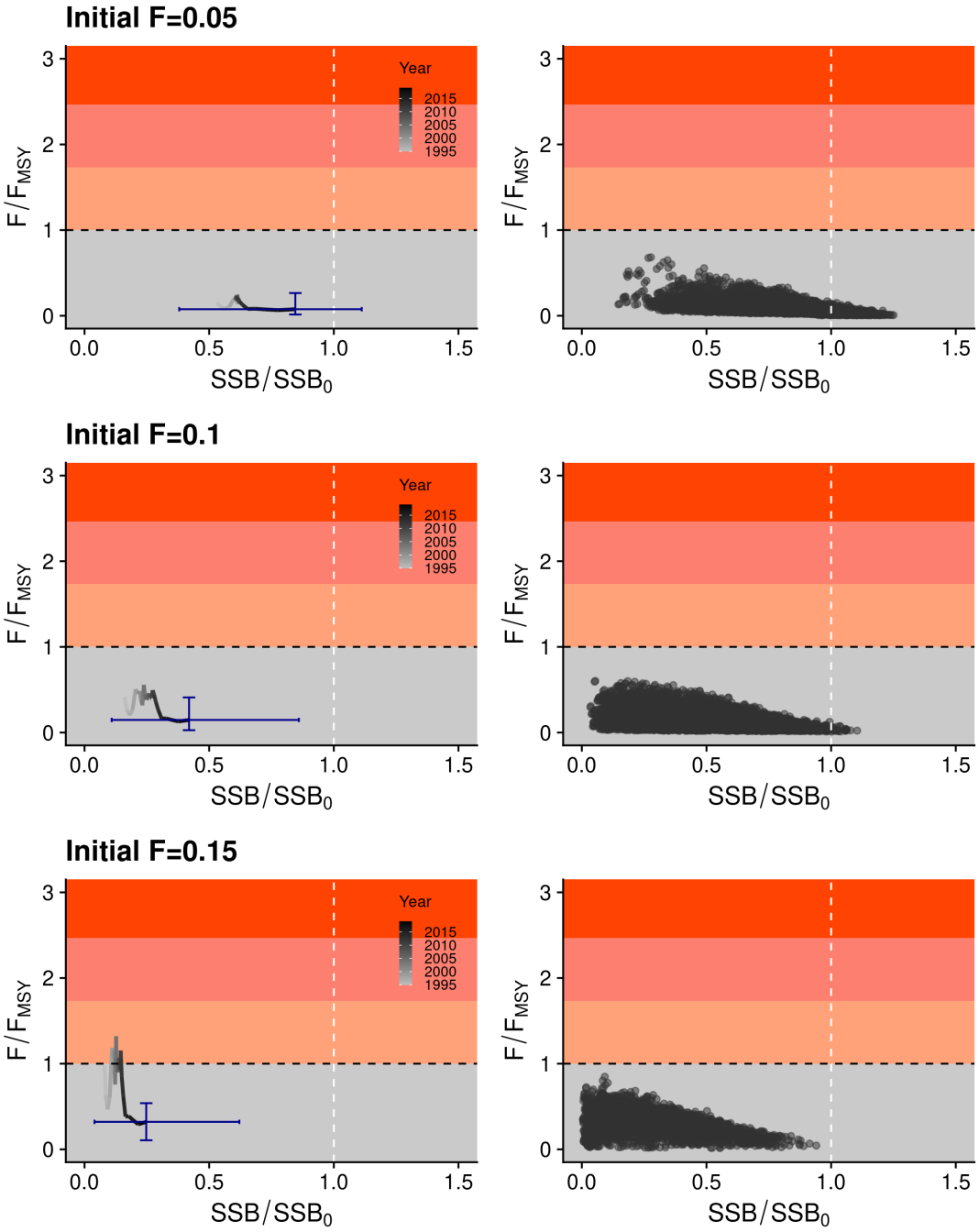

Figure 61: Majuro plots for silky shark assessments with a length and age-structured model with sensitivities on initial F ($F_{init} = 0.05, 0.1, 0.15$, respectively). The first column shows stock status (SSB/SSB_0) trajectories over time, with error bars for the recent (2019-2020) stock status level indicating 95% uncertainty intervals. The second column shows the individual draws from the posterior distributions for recent (2019-2020) years. The reddish color gradient indicates F_{lim} and F_{crash} relative to F_{MSY}. The horizontal dashed line represents $F/F_{\text{MSY}} = 1$, and the vertical dashed line represents $SSB/SSB_0 = 1$.

11.2.2 Dynamic surplus production model

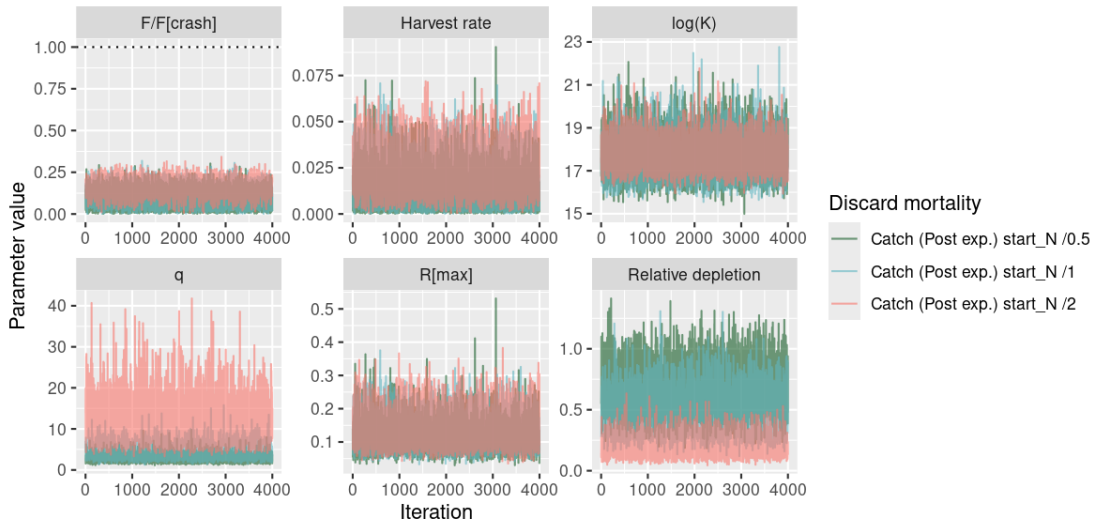

Figure 62: MCMC traces for derived parameters (harvest rate, risk of population collapse F/F_{Crash}) and selected estimated parameters (initial depletion, carrying capacity K, intrinsic population growth R_{max} and relative depletion) for different model runs with alternative prior assumptions about initial depletion.

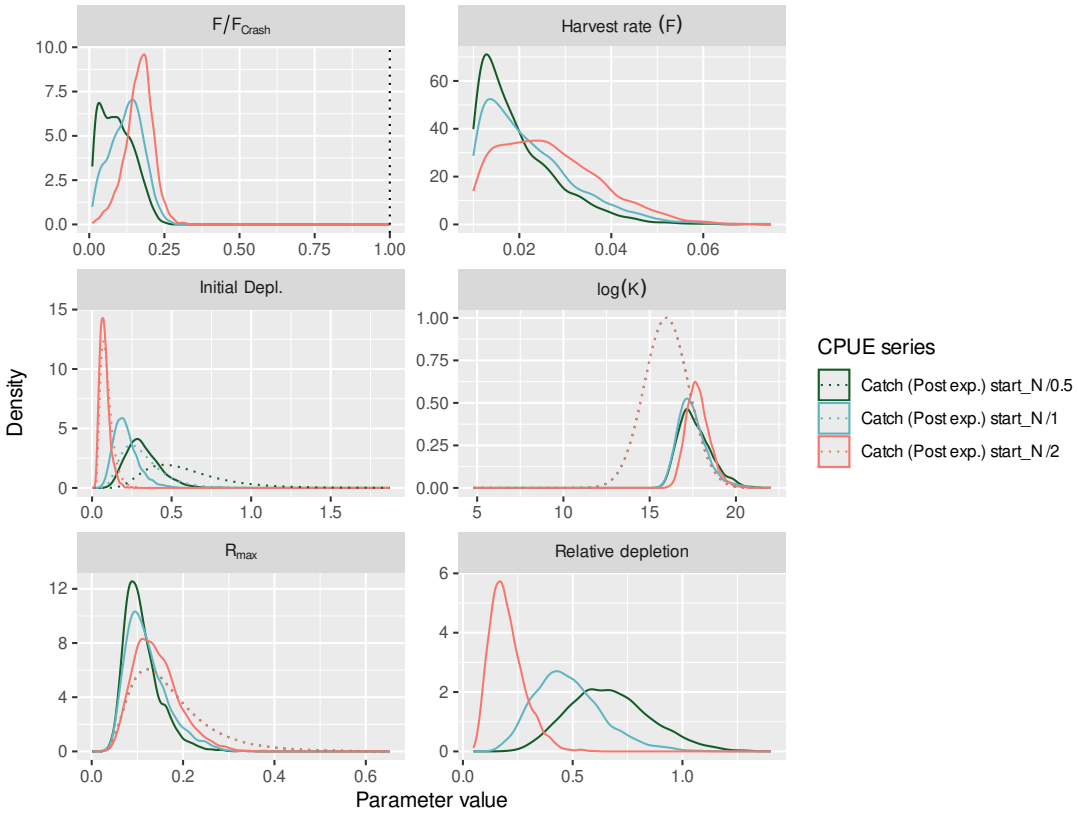

Figure 63: Marginal posterior densities for derived parameters (harvest rate, risk of population collapse F/F_{Crash}) and selected estimated parameters (initial depletion, carrying capacity K, intrinsic population growth R_{max} and relative depletion) for different model runs with alternative prior assumptions about initial depletion.

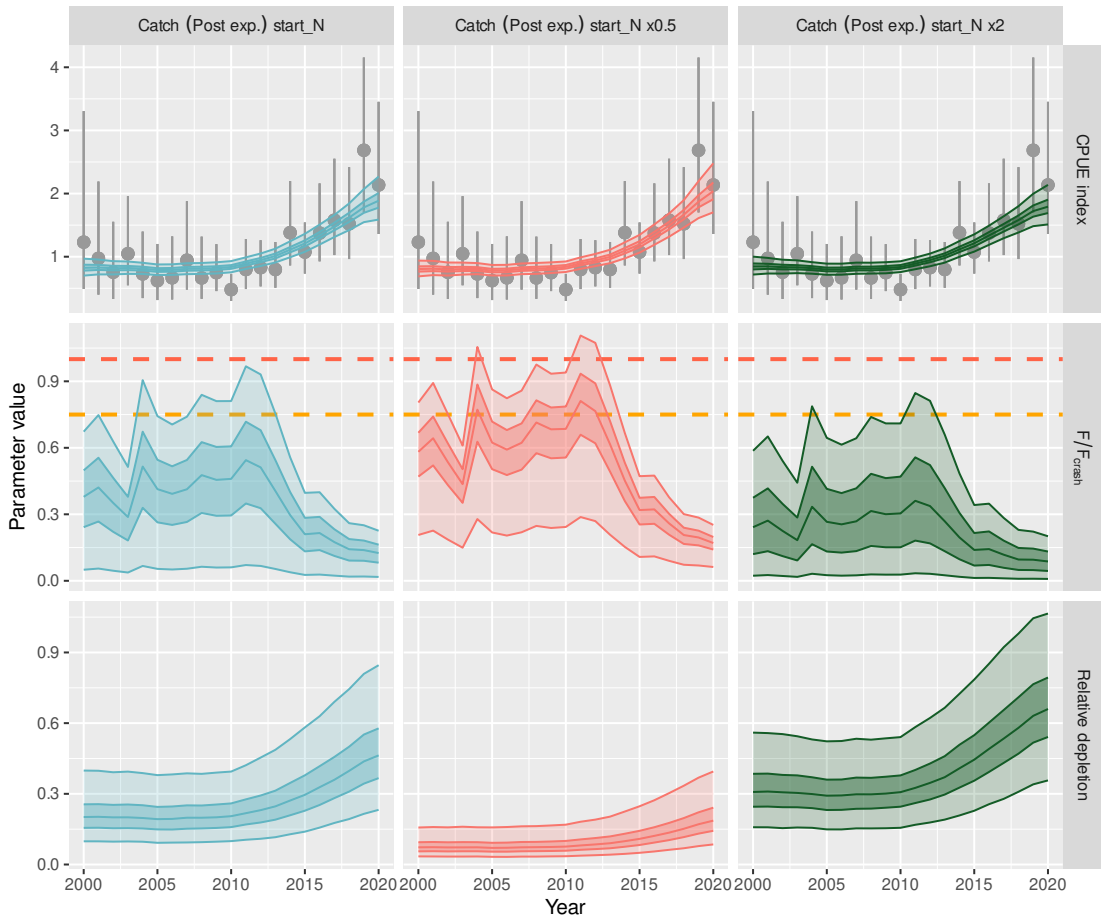

Figure 64: Fitting of catch-per-unit-effort (CPUE) data using a dynamic surplus production model with independent model runs for each CPUE indices (dark shading, inter-quartile; light shading, 95% credible interval). Top row: Predicted CPUE with input CPUE (points) and observation error (inter-quartile range). Middle row: Time series of fishing mortality relative to the F_{Crash} (red) and $F_{lim} = 0.75 \cdot F_{Crash}$ (orange) as estimated in the dynamic surplus production model. Bottom row: Estimated relative depletion (relative to unfished abundance K). The stock was not unfished in the first year of the time-series, and each column shows an alternative prior assumption about initial depletion.

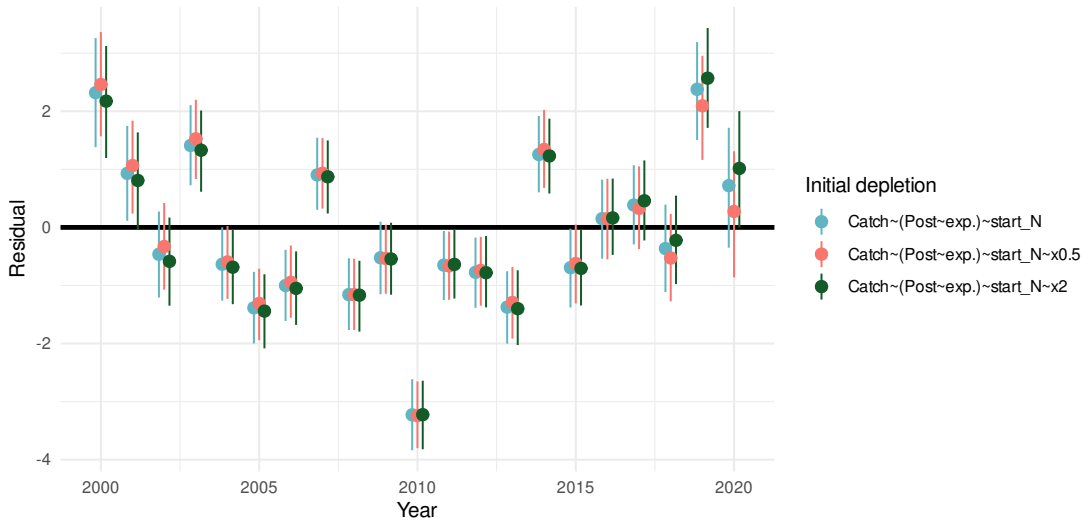

Figure 65: Standardised residuals for CPUE fits by initial depletion assumption.

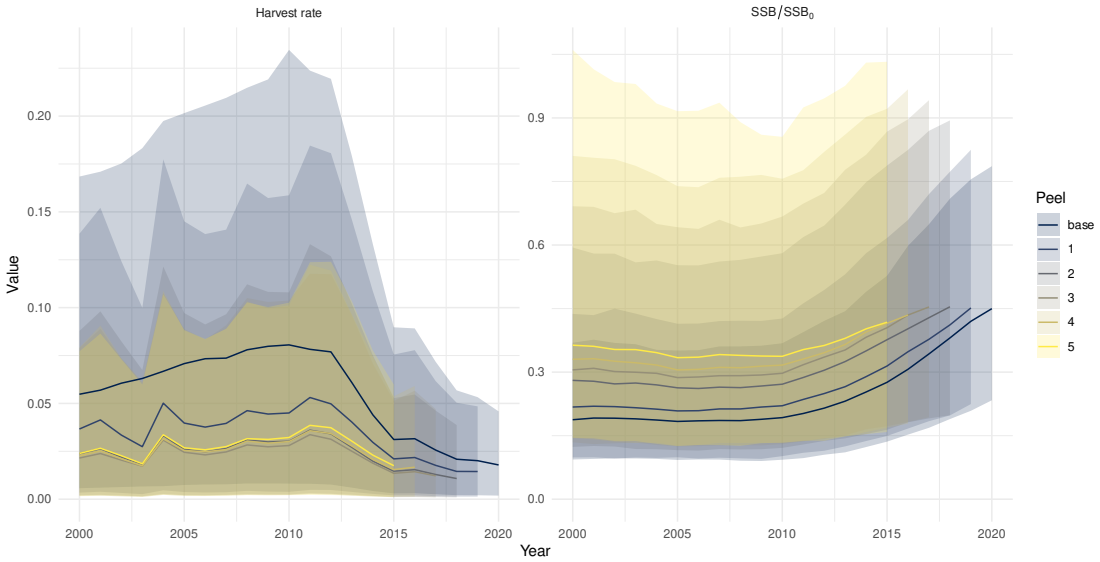

Figure 66: Retrospectives for harvest rate and biomass depletion for the base initial depletion assumption used for the dynamic surplus production model for silky shark.

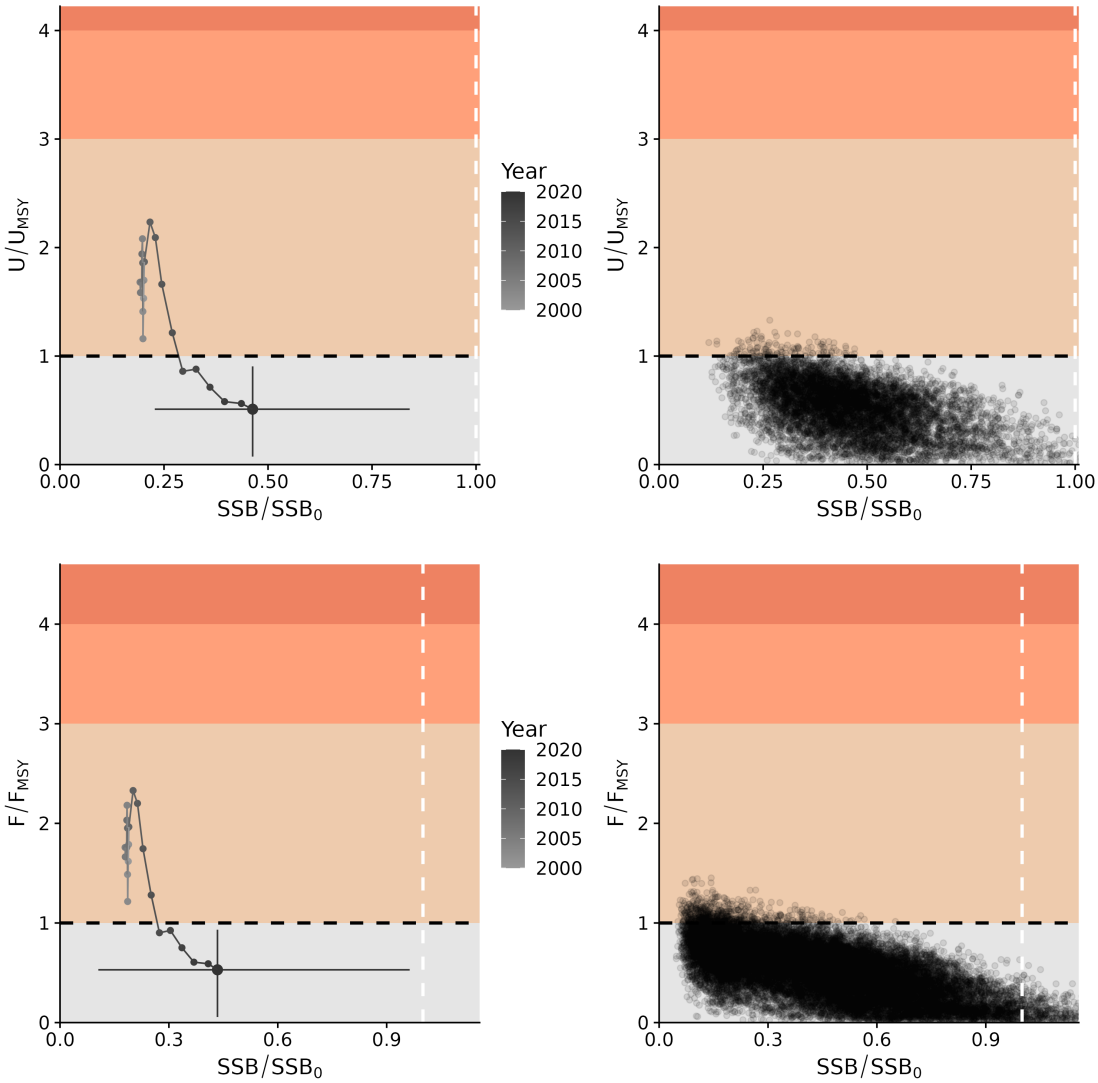

Figure 67: Majuro plots for recent (2019–2020) stock status based on the dynamic surplus production model for silky shark in the WCPFC. The top row shows outcomes for the base scenario, whereas the bottom row shows the outcomes across all three assumptions of initial depletion. Left hand plots show the stock trajectory, with uncertainty shown for the most recent year in the analysis (2020), whereas the plot on the right-hand side show individual draws from the posterior distribution(s) for recent (2019–2020) years.

11.2.3 Length-based spatial risk assessment

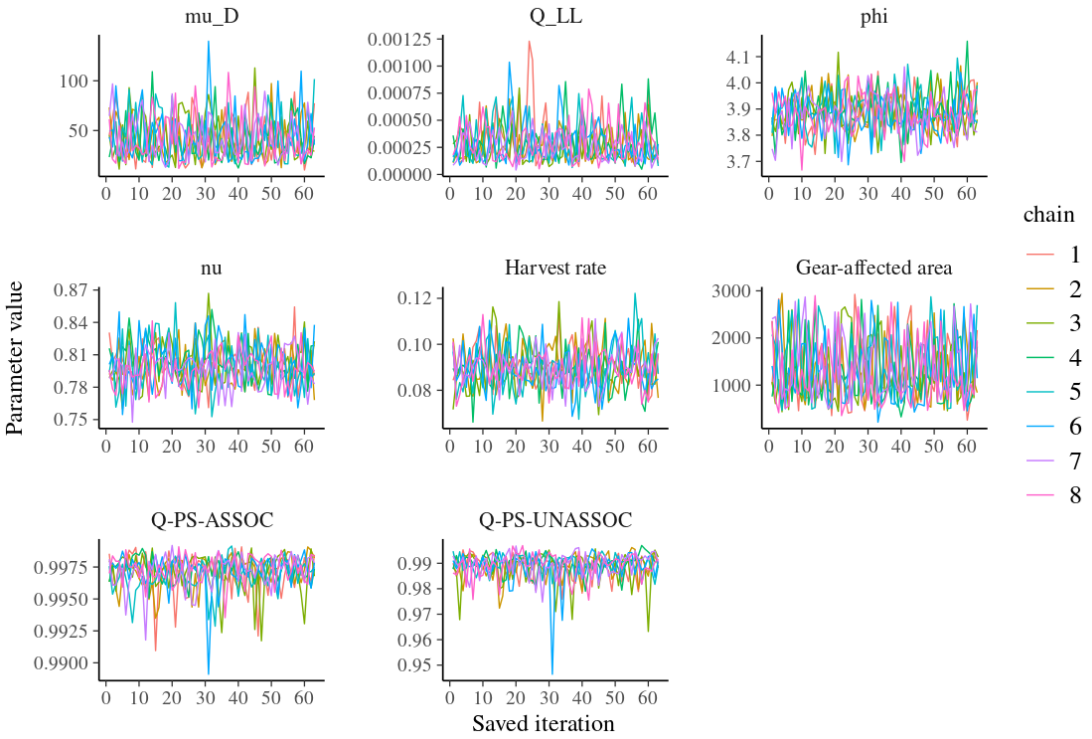

Figure 68: MCMC traces for key parameters in the hybrid length-based spatial risk assessment.

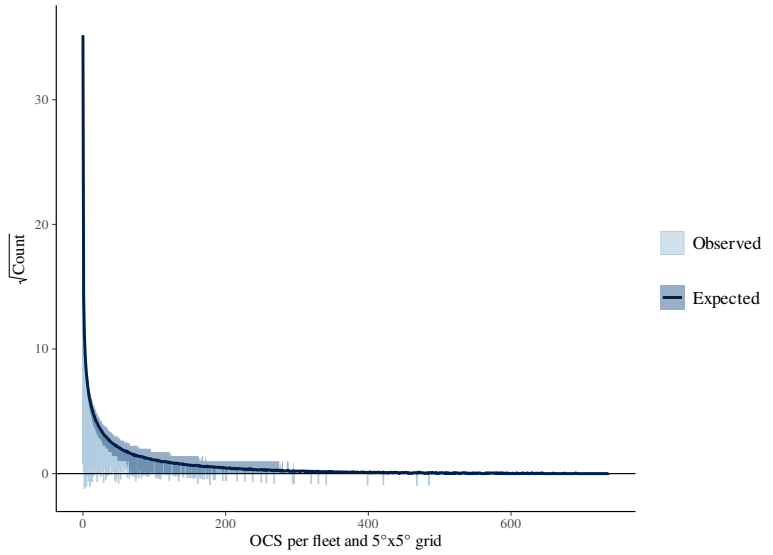

Figure 69: Posterior predictive draws (ribbon) and "rootogram" showing the histogram of observed data shifted on the y-axis to meet the prediction, thereby showing residuals along the x-axis (i.e., bars ending above the x-axis show a negative residual and vise-versa.)

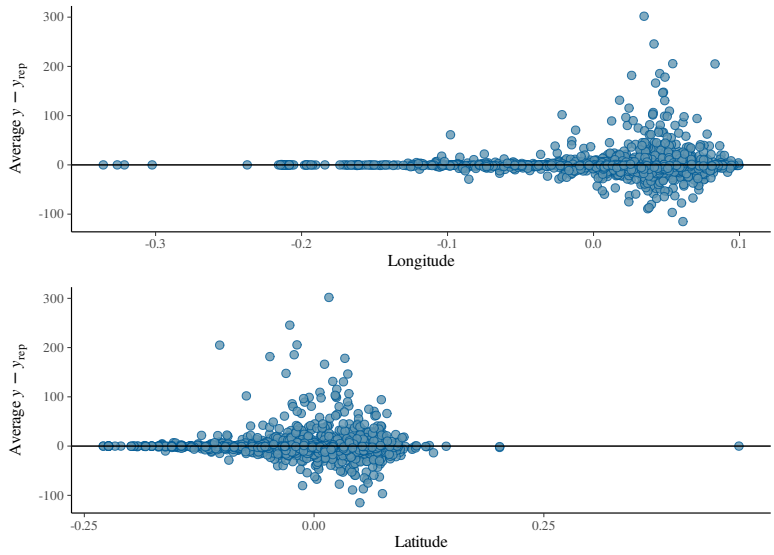

Figure 70: Posterior predictive histograms of observed versus predicted (yrep) interactions by gear (1: longline; 2: Object-associated purse-seine; 3: free-school purse-seine) and residuals from the hybrid length-based spatial risk assessment plotted against standardised longitude and latitude.

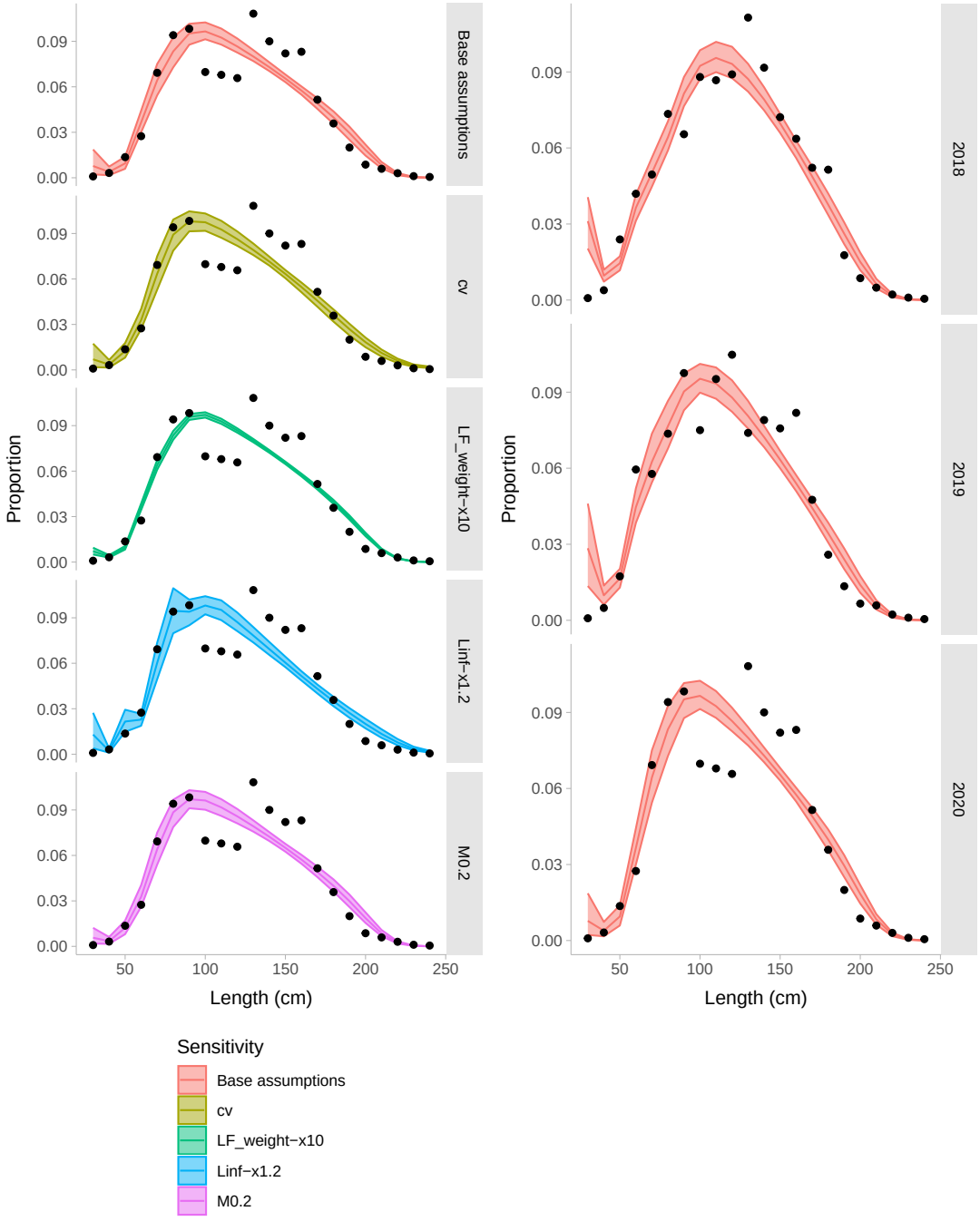

Figure 71: Fits (line (posterior median) and ribbon (95% credible intervals) for length frequencies used in the hybrid length - based spatial risk assessment to estimate fishing mortality.

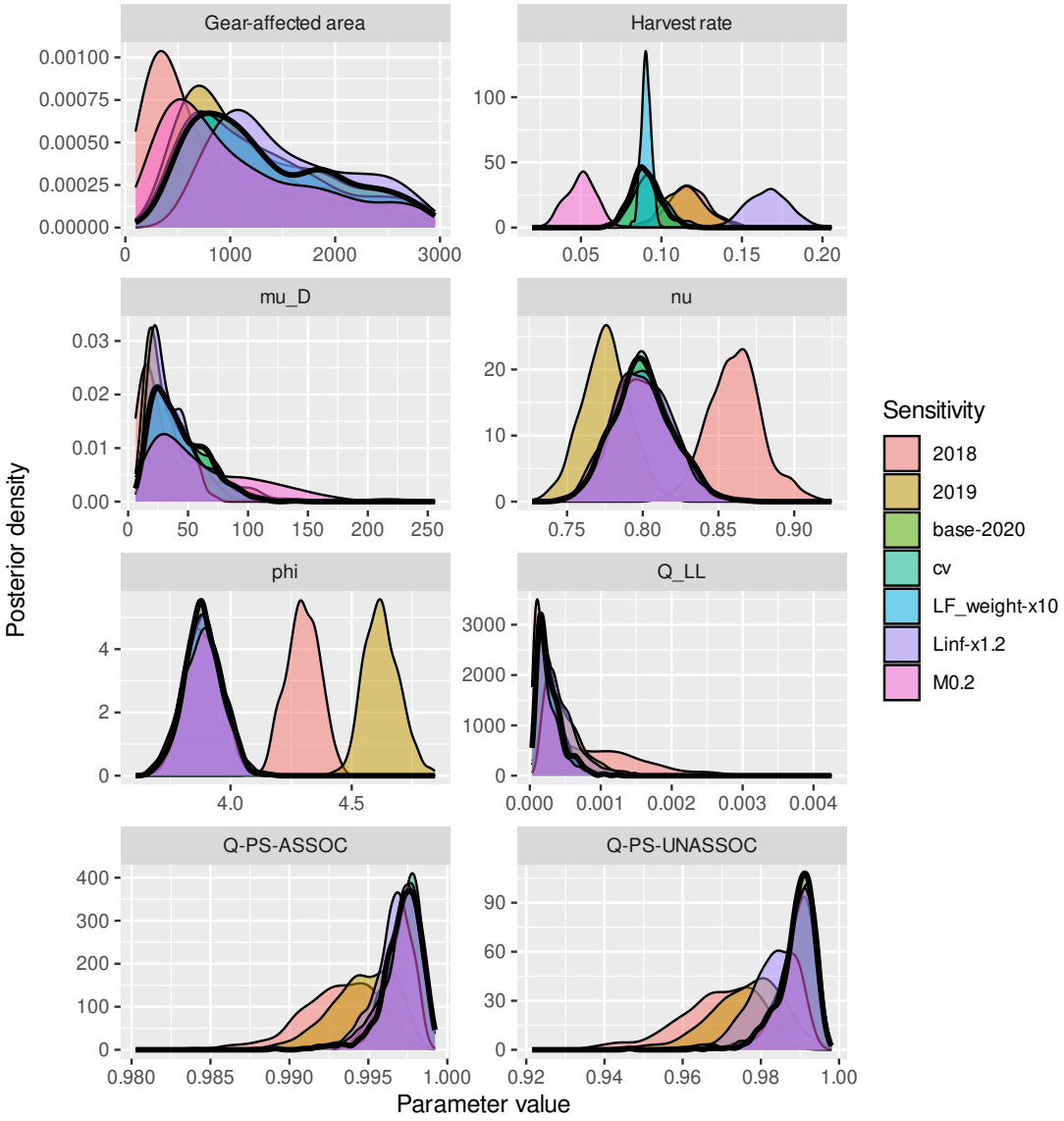

Figure 72: Posterior densities for key model parameters, with the base scenario highlighted with the thick black line.

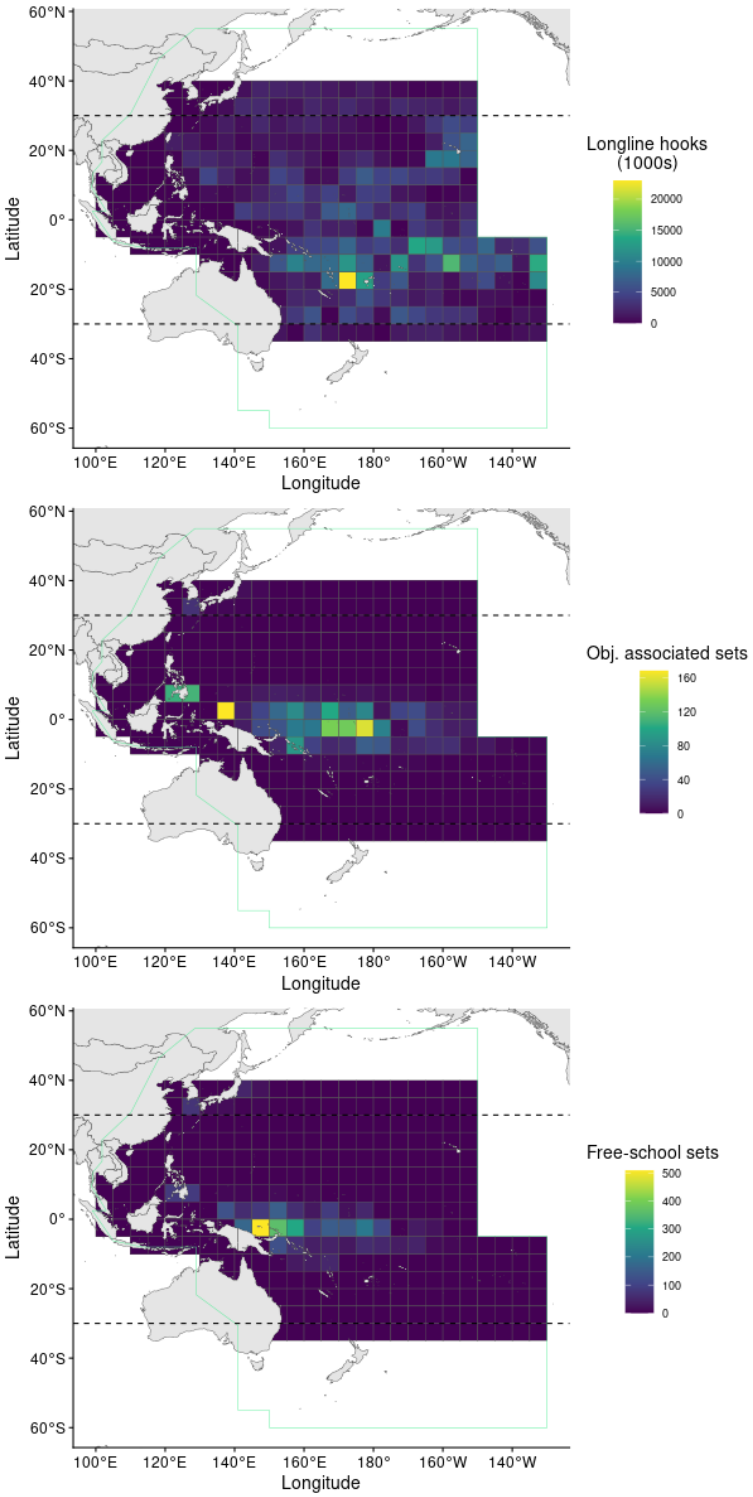

Figure 73: Effort by gear (top: longline; middle: Object-associated purse-seine; bottom: free-school purse-seine) used to predict spatial captures and harvest rate. Only effort from the 2020 year is shown.

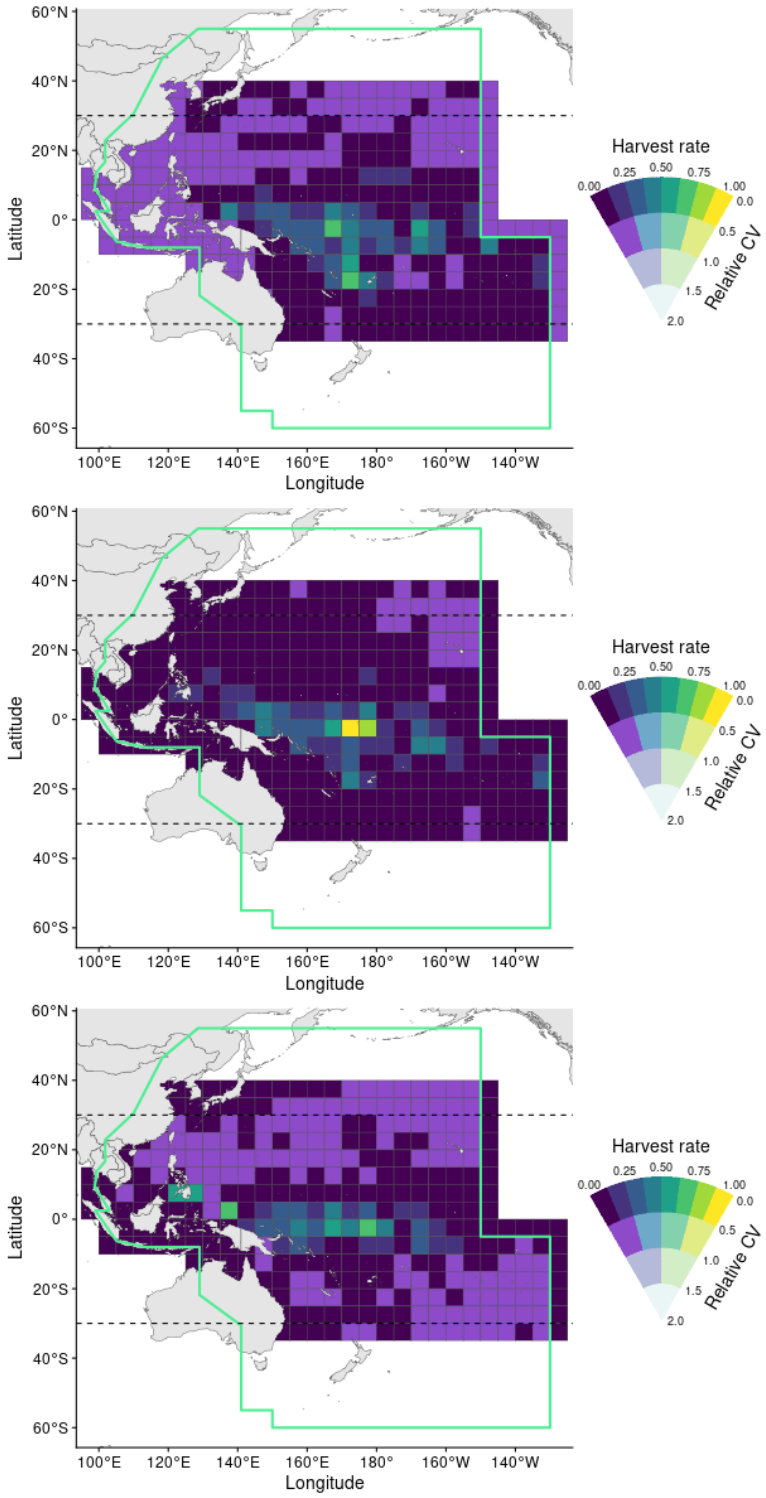

Figure 74: Estimated harvest rate and uncertainty from the hybrid length-based spatial risk assessment of silky shark by year, for 2018 (top), 2019 (middle) and 2020 (bottom).

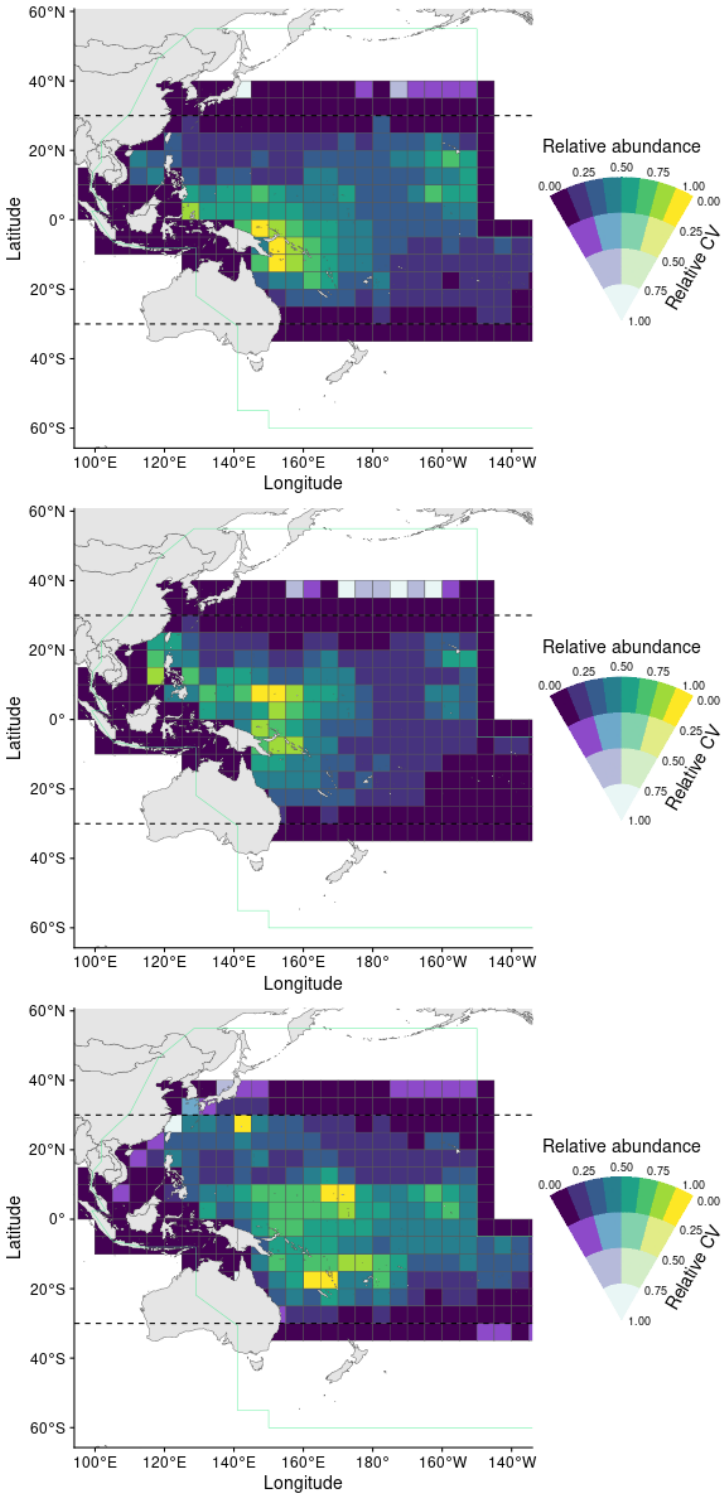

Figure 75: Estimated relative density and uncertainty from the hybrid length-based spatial risk assessment of silky shark by year, for 2018 (top), 2019 (middle) and 2020 (bottom).

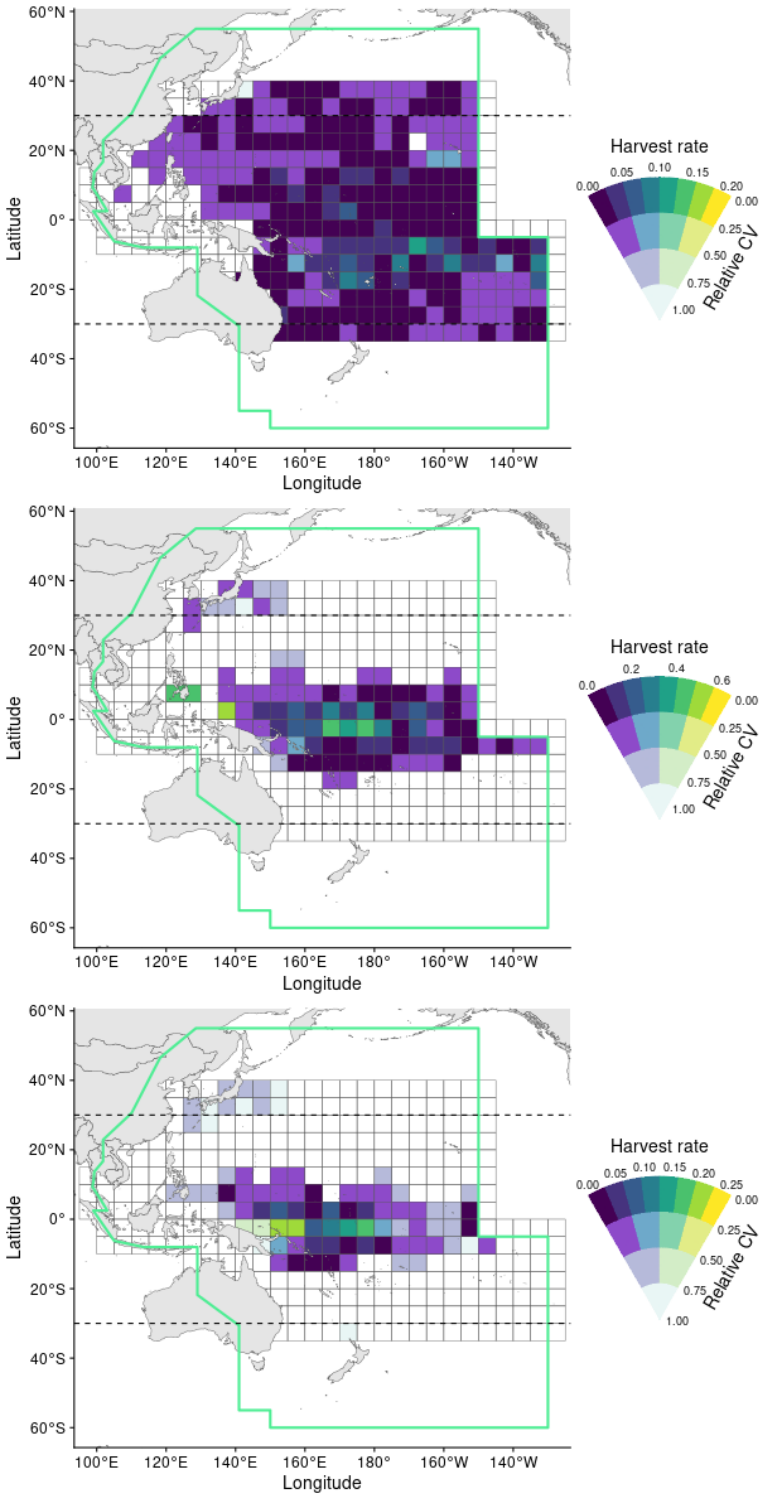

Figure 76: Estimated harvest rate and uncertainty from the hybrid length-based spatial risk assessment of silky shark by gear (top: longline; middle: Object-associated purse-seine; bottom: free-school purse-seine).

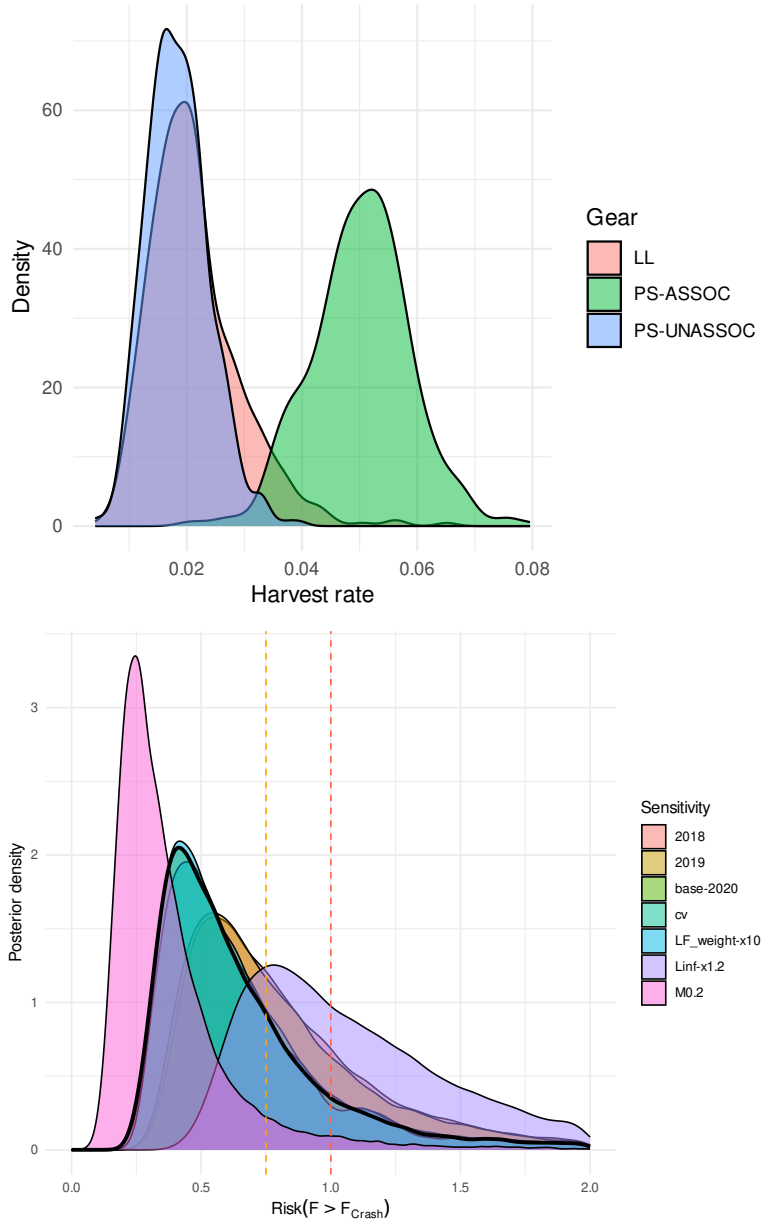

Figure 77: Estimated total harvest rate by gear (top) and associated risk estimated across years and sensitivities (for 2020).

11.2.4 Model Comparison

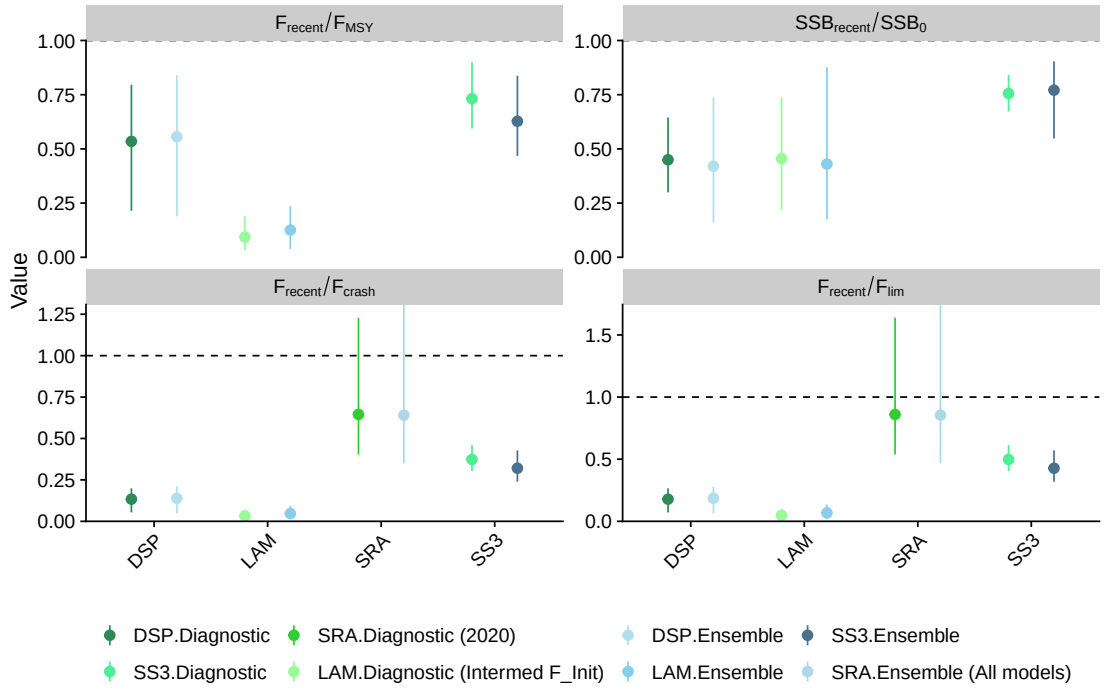

Figure 78: Estimates of management quantities (stock status as SSB_{recent}/SSB_0, and fishing mortality (F) relative to indicators (F_{MSY}) and possible limit reference points F_{lim}, F_{crash}) across models and subsets within models (diagnostic vs ensemble). P(>RP) refers to the probability that the metric (status, fishing mortality) is above the respective indicator (B_0, F_{MSY}, F_{lim}, F_{crash}). SS3: Stock Synthesis 3, DSP: Dynamic surplus production, LAM: Length and age-structured model, SRA: Spatial length-based risk assessment.

APPENDIX A TECHNICAL DETAILS OF THE LAM

A.1 Survival matrix

The survival matrix, $\mathbf{S}_t$, is a square matrix with length I, where I is the number of length bins. The survival matrix is defined as

$$\mathbf{S}_t = \begin{bmatrix} S_{1,t} & 0 & \cdots & 0 \\ 0 & S_{2,t} & \cdots & 0 \\ \vdots & \vdots & \ddots & \vdots \\ 0 & 0 & \cdots & S_{I,t} \end{bmatrix}, \tag{A-1}$$

where $S_{i,t}$ is the survival probability of a fish in length bin i at year t. The survival probability is calculated as

$$S_{i,t} = \exp\left(-M - \sum_f F_{i,t,f}\right), \tag{A-2}$$

where M is the natural mortality rate, and $F_{i,t,f}$ is the fishing mortality rate for fish in length bin i at year t of fishing fleet f.

A.2 Recruitment vector

The recruitment vector, $\mathbf{R}_t$, is a vector with length I, where I is the number of length bins. The recruitment vector is defined as

$$\mathbf{R}_t = \tilde{R}_t \cdot \begin{bmatrix} \pi_{1|r} \\ \pi_{2|r} \\ \vdots \\ \pi_{I|r} \end{bmatrix}, \tag{A-3}$$

where $\tilde{R}_t$ is the total recruitment at year t and $\pi_{i|r}$ is the probability of a fish being in length bin i at age of recruitment r.

For the length distribution of the initial age group $\pi_{i|r}$, a normal distribution is assumed with the mean length at age of recruitment, μ_r, and the variance of the length at recruitment, σ_r^2. The probability of a fish being in length bin i at age of recruitment

is defined as

$$\pi_{i|r} = \begin{cases} \int_0^{L_i+w/2} f(L|\mu_r, \sigma_r^2)\, dL & \text{for } i = 1 \\ \int_{L_i-w/2}^{L_i+w/2} f(L|\mu_r, \sigma_r^2)\, dL & \text{for } 1 < i < I\,, \\ 1 - \int_0^{L_i-w/2} f(L|\mu_r, \sigma_r^2)\, dL & \text{for } i = I \end{cases} \tag{A-4}$$

where L_i is the midpoint of length bin i, w is the length bin width, μ_r is the mean length at age of recruitment, σ_r^2 is the variance of the length at recruitment, and $f(\cdot)$ is the normal probability density function.

A.3 Growth transition matrix

The age-specific growth transition probability matrix, $\mathbf{G}_a$, is a square matrix with dimension $I \times I$, where I is the number of length bins. The growth transition probability matrix is defined as

$$\mathbf{G}_a = \begin{bmatrix} G_{1|1,a} & G_{1|2,a} & \cdots & G_{1|I,a} \\ G_{2|1,a} & G_{2|2,a} & \cdots & G_{2|I,a} \\ \vdots & \vdots & \ddots & \vdots \\ G_{I|1,a} & G_{I|2,a} & \cdots & G_{I|I,a} \end{bmatrix}, \qquad \text{for } r \leq a < A, \tag{A-5}$$

where $G_{j|i,a}$ is the probability that a fish in length bin i at age a will grow to length bin j at age $a+1$. The growth transition probability, $G_{j|i,a}$, is modelled as a normal distribution with mean $\bar{L}_{i,a+1}$ and variance σ_{a+1}^2, where $\bar{L}_{i,a+1}$ is the expected length for fish in length bin i after one growth increment and σ_{a+1}^2 is the corresponding variance:

$$G_{j|i,a} = \begin{cases} 0 & \text{for } j < i \\ \int_0^{L_j+w/2} f(L|\bar{L}_{i,a+1}, \sigma_{a+1}^2)\, dL & \text{for } j = i \\ \int_{L_j-w/2}^{L_j+w/2} f(L|\bar{L}_{i,a+1}, \sigma_{a+1}^2)\, dL & \text{for } j > i \\ 1 - \int_0^{L_j-w/2} f(L|\bar{L}_{i,a+1}, \sigma_{a+1}^2)\, dL & \text{for } j = I \end{cases}, \qquad \text{for } r \leq a < A \tag{A-6}$$

A.4 Growth model

The expected length for fish in length bin i after one growth increment, $\bar{L}_{i,a+1}$, was derived by reparameterizing the von Bertalanffy growth model. The expected length, $\bar{L}_{i,a+1}$, is defined as

$$\bar{L}_{i,a+1} = L_\infty \cdot (1 - \rho) + \rho \cdot L_i \quad , \tag{A-7}$$

where L_∞ is the asymptotic length, ρ is the brody growth coefficient (i.e., $\exp(-k)$, where k is the von Bertalanffy growth coefficient), and L_i is the midpoint of length bin i.

A.5 Growth variability

The variance of the expected length growth, σ^2_{a+1}, was assumed to be a function of the mean length at age a, which follows the two-parameter growth variability model used in the Stock Synthesis software (Methot Jr & Wetzel 2013, Methot et al. 2021):

$$\sigma_a = \mu_a \cdot \left(CV_1 + \left(\frac{\mu_a - L_{min}}{L_{max} - L_{min}} \cdot (CV_2 - CV_1) \right) \right), \tag{A-8}$$

where μ_a is the mean length at age a, CV_1 and CV_2 are the coefficients of variation for growth variability at the minimum and maximum lengths, and L_{min} and L_{max} are the minimum and maximum lengths, respectively.

The mean length at age a, μ_a, is calculated using the von Bertalanffy growth model:

$$\mu_a = L_\infty \cdot [1 - \exp(-k \cdot (a - a_0))], \tag{A-9}$$

where a_0 is the theoretical age at which fish are of zero length.

A.6 Length-at-age distribution

Length-at-age distributions under equilibrium conditions (i.e., $\pi_{i|a}$, defined as the probability of a fish being in length bin i at age a) with varying levels of length-dependent mortality across length bins can be calculated using the growth transition probability. This property is useful for understanding the impact of length-dependent mortality on the length-at-age distribution in relation to the growth traits of a fish population.

This equilibrium distribution can be calculated by multiplying the age-specific growth transition probability $G_{j|i,a}$ with the corresponding length-at-age distribution $\pi_{i|a}$ and the total mortality rate, $Z_i = M + F_i$. Then, summing over all length bins i to obtain the length-at-age distribution in the next age class $\pi_{j|a}$:

$$\pi_{j|a} = \frac{\sum_{i=1}^{I} \pi_{i|a-1} \cdot \exp(-Z_i) \cdot G_{j|i,a-1}}{\sum_{j=1}^{J} \sum_{i=1}^{I} \pi_{i|a-1} \cdot \exp(-Z_{i,a-1}) \cdot G_{j|i,a-1}}, \qquad \text{for } r < a \leq A, \tag{A-10}$$

where $Z_{i,a}$ is the total length-dependent mortality rate for fish in length bin i, and the denominator of the equation normalises the distribution to sum to 1. This process is repeated iteratively with $j = i$ until $a = A$ to obtain the length-at-age distribution across all age classes defined in the model.